![US.NRC logo] **U.S.NRC**

United States Nuclear Regulatory Commission

Protecting People and the Environment

NUREG-2196

BWR ECCS Pump Suction Concerns following a LOCA

Office of Nuclear Regulatory Research

AVAILABILITY OF REFERENCE MATERIALS
IN NRC PUBLICATIONS

NRC Reference Material

As of November 1999, you may electronically access NUREG-series publications and other NRC records at NRC's Library at www.nrc.gov/reading-rm.html. Publicly released records include, to name a few, NUREG-series publications; *Federal Register* notices; applicant, licensee, and vendor documents and correspondence; NRC correspondence and internal memoranda; bulletins and information notices; inspection and investigative reports; licensee event reports; and Commission papers and their attachments.

NRC publications in the NUREG series, NRC regulations, and Title 10, "Energy," in the *Code of Federal Regulations* may also be purchased from one of these two sources.

1. **The Superintendent of Documents**
   U.S. Government Publishing Office
   Mail Stop IDCC
   Washington, DC 20402-0001
   Internet: bookstore.gpo.gov
   Telephone: (202) 512-1800
   Fax: (202) 512-2104

2. **The National Technical Information Service**
   5301 Shawnee Rd., Alexandria, VA 22312-0002
   www.ntis.gov
   1-800-553-6847 or, locally, (703) 605-6000

A single copy of each NRC draft report for comment is available free, to the extent of supply, upon written request as follows:

Address: **U.S. Nuclear Regulatory Commission**
Office of Administration
Publications Branch
Washington, DC 20555-0001
E-mail: distribution.resource@nrc.gov
Facsimile: (301) 415-2289

Some publications in the NUREG series that are posted at NRC's Web site address www.nrc.gov/reading-rm/doc-collections/nuregs are updated periodically and may differ from the last printed version. Although references to material found on a Web site bear the date the material was accessed, the material available on the date cited may subsequently be removed from the site.

Non-NRC Reference Material

Documents available from public and special technical libraries include all open literature items, such as books, journal articles, transactions, *Federal Register* notices, Federal and State legislation, and congressional reports. Such documents as theses, dissertations, foreign reports and translations, and non-NRC conference proceedings may be purchased from their sponsoring organization.

Copies of industry codes and standards used in a substantive manner in the NRC regulatory process are maintained at—
The NRC Technical Library
Two White Flint North
11545 Rockville Pike
Rockville, MD 20852-2738

These standards are available in the library for reference use by the public. Codes and standards are usually copyrighted and may be purchased from the originating organization or, if they are American National Standards, from—
American National Standards Institute
11 West 42nd Street
New York, NY 10036-8002
www.ansi.org
(212) 642-4900

U.S.NRC

United States Nuclear Regulatory Commission

Protecting People and the Environment

BWR ECCS Pump Suction Concerns following a LOCA

Manuscript Completed: February 2016
Date Published: May 2016

Prepared by:
W.J. Krotiuk, C. Boyd, T. Zaki, W. Wang

Office of Nuclear Regulatory Research

ABSTRACT

This document describes a method to perform a plant-specific assessment to determine whether an emergency core cooling system (ECCS) pump will operate acceptably following a loss-of-coolant accident (LOCA) in a boiling water reactor (BWR) pressure suppression pool. The assessment approach uses the ECCS pump strainer location, the ECCS pump operation criteria, the ECCS pump startup and full operation timing information, and an estimate of the transient pool void fraction information to make the determination.

To support the developed assessment method, this report describes the acceptable ECCS pump operating range necessary to prevent pump damage if noncondensable gas ingestion occurs or to permit recovery from noncondensable gas ingestion. Additionally, this report uses computational fluid dynamics (CFD) analyses to define a noncondensable gas bubble "exclusion zone" and to provide the time-dependent noncondensable void fraction distribution in the suppression pool outside the large gas bubble following a LOCA. The report also lists the test facilities used to test BWR pressure suppression systems and summarizes the available test data that are used to verify the acceptability of the CFD analyses.

TABLE OF CONTENTS

TABLE OF CONTENTS

LIST OF FIGURES

LIST OF FIGURES

LIST OF TABLES

EXECUTIVE SUMMARY

This report summarizes the work and recommendations developed to support the technical basis for resolving U.S. Nuclear Regulatory Commission (NRC) Generic Safety Issue (GI) 193, "Boiling Water Reactor (BWR) Emergency Core Cooling System (ECCS) Suction Concerns." The following text from Reference 1 provides the background for this activity:

> *GSI-193 addresses the possible failure of the ECCS pumps due to unanticipated, large quantities of entrained gas in the suction piping from BWR suppression pools. The issue applies to Mark I, II, and III containments during large- and medium-break LOCAs, and could potentially cause pump failure or degraded performance due to gas binding, vapor locking, or cavitation.*

BWRs in the United States use containment pressure suppression (PS) systems to minimize the containment pressure rise following a loss of coolant accident (LOCA). The containment systems include a drywell that contains the reactor vessel and piping, a suppression chamber or wetwell that contains a gas atmosphere and a pool of water to provide the pressure suppression function, and a downcomer vent system that connects the drywell to a submerged position in the wetwell suppression pool. Following a LOCA the drywell atmosphere and the break mass flows through the downcomer vent system and enters the suppression pool. The pool condenses the break steam flow and removes energy from any noncondensable gas (NCG).

This report describes the technical specifics of the GI-193 problem and summarizes the assessment of two analytical approaches, a scaling method and computational fluid dynamics (CFD) analyses, to support the development of the technical basis for developing criteria to perform a plant assessment.

Section 3 lists the facilities used to test BWR pressure suppression systems and summarizes the test data available from these facilities, which are applicable to the GI-193 activity. The primary tests and facilities which provide data specific to the GI-193 activities are the tests performed at Lappeenranta University and Purdue University.

Section 4 of this report describes the acceptable ECCS pump operating range necessary to prevent pump damage if NCG ingestion occurs or to permit recovery from condensable gas ingestion.

Section 5 of this report summarizes the CFD analyses used to define an NCG large bubble "exclusion zone" and to provide the time dependent noncondensable void fraction distribution in the suppression pool outside the large gas bubble following a LOCA.

Section 6 describes a method to perform a plant-specific assessment to determine whether an ECCS pump will operate acceptably following a design-basis accident (DBA) LOCA in a Mark I suppression pool using the analyses results and criteria presented in this report. The assessment approach uses the ECCS pump strainer location, the ECCS pump operation criteria, the ECCS pump startup and full operation timing information, and the pool void fraction information to make the determination.

Post-LOCA Suppression Pool Behavior

Following a LOCA, the downcomer vent flow into the suppression pool can be divided into four different phases: (1) the vent water clearing phase, (2) the large noncondensable gas flow and small noncondensable gas bubble phase, and (3) the steam condensation oscillation and chugging phase.

1.   Vent water clearing—A water column exists in the downcomer vent before the start of a LOCA. As the drywell pressure increases following a LOCA the water column is pushed into the suppression pool because of the increased pressure differential between the drywell and wetwell. The water clearing phase lasts about 0.3 seconds for a double-end DBA LOCA, but can take longer for smaller break sizes.

2.   Noncondensable gas flow and small gas bubble phase—The noncondensable gas flow behavior can be divided into two phases, a large gas bubble phase followed by a longer small gas bubble phase. After the completion of vent water clearing, the NCG-steam mixture in the drywell begins to flow out of the vent and into the suppression pool. The initial flow in this phase contains a significant amount of NCG. This initial large gas "jet" can penetrate a significant depth into the pool as it follows the initial water jet downward. The amount of NCG in the vent flow decreases quickly and reaches very small levels after 2–3 seconds for a DBA LOCA. The size of the initial large NCG "jet" can define an "exclusion zone" volume at the vent exit which possesses a large fraction of noncondensable gas. The ECCS strainer and pump suction should not extend into the "exclusion zone" during ECCS pump operation. After 2–3 seconds the size of the NCG volume decreases as the initial large gas bubble rises and exits the top of the suppression pool. After the large NCG bubble exits, small gas bubbles are still present in the suppression pool water; however the void fraction of this gas is significantly less than the initial large gas "jet". The average suppression pool void fraction is expected to decrease to low levels by about 10 seconds, but much lower levels of noncondensable gas void fractions levels may last in the suppression pool for about 30–40 seconds.

3.   Steam condensation oscillation (CO) and chugging—After the NCG flow reaches very low levels, the bulk of the flow exiting the vent is a steam-water mixture. Initially this flow rate can be significant but will decrease as a function of time following the LOCA. These steam condensation modes, which generally exist at times later than 10 seconds after the LOCA, are not expected to impair ECCS pump operation because the fraction of NCG exiting the vent and entering the suppression pool is small, and because any steam in the suppression pool is expected to condense before entering the ECCS pump inlet.

The determination of vent flow rates into the suppression pool following a LOCA is dependent on the break mass and energy flow and the resultant drywell pressure. This information is analytically provided by a containment analysis computer code. This report concentrates on the post-LOCA predictions for a typical Mark I plant design. A Mark I containment results in the most limiting NCG suppression pool conditions because of its relatively small suppression chamber (wetwell) volume and the small downcomer vent submergence when compared to the larger Mark II and Mark III suppression pool designs (Figure 2.1-2). Additionally, the ECCS pump strainers are generally located closer to the downcomer vent exits in a Mark I design.
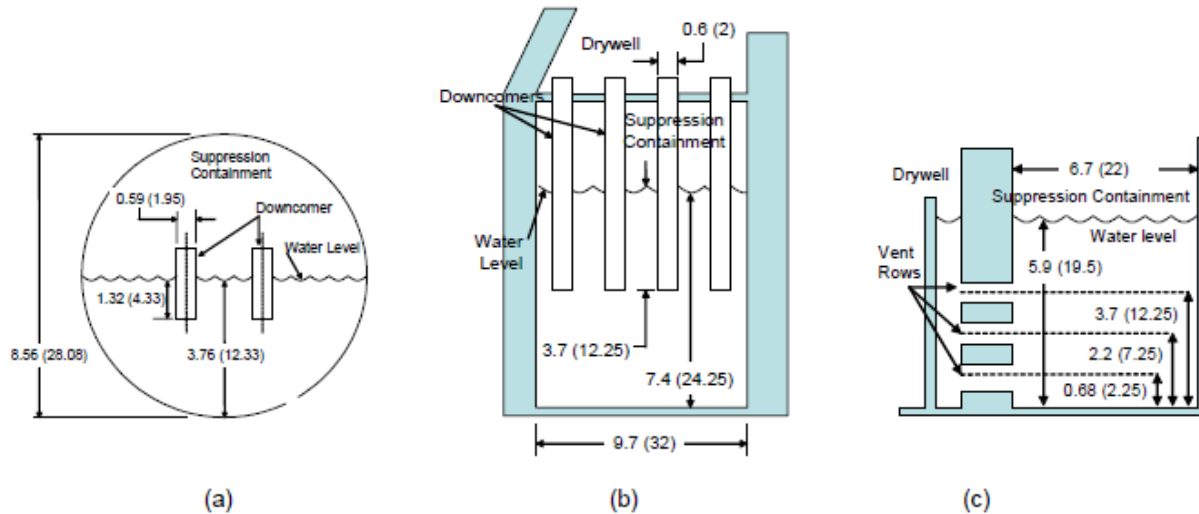
Figure 2.1-2: Cross Section and Dimensions of Typical (a) Mark I, (b) Mark II and (c) Mark III Suppression Chambers (Dimensions in meters (feet))

Considerations for ECCS Pump Operation

ECCS pump operation could primarily be affected if the pump operates within the first 2–3 seconds following a DBA LOCA. Concerns regarding NCG ingestion by the ECCS pumps would be expected to last until the bulk of the noncondensable gas rises and exits the pool surface.

For a DBA LOCA, the ECCS (low-pressure core spray (LPCS) and low-pressure core injection (LPCI)) pump startup signal is typically generated at the high drywell pressure set point. A survey by the BWR Owners Group for Mark I containment designs (Ref. 4) reveals that a high-containment pressure signal can occur as early as 1 second following the start of a DBA large-break LOCA (LBLOCA). An additional 3-to-10 second pump startup delay is to be expected if a loss of offsite power is considered concurrent with the DBA LBLOCA to account for emergency diesel generator startup and ECCS pump initiation sequencing. Therefore, the earliest start time of the ECCS pumps with the availability of offsite power is about 1 second, but is about 4 seconds with an associated loss of offsite power.

During the initial period after receipt of a startup signal the LPCS and LPCI pumps are operated to reach full speed. Additionally, the initial pump flow is recirculated to the suppression pool and is not injected into the core. Regardless of the availability of offsite power, the LPCS and LPCI systems are expected to pump flow into the core at about 40 and 50 seconds after appropriate valve reconfiguration. Consequently, during the first 40 to 50 seconds following a LOCA, when the ECCS pumps circulate flow within the suppression pool, the effects of NCG ingestion do not affect the ability of the ECCS pumps to provide flow to the core. The primary concerns in this early time frame concerns the possibility of incurring pump damage or, if pump damage does not occur, the ability of the ECCS pumps to recover to full operation after possible noncondensable gas ingestion during the early period.

Figure 6.1-1 presents a summary of the NCG behavior in the suppression pool. Information regarding the typical startup and full operation timing of the ECCS pumps of a Mark I containment design following a DBA LOCA is also presented on Figure 6.1-1.
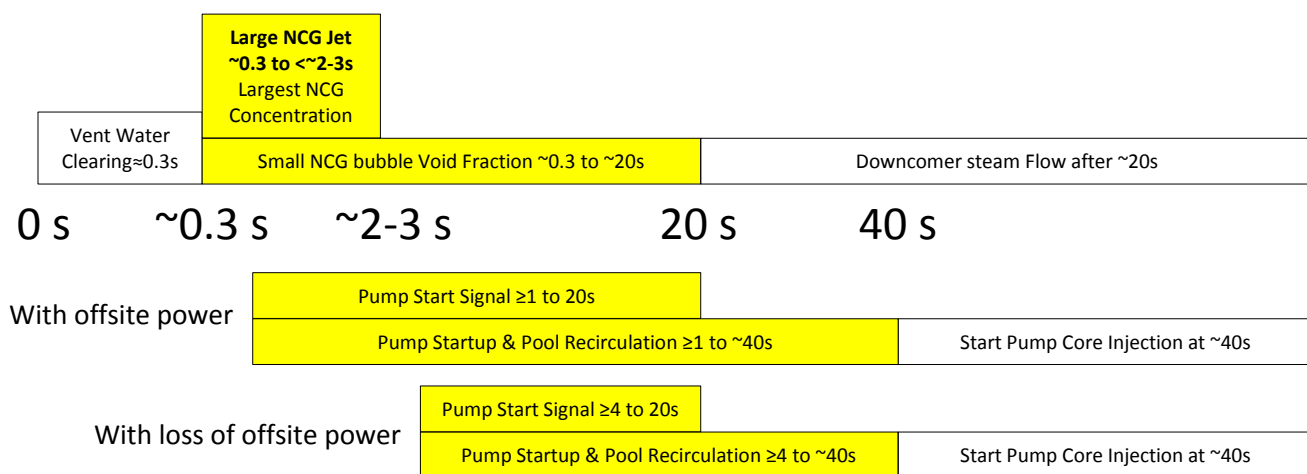
Figure 6.1-1: Downcomer Flow/Suppression Pool Conditions and ECCS Pump Operation Comparisons

Prediction of Post-LOCA Suppression Pool Flow Conditions

Although many of the earlier tests did not provide specific measurements of suppression pool thermal-hydraulic conditions, many of the programs included activities to develop analytical and computer models for the noncondensable gas phenomena in the suppression pool. CFD computer codes have been used to simulate the thermal-hydraulic behavior in the suppression pool following a LOCA. These analytical models and methods must be verified for application to an actual plant geometry. Consequently, the CFD analysis methods were compared to test data from several of the test facilities.

Considering the experience with CFD analyses for analyzing the vent clearing and noncondensable gas portions of the downcomer vent flow into the suppression pool following a LOCA, it is reasonable to assume that a CFD analysis could be used to analyze the initial vent clearing and noncondensable gas flow transient in a full-scale plant geometry. In Section 5, the analysis techniques for a current CFD code were benchmarked against data from two scaled test facilities and qualitatively compared to a video of the Mark II full-scale tests. The CFD techniques were then used to develop models of a full-scale plant geometry and used to simulate the noncondensable gas behavior in a suppression pool. Section 5 of this report describes the CFD analyses used to define a noncondensable gas bubble "exclusion zone" and also provides an estimate of the time dependent noncondensable void fraction distribution in the suppression pool around the vent pipe location following a LOCA.

It should be noted that the CFD models are primarily applicable to the analyses of the vent clearing and noncondensable bubble phase. CFD analysis of the steam bubble CO and chugging phases require modeling of contact condensation at the steam bubble surface. The contact condensation phenomenon is not considered in the current analysis.

Figures 5.2.3-5, 5.2.3-6, 5.2.3-7 and 5.2.3-8 provide a time dependent definition of the "exclusion zone" and the suppression pool void fraction.
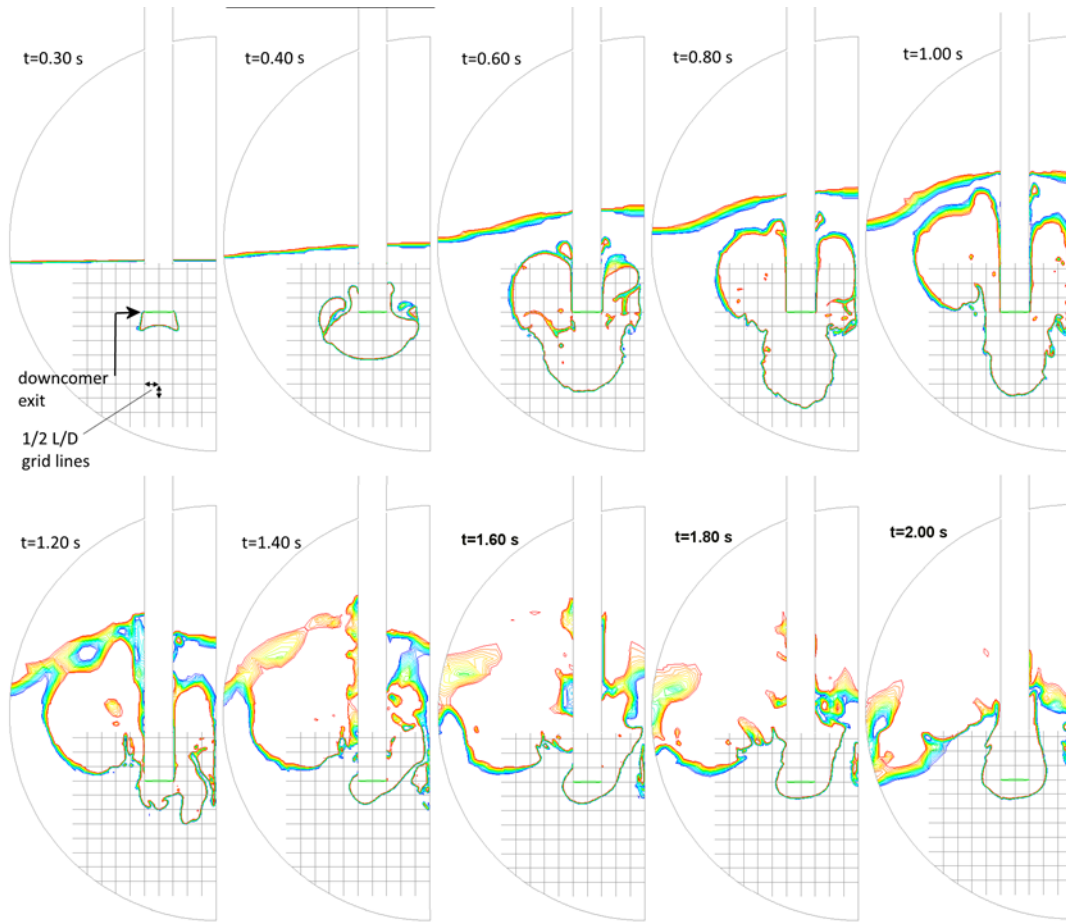
Figure 5.2.3-5: Contour Plots of Time Dependent Bubble Interface (VOF Method)
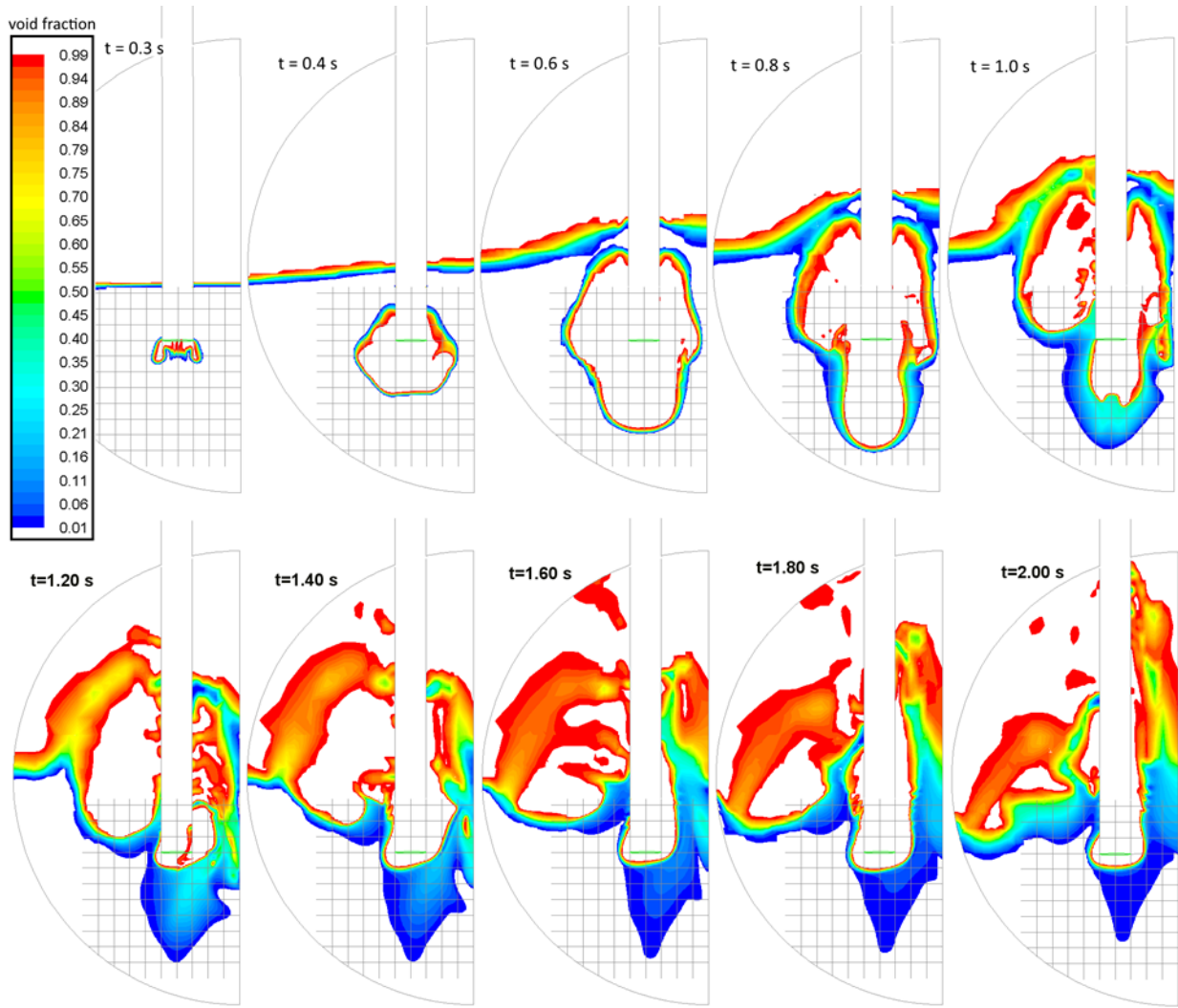
Figure 5.2.3-6: Contour Plots of Time Dependent Void Fraction (Eulerian Method)
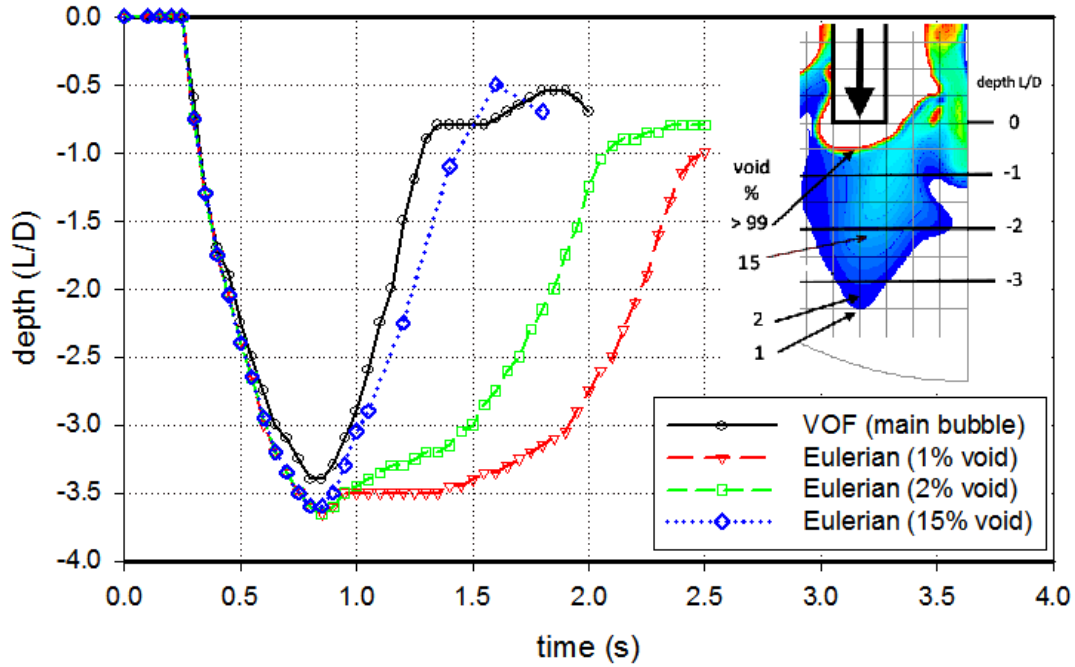
Figure 5.2.3-7: Time Dependent Maximum Penetration Depth
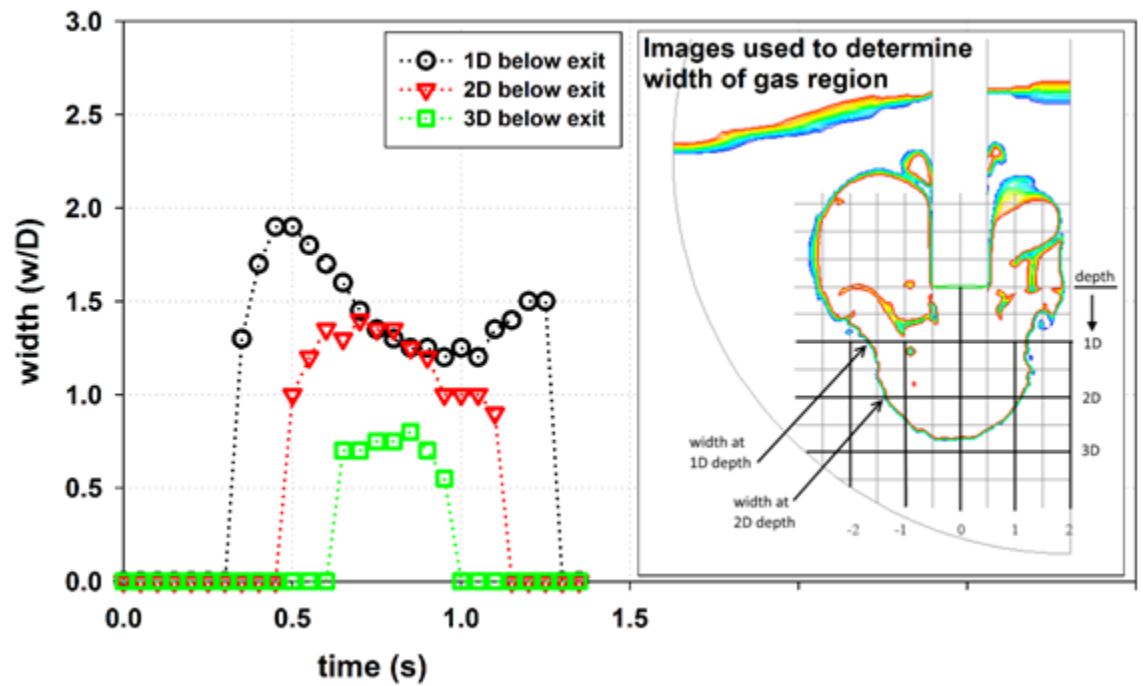
Figure 5.2.3-8: Time Dependent Radial Width of Main Bubble

Section 4 of this report addresses the acceptable operating range of the ECCS pumps to define the operating conditions necessary to prevent pump damage if noncondensable gas ingestion occurs or to determine the ability of the pump to recover from noncondensable gas ingestion.

The pump requires additional time to reach full speed after receipt of the startup signal; however, for conservatism, the pump is assumed to instantaneously reach full speed.

An ECCS pump can sustain damage caused by over speed and vibration if gas is ingested. The acceptable ECCS pump operating range for noncondensable gas inlet void fraction is discussed in Section 4 which also discusses the ability of the ECCS pump to recover after a limited amount of gas is ingested.

The BWR ECCS operational criteria presented in Section 4 is summarized below.

1.   Low transient flow rates (less than 70 percent of the best efficiency point) with an inlet void fraction greater than 5 percent for more than 5 seconds will result in pump damage unless pump specific testing can show otherwise.

2.   Higher transient flow rates (between 70 percent and 120 percent of the best efficiency point) with an inlet void fraction greater than 10 percent for more than 5 seconds will result in pump damage unless pump specific testing can show otherwise.

3.   Low flow operation (less than 40 percent of the best efficiency point) at greater than 1 percent by volume continuous suction noncondensable gas void fraction results in pump damage unless pump specific testing can show otherwise.

4.   Full flow operation (40 percent to 120 percent of the best efficiency point) at greater than 2 percent by volume continuous suction noncondensable gas void fraction results in pump damage unless pump specific testing can show otherwise.

ECCS pumps that operate within the void fraction conditions specified in Table 4.1-1 and within the gas void fractions indicated above in items 1 to 4 can be considered capable of recovery without damage, and will operate at normal pump head and flow conditions if the inlet void fraction is reduced to a value below 1 percent.

An ECCS pump assessment would be permitted to use other operation criteria if pump specific tests are performed to provide better operational guidance.

Assessment Approach for ECCS Pump Operation in BWR Pressure Suppression Containments

Section 6 describes a method to perform a plant-specific assessment to determine whether an ECCS pump will acceptably operate following a DBA LOCA in a Mark I suppression pool using the analyses results and criteria presented in this report. The assessment approach uses the ECCS pump strainer location, the ECCS pump operation criteria, the ECCS pump startup and full operation timing information, and the pool void fraction information to make its determination.

It should be noted that ultimately the plant operators will be responsible for applying the methods and criteria to their specific plant geometry to complete assessment for a particular plant. The assessment of ECCS pump operation following a LOCA would follow the following steps:

1.	Determine the post-LOCA noncondensable gas "exclusion zone" in the suppression pool.

2.	Determine the void fraction in the pool water outside the "exclusion zone".

3.	Determine the location of the ECCS pump strainer in relation to the "exclusion" zone.

4.	Determine the ECCS pump performance if noncondensable gas is present at the pump strainers.

5.	If the assessment determines that the ECCS pump operation would be affected, the plant operator would need to determine a course of action to correct the condition.

After pump startup, the criteria for acceptable pump operation will be determined using the flow logic presented in Figure 6.5-1, which provides a logic stream for this procedure to assess the post-LOCA operation of the ECCS pumps. The procedure proposes that the ECCS pump operation be assessed using the maximum and transient noncondensable gas void fraction at the strainer location using the graphs contained in Figures 5.2.3-5, 5.2.3-6, 5.2.3-7 and 5.2.3-8. Additionally, Section 5.2.3.5 and Figure 5.2.3-9 show that the void fraction at a strainer located below the downcomer exit and outside of the large bubble will be 1 percent or less for times greater than about 2 seconds. This assessment approach is proposed because of the short duration of the large NCG large bubble which is less than 3 seconds. For this assessment it is assumed that the "exclusion zone" for the large NCG bubble is defined by the boundary where the pool void fraction exceeds 10 percent. This assumption is consistent with the ECCS pump acceptable operation criteria listed in Section 6.4.1. Other void fraction criteria are also consistent with the information listed in Section 6.4.2.

The assessment procedure presented in Figure 6.5-1 was developed using information for a Mark I containment. Because of similar vertical downcomer geometry, the results of this study can be conservatively applied to a Mark II containment design, which possesses a larger suppression chamber. A Mark III design includes a horizontal vent pipe orientation and the ECCS pump inlets are located significantly further from the vent exits. Consequently, the ECCS pumps in a Mark III design are expected to be less affected by NCG because lower void fractions are expected at their inlets.

Figure 6.5-1 includes an option to perform ECCS pump specific testing if the application of the flow logic determined that the timing and void fraction criteria results in pump failure including the inability to recover. This testing option would provide the actual operability assessment of a particular ECCS pump.

If an ECCS pump assessment concludes that a pump would fail and not recover, the plant operator must determine what corrective action would be necessary. Four possible corrective actions could be considered:

1.	The ECCS start time could be delayed to ensure that the pump would start after elevated gas void fraction conditions are reduced in the suppression pool at the elevation of the pump strainer and intake.

2.	The location of the ECCS pump strainer and intake could be moved to eliminate or minimize the gas void fraction concern at the pump strainer and intake.

3.   Closing off a specific pump strainer is also an option if other strainer intakes provide sufficient flow into a common header feeding a pump.

4.   As outlined below, the licensee may also choose a more detailed plant-specific analysis that models the strainer and downcomer locations and explicitly calculates the voiding at the ECCS pump inlet.

The method outlined in this report is limited by the assumptions used to develop the criteria. For instance the assumptions regarding the typical ECCS pump start times is based on the survey information present in Reference 4. The analyses used to develop the criteria were developed for a DBA LBLOCA in the suppression pool of a Mark I containment using the information provided in References 2. The DBA LOCA results in the most severe NCG conditions in a suppression pool because it provides the largest and fastest break flowrates that result in the largest gas flow into the suppression pool in the shortest time. Additionally, the ECCS pump strainers are generally located closest to the downcomers in a Mark I design. The pump operation acceptance criteria were obtained from the literature search and testing information described in Sections 3 and 4. The CFD approach used to predict the location and duration of the NCG phase is also limited to the simplified cases considered. Other phenomena, such as suppression pool structures or flow patterns that could further enhance, mix, or distribute the NCG region, should be considered on a case-by-case basis.

For this assessment, ECCS pump performance during operation with void fraction conditions at the pump inlet was considered from a general, not plant-specific perspective. A review of Figure 6.5-1 reveals that an ECCS pump start time greater than about 2–3 seconds may be sufficient to conclude that pump operation is unaffected. This assessment supports the technical conclusion that delayed ECCS pump flow initiation beyond 3 seconds, plus a possible safety factor, following a DBA LOCA initiation will adequately protect the ECCS pumps from damage.

Similarly, consideration of the void fraction at the strainer location may be sufficient to conclude that pump operation is unaffected. This assessment approach assumes that the void fraction at the strainer location is transferred unchanged through the strainer and piping to the pump inlet. This is a conservative assumption with regards to the determination of acceptable pump operation. The assessment includes the option to refine the pump operation assessment by using calculations to determine the void fraction at the pump inlet. Other studies and tests have demonstrated that the void fraction at the strainer location could be substantially different after traveling a distance through a pipe to the pump inlet. Consequently, calculational methods outlined in Reference 44 can be used to estimate the gas transport in the pipe from the strainer to the pump inlet in order to determine the actual void fraction at the pump inlet. Additionally, a defensible method would need to be developed to calculate the transport of noncondensable gas from the large bubble or small bubbles in the suppression pool, through the strainer and into the pipe downstream of the strainer. Of course, the method used to perform this calculation (e.g. a thermal-hydraulic computer code) must be verified against applicable test data before it could be used in this application.

Another approach to determine the void fraction at the pump inlet would be to include the strainer inlet and piping leading to the ECCS pump in the full CFD model used to predict the noncondensable gas bubble behavior. This model would include details of the pump strainer and piping along with the time dependent pump suction flow at the end of the piping. This approach would not only estimate the void fraction in the piping approaching the pump inlet, but would also predict the interactions between the size and location of the noncondensable gas bubble and the calculated suppression pool flow field and void fraction distribution that includes

the effect of the pump suction. Of course, the CFD method used to perform this calculation should be benchmarked against applicable test data before it is used in this application.

Determine pump start time

Is pump start time
≥ 3 s? — Yes → Acceptable pump operation

No

Determine time dependent void fraction (α) at strainer location

Is strainer location
α > 10% for > 5 s? — No → Is strainer location
α ≤ 1%? — Yes → Acceptable pump operation

Yes

No

Is strainer location
α ≤ 5% for ≤ 5 s — Yes → Acceptable pump operation

No

Determine time (t_α) when α ≤ 5%

Is pump start time
≥ t_α — Yes → Acceptable pump operation

No

Perform pump specific testing? AND/OR
Perform detailed plant specific analysis to determine pump
inlet void fraction? — No → Assume pump failure.
Move strainer, block strainer or adjust start time

Yes

Will pump fail? — No → Acceptable pump operation

Yes

Can pump recover? — Yes →

No

Pump failure
Move strainer, block strainer or adjust start time

Figure 6.5-1: Approach for Assessing Effects of Noncondensable Gas on ECCS Pump Operation

ACRONYMS AND ABBREVIATIONS

BEP   best efficiency point
BWR   boiling water reactor
CFD   computational fluid dynamics
CO   condensation oscillation
CS   containment spray
DBA   design-basis accident
DW   drywell
ECCS   emergency core cooling system
GE   General Electric
GI   generic safety issue
ID   internal diameter
LLL   Lawrence Livermore Laboratory
LOCA   loss-of-coolant accident
LPCI   low-pressure core injection
LPCS   low-pressure core spray
MIT   Massachusetts Institute of Technology
NCG   noncondensable gas
NOG   Nordic Owners Group
NPP   nuclear power plant
NPSH   net positive suction head
NPSHR   net positive suction head required
NRC   U.S. Nuclear Regulatory Commission
PS   pressure suppression
PSI   Paul Scherrer Institute
PUMA   Purdue University Multi-Dimensional Integral Test Assembly
PWR   pressurized water reactor
RHR   residual heat removal
SRV   safety relief valve
VOF   volume of fluid
WW   wetwell

1.   INTRODUCTION

This report summarizes the work and recommendations developed to support the technical basis for resolving U.S. Nuclear Regulatory Commission (NRC) Generic Safety Issue (GI) 193, "Boiling Water Reactor (BWR) Emergency Core Cooling System (ECCS) Suction Concerns." The following text from Reference 1 states the safety concerns related to this activity:

> *GSI-193 addresses the possible failure of the ECCS pumps due to unanticipated, large quantities of entrained gas in the suction piping from BWR suppression pools. The issue applies to Mark I, II, and III containments during large- and medium-break LOCAs, and could potentially cause pump failure or degraded performance due to gas binding, vapor locking, or cavitation.*

Section 2 describes the analytical methods used to calculate post loss-of-coolant accident (LOCA) BWR pressure suppression containment conditions including suppression pool behavior.

Section 3 lists the test facilities used to test BWR pressure suppression systems and summarizes the test data available from these facilities, which are applicable to the GI-193 activity.

Section 4 of this report describes the acceptable ECCS pump operating range necessary to prevent pump damage if noncondensable gas ingestion occurs or to permit recovery from noncondensable gas ingestion. Information regarding the typical startup and full operation timing of the ECCS pumps of a Mark I containment design following a design-basis accident (DBA) LOCA is also presented.

Section 5 of this report uses analyses to define a noncondensable gas bubble "exclusion zone" and also provides the time-dependent noncondensable void fraction distribution in the suppression pool outside the large gas bubble following a LOCA.

Section 6 describes a method to perform a plant-specific assessment to determine whether an ECCS pump will operate acceptably following a DBA LOCA in a Mark I suppression pool using the analyses results and criteria presented in this report. The assessment approach uses the ECCS pump strainer location, the ECCS pump operation criteria, the ECCS pump startup and full operation timing information, and the pool void fraction information to make its determination.

2. BWR POST-LOCA CONTAINMENT ANALYSIS AND SUPPRESSION POOL BEHAVIOR

Boiling water reactors (BWRs) in the United States use containment pressure suppression systems to minimize the containment pressure rise following a loss-of-coolant accident (LOCA). The containment systems include a drywell that contains the reactor vessel and piping, a suppression chamber or wetwell that contains a gas atmosphere and a pool of water to provide the pressure suppression function, and a downcomer vent system that connects the drywell to a submerged position in the wetwell suppression pool. Following a LOCA, the drywell atmosphere and break mass flow through the downcomer vent system and enter the suppression pool. The pool condenses the break steam flow and removes energy from any noncondensable gas (NCG).

2.1 Containment Analysis

The determination of vent flow into the suppression pool following a LOCA is dependent on the break mass and energy flow and the resulting drywell pressure. This information is analytically provided by a containment analysis computer code. Reference 2 describes the containment analyses and provides the predictions for typical Mark I, Mark II, and Mark III (Figure 2.1-1) containments following a DBA LOCA. The DBA LOCA for a BWR pressure suppression (PS) system is typically a double-end rupture of a main steam line or a recirculation line. The following sections concentrate on the post-LOCA predictions for a typical Mark I plant design. This design is considered the most limiting for GI-193 concerns because it contains a relatively small suppression chamber (wetwell) volume and small downcomer vent submergence when compared to Mark II and III containment designs (Figure 2.1-2). The Mark I designs can also possess ECCS pump inlet strainer locations closer to the discharge end of the downcomer vent (Figure 2.1-3). Because of similar vertical downcomer geometry, the results of this study can be conservatively applied to a Mark II containment design, which possess a larger suppression chamber. A Mark III design includes a horizontal vent pipe orientation and the ECCS pump inlets are located significantly further from the vent exits. Consequently, the ECCS pumps in a Mark III design are expected to be less affected by NCG because lower void fractions are expected at their inlets.

MARK I   MARK II   MARK III
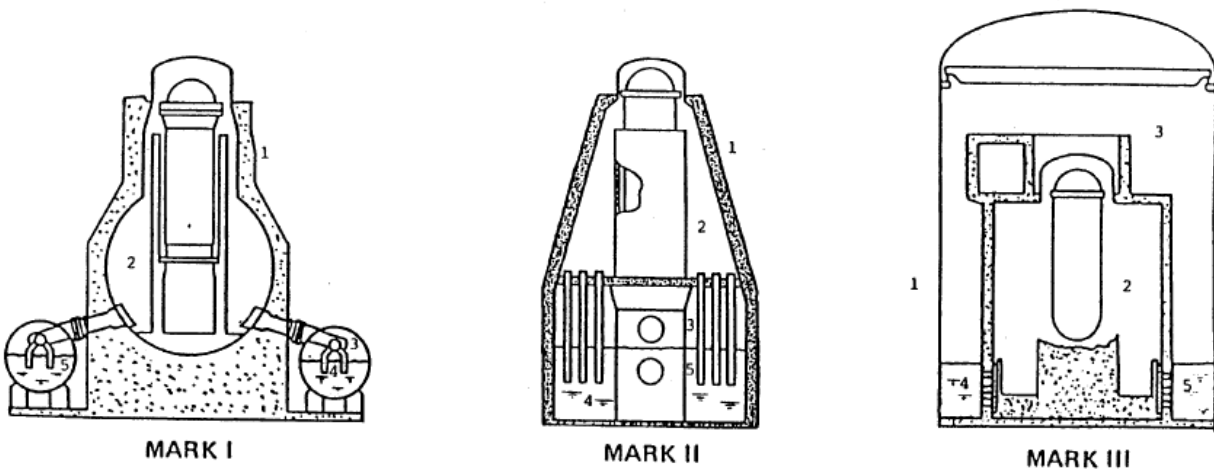
**Figure 2.1-1: BWR Pressure Suppression System Designs
(1-Primary Containment, 2-Drywell, 3-Wetwell, 4-Suppression Pool, 5-Vent System)**
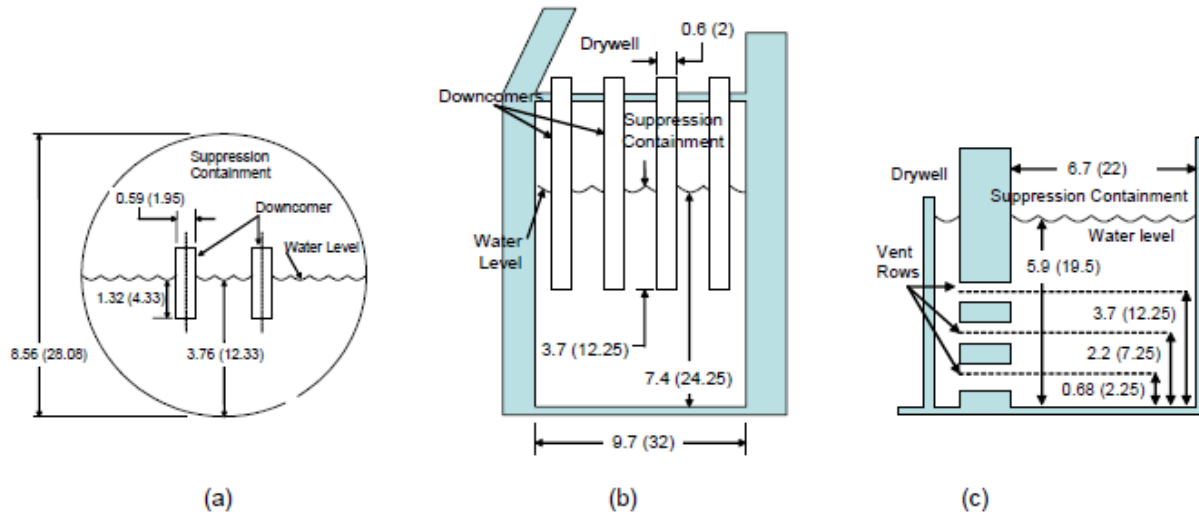
Figure 2.1-2: Cross Section and Dimensions of Typical (a) Mark I, (b) Mark II and (c) Mark III Suppression Chambers (Dimensions in meter (foot))
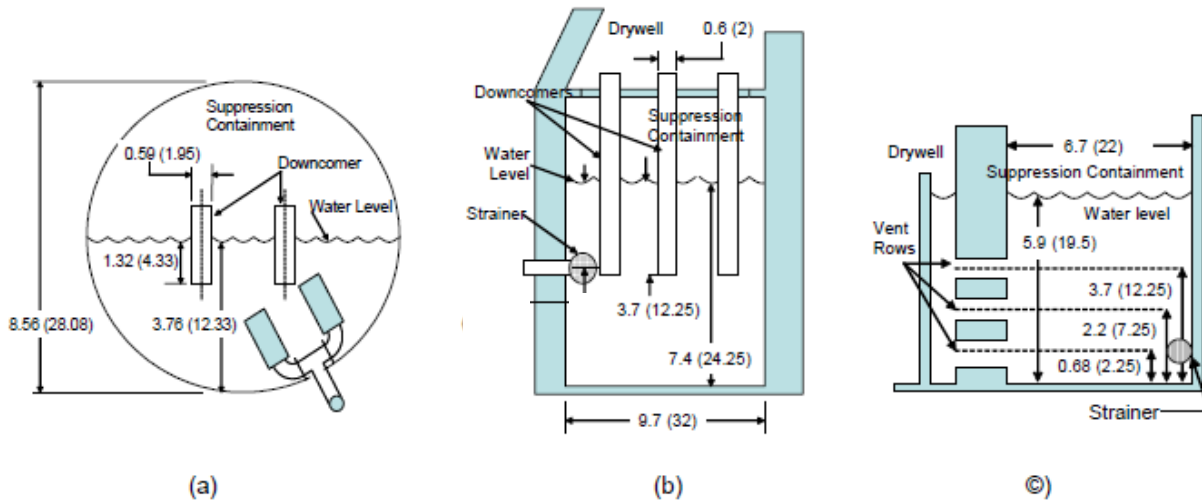
Figure 2.1-3: Typical ECCS Pump Strainer Locations in (a) Mark I, (b) Mark II and (c) Mark III Suppression Chambers (Dimensions in meter (foot))

The DBA LOCA is considered the most severe for assessing the effects of possible NCG flow on the ECCS pump operation because a large double-ended DBA LOCA produces the largest drywell pressure rise rates and the highest containment pressures resulting in the largest vent flow rate into the suppression pool. The larger vent flow produces a larger NCG vent "jet" than a smaller break. The larger gas "jet" defines the suppression pool "exclusion zone," which can possess a large NCG mass. Typically, ECCS pump suctions should not be located in or near the "exclusion zone" to ensure successful pump operation.

As shown on Table 2.1-1, the downcomer flow following the initial clearing of the submerged water volume in the downcomer pipe can be divided into four phases: (1) a phase when the water contained in the submerged downcomer pipe is cleared, (2) a large NCG bubble or "jet" phase, (3) a small NCG bubble phase, and (4) an all steam flow phase. Table 2.1-1 indicates that the largest break DBA LOCA produces the largest NCG volume in the suppression pool. Consequently, the DBA LOCA is assessed in this study.

Table 2.1-1: Post-LOCA Downcomer Flow Phases after Vent Water Clearing

Downcomer Flow Phase	Largest Break DBA LOCA	Medium Break	Small Break
Phase 1: Clearing of submerged vent water	• Fastest water clearing	• Slower water clearing	• Slowest water clearing
Phase 2: Large NCG Bubble	• Largest NCG bubble • Largest bubble penetration • Smallest large bubble duration	• Smaller NCG bubble • Smaller bubble penetration • Longer large bubble duration	• Smallest or negligible large NCG bubble • Smallest bubble penetration
Phase 3: Small NCG Bubbles	• Smallest small NCG bubble duration • Largest small NCG bubble penetration	• Longer small NCG bubble duration • Smaller small NCG bubble penetration	• Longest small NCG bubble duration • Smallest small NCG bubble penetration
Phase 4: All steam flow	• Localized condensation oscillation or chugging	• Localized condensation oscillation or chugging	• Localized condensation oscillation or chugging

2.1.1   Vent Discharge Flow

Figures 2.1-4 and 2.1-5 show typical Mark I pressure and temperature response plots following a DBA double-ended recirculation line break, which is the DBA LOCA presented in Reference 2. The plots indicate the similarity of calculated results using either the MELCOR or CONTAIN computer codes.
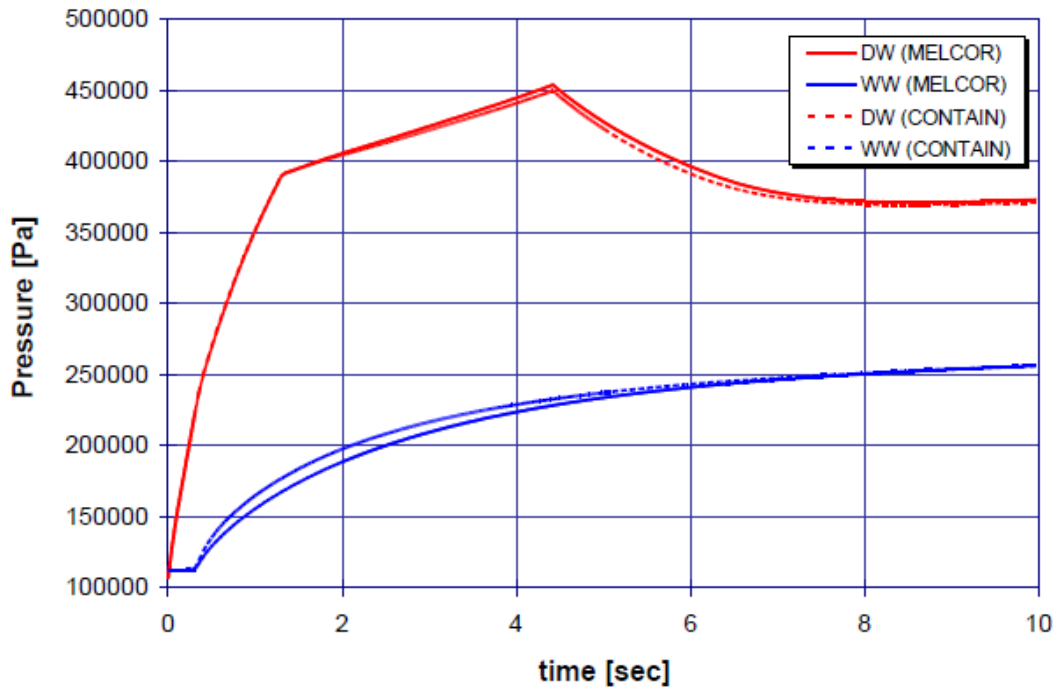
Figure 2.1-4: Predictions of Mark I Containment Drywell (DW) and Wetwell (WW) Pressures following a DBA LOCA
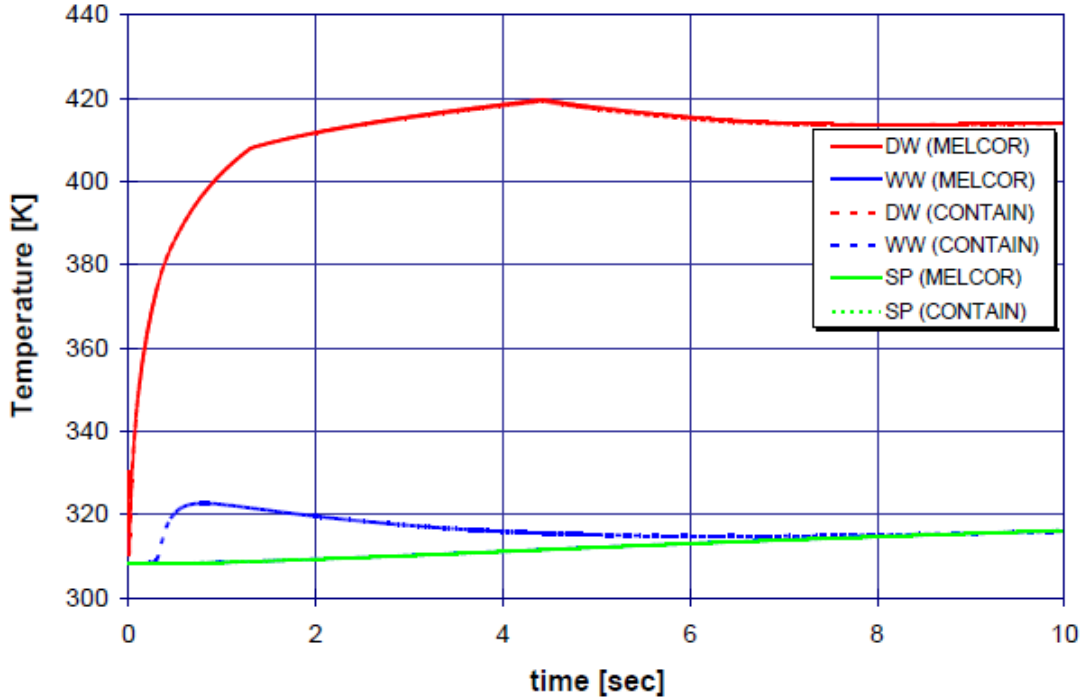
Figure 2.1-5: Predictions of Mark I Containment Drywell (DW), Wetwell (WW) and Suppression Pool (SP) Temperatures following a DBA LOCA

6

The vent discharge flow rate and the resultant discharge "jet" are important considerations in the determination of the "exclusion zone" and successful post-LOCA operation of the ECCS pumps. Reference 2 describes the calculation of the downcomer vent flow from the drywell to the wetwell suppression pool following a Mark I DBA LOCA using the MELCOR computer code. Figure 2.1-6 shows steam, water droplet, and NCG flows at the entrance to the vent system between the drywell and wetwell. Figure 2.1-7 shows the downcomer vent system exit flow rates for liquid, steam, water drops, and a nitrogen-oxygen gas mixture, which typifies the NCG, between the drywell and suppression pool. Figure 2.1-8 plots the time-dependent noncondensable mass fraction at the downcomer exit. The total downcomer NCG flow is limited by the total mass of noncondensables initially present in the drywell. The LOCA is assumed to occur at 0 seconds. The initial clearing of the downcomer water column is predicted to occur by 0.3 seconds following the start of the LOCA after which the steam, water droplet, and NCG flow begins to exit the downcomers. These figures show that the NCG flow peaks before 1 second and reaches very small values before 10 seconds. Consequently consideration of NCG effects on ECCS pump operation is not considered to be a significant concern after the first few seconds following the LOCA because the large NCG volume "exclusion zone" at the vent exit will dissipate within 10 seconds. Based on analyses presented in Section 5.2, concerns regarding NCG ingestion by the ECCS pumps are expected to be largest during the first 2 seconds and drop significantly after that time because the major portion of NCG rises and exits the pool surface. The average suppression pool void fraction is expected to significantly decrease within 10 seconds. However, much lower levels of NCG void fractions may remain in the suppression pool for about 30–40 seconds.
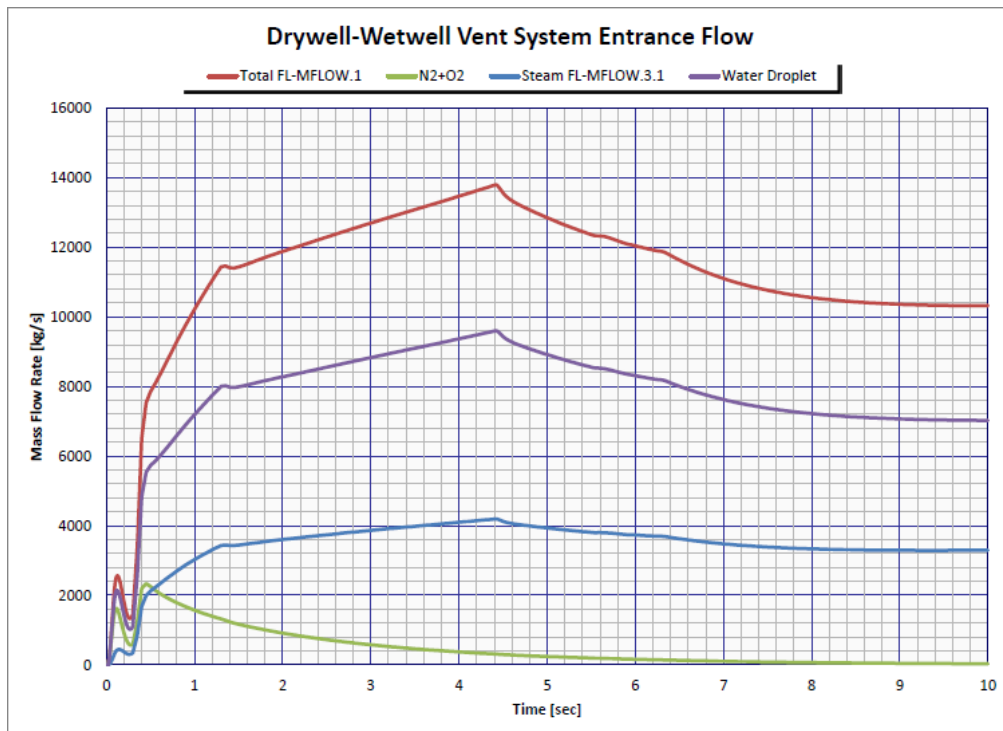
Figure 2.1-6: MELCOR Predictions of Mark I Post-DBA LOCA Constituents of Vent System Entrance Flow
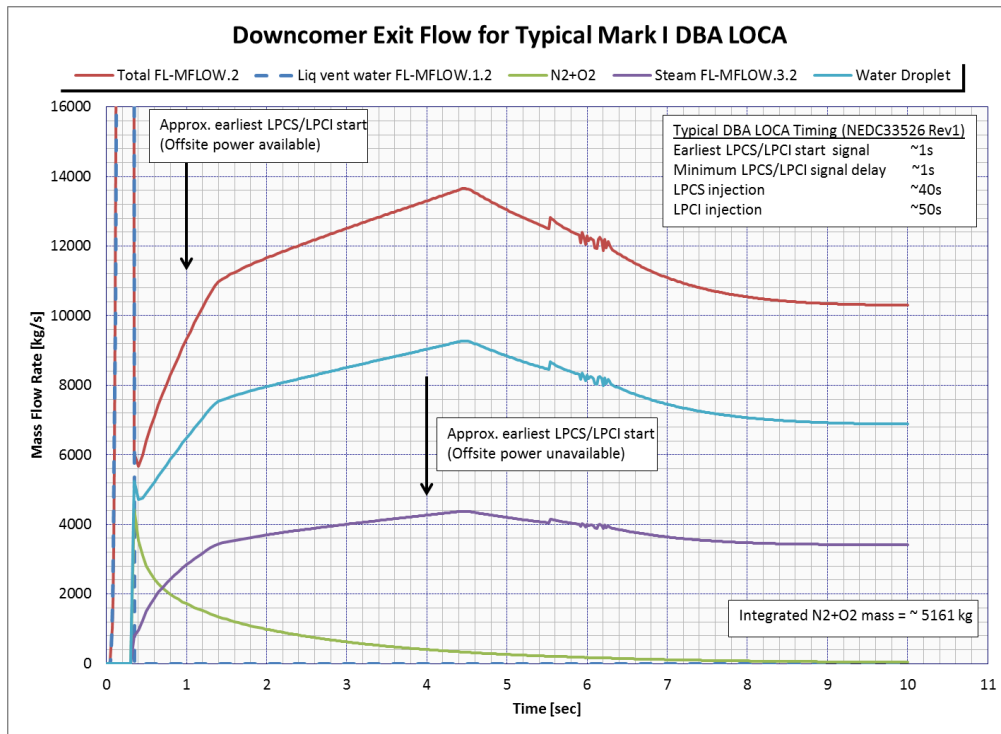
Figure 2.1-7: MELCOR Predictions of Mark I Post-DBA LOCA Constituents of Downcomer Exit Flow
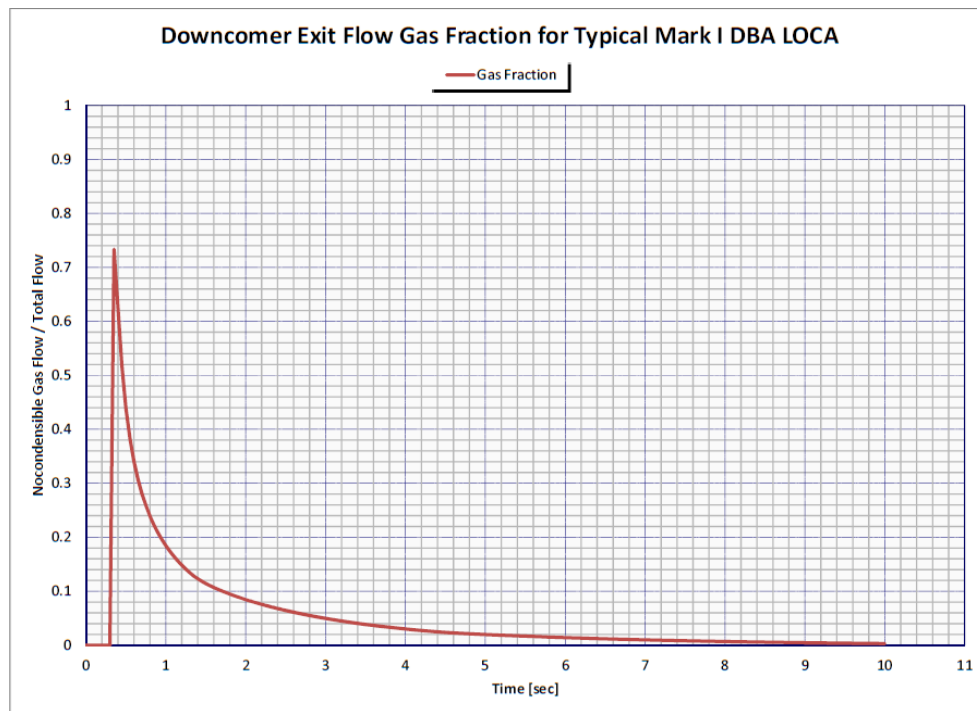
Figure 2.1-8: MELCOR Predictions of Mark I Post-DBA LOCA Noncondensable Gas Mass Fraction of Downcomer Exit Flow

2.2   Post-LOCA Suppression Pool Behavior

As indicated in Figure 2.1-7, suppression pool behavior due to vent flow following a LOCA can be divided into phases: (1) the vent water clearing phase, the large NCG flow and small bubble phases, and (2) the steam condensation oscillation and chugging phase. The following sections describe the suppression pool phenomena occurring in each phase and identify the phase that presents the major concern for NCG ingestion into the ECCS pump suction.

2.2.1   Downcomer Vent Water Clearing

A water column exists in the downcomer vent before the start of a LOCA. As the drywell pressure increases following a LOCA the water column is pushed into the suppression pool because of the increased pressure differential between the drywell and wetwell. The water clearing phase lasts about 0.3 seconds for a double-ended DBA LOCA, but can take longer for smaller break sizes. The vent clearing phenomenon can produce significant turbulence in the suppression pool and pressure loads on the walls of the suppression pool and on submerged structures.

2.2.2   Noncondensable Gas Flow and Bubble Behavior

NCG flow behavior can be divided into two phases, a large gas bubble phase followed by a longer small gas bubble phase. Following the completion of vent water clearing, the NCG-steam mixture in the drywell begins to flow out of the vent and into the suppression pool. As shown on Figure 2.1-7, the initial flow in this phase contains a significant amount of NCG. However, as previously indicated, the amount of NCG in the vent flow decreases quickly and reaches very small levels before 10 seconds for a DBA LOCA. The initial large NCG "jet" can possess a length extending to the bottom of the pool with a radially expanding and oscillating surface. The initial gas discharge produces large and small bubbles which causes a swelling of the suppression pool surface. As discussed in Reference 3, the gas bubble can undergo expansion-contraction oscillations that have been shown to follow a Rayleigh bubble oscillation behavior (Figure 2.2-1). The pool swell and bubble oscillation can create loadings on the suppression pool walls and on submerged structures. The size of the initial NCG "jet" can be used to define a volume at the vent exit, which possesses a large fraction of NCG. This volume can be used to define an "exclusion zone" in which an ECCS strainer and pump suction should not extend during ECCS pump operation. However, it should be noted that the size of the NCG volume will decrease as the gas flow decreases, and as the gas rises and exits the top of the suppression pool.
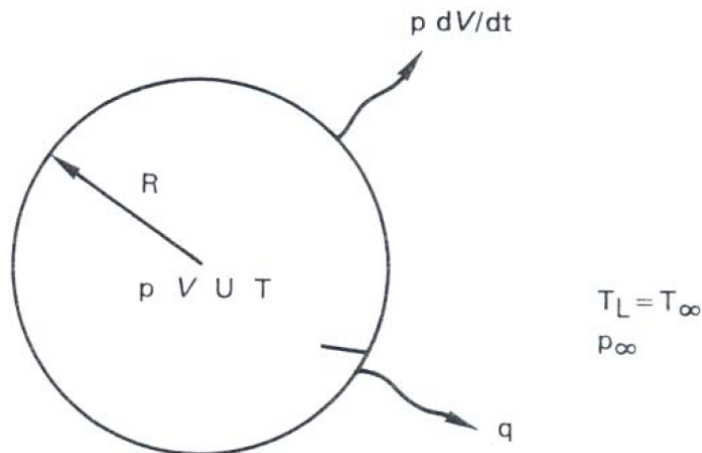
Figure 2.2-1: Raleigh Gas Bubble Oscillation in Liquid (Ref. 3)

2.2.3   Condensation Oscillation and Chugging

As shown in Figure 2.1-7, the NCG flow increases quickly after vent clearing and subsequently decreases reaching very small levels well before 10 seconds following a DBA LOCA. After vent clearing the vapor-liquid vent flow increases and peaks before 5 seconds following the DBA LOCA and subsequently decreases. Consequently, the vent flow between 0.3 and 10 seconds consists of a decreasing amount of noncondensable gas with an increasing amount of vapor and liquid. The steam condensation mode, which generally exists at later times following a DBA LOCA when the vent flow is primarily steam-liquid flow, is not expected to impair ECCS pump operation because the fraction of NCG exiting the vent and entering the suppression pool is small and because any steam in the suppression pool is expected to condense before entering the ECCS pump inlet.

After the NCG flow reaches very low levels, the bulk of the flow exiting the vent is a steam-water mixture. Initially this flow rate can be significant but will decrease as the vent flow decreases following the LOCA. Figure 2.2-2 shows the condensation modes that have been observed during a LOCA discharge. High steam flow results in steady condensation. Decreasing steam flow can produce oscillating bubbles at the vent exit resulting from steam condensation at the bubble surface. This phenomenon is called condensation oscillation (CO) (Figure 2.2-3). At even lower steam flow conditions, the exiting steam flow can create a bubble which rapidly, fully condenses or collapses at the vent exit causing backflow of water into the vent pipe. This condition can occur in a cyclical fashion consisting of steam bubble formation and full collapse. This phenomenon is called chugging. Figure 2.2-4 presents a typical flow map showing the conditions which support chugging conditions. The CO and chugging phenomena are the dominant condensation modes that can cause loadings on the suppression pool walls and on submerged structures.
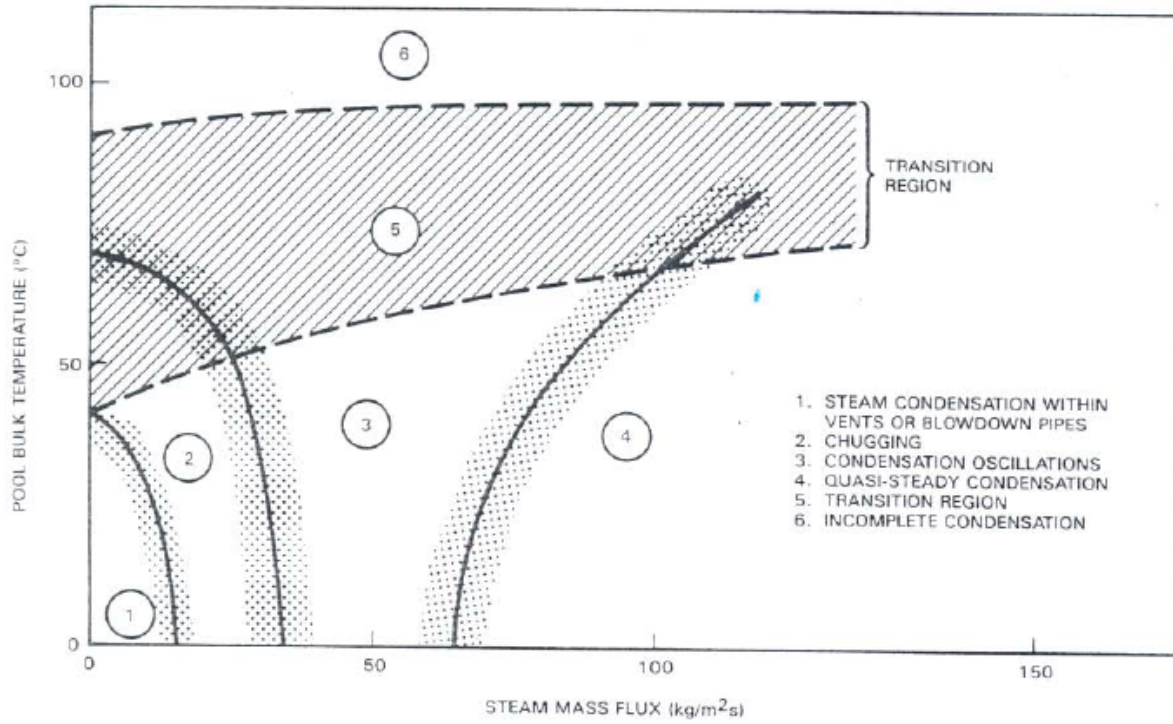
Figure 2.2-2: Schematic of Typical Condensation Mode Regions during LOCA Blowdown (Ref. 3)
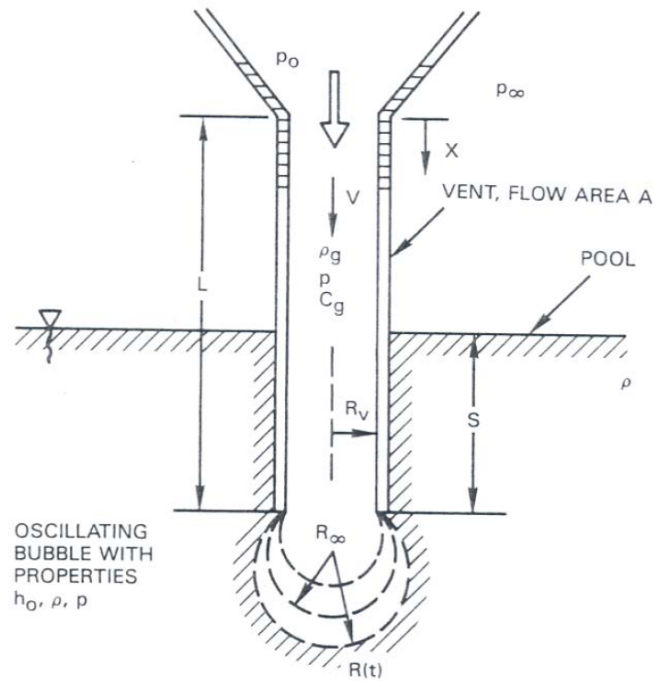
Figure 2.2-3: Steam Condensation Oscillation at Vent Exit (Ref. 3)
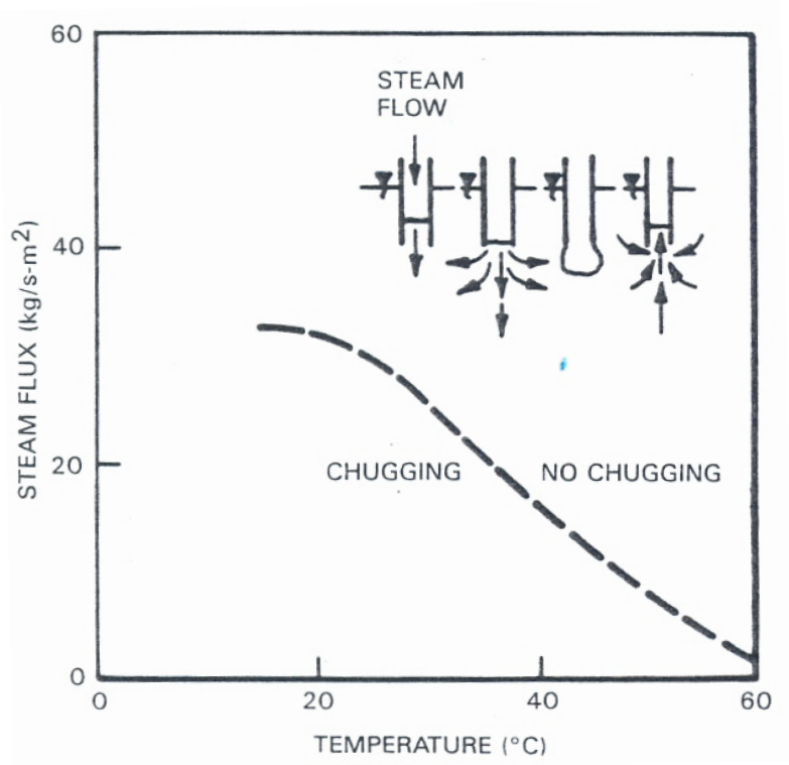
Figure 2.2-4: Sampling Chugging Map for Vertical Vents (Ref. 3)

3. LITERATURE SURVEY

This section lists the facilities used for testing BWR pressure suppression systems and summarizes the test results applicable to addressing the GI-193 issue. A summary of the analytical techniques used to predict the post-LOCA suppression pool conditions is also presented.

3.1 Pressure Suppression Experimental Facilities and Test Data

Since the late 1970s, numerous test facilities have been used to provide test data for the behavior of a pressure suppression system. However, the primary objective of many of these test facilities was to assess the pressure loadings on the walls of the suppression pool and not to provide information regarding the thermal-hydraulic conditions in the suppression pool. A listing of the pressure suppression tests and facilities, and the associated reference documents are provided in Table 3.1-1. This table also identifies the main purpose of the test facility and lists associated analytical efforts to model pool behavior following air injection through a vent pipe.

The primary tests and facilities that provide data specific to GI-193 activities are those tests performed at Lappeenranta University and Purdue University. Because both these tests use scaled facilities, it is necessary to develop an approach to apply the scaled test results to a plant geometry.

3.1.1 General Electric Pressure Suppression Testing

General Electric (GE) performed many full-scale tests and tests scaled to the wetwells and suppression pools of Mark I, Mark II, and Mark III containments in the late 1970s and early 1980s. The suppression pool testing modeled the post-LOCA vent flow entering the suppression pool and discharge flow entering the suppression pool from safety relief valve (SRV) operation. The primary purpose of these tests was to assess loadings on the suppression pool walls and submerged structures following a LOCA or SRV actuation. The test data was used to develop and verify calculational methods to determine the wall and structure loadings, and to support design modifications as required.

The GE tests did not specifically measure the thermal-hydraulic conditions in the suppression pool following a LOCA or SRV actuation. However some thermal-hydraulic models of the vent discharge phenomena were developed as part of the efforts to determine wall and structure loads. For example efforts related to the GE testing developed models to calculate NCG bubble oscillations at the vent exit using Rayleigh bubble theory. Thermal-hydraulic models of the CO and chugging phenomena were also developed.

Videos were taken during performance of the GE Mark I and Mark II pressure suppression tests. The Mark I and Mark II test videos primarily recorded the chugging phenomena in the suppression pool. Thermal-hydraulic measurements were not taken in the suppression pool during these tests. Visual examination of the video cannot support or dispel with certainty the presence of an ECCS pump safety concern which confirms the need for additional information to reach a definitive conclusion on the existence of a safety concern.

13

3.1.2   NRC 1/5 Scale Mark I Pressure Suppression Testing

The NRC-scaled Mark I pressure suppression tests were performed in the early 1980s to support efforts to verify the findings from the GE pressure suppression tests and to support rulemaking activities. Testing was performed using a one-fifth scaled test facility built at Lawrence Livermore Laboratory (LLL) which modeled a section of a Mark I containment. As with the GE tests the primary purpose of these tests was to assess the loads on the suppression pool walls and submerged structures resulting from a LOCA.

No specific measurements of suppression pool thermal-hydraulic conditions were made. However, efforts were made as part of this program to develop models for the NCG and steam blowdown phenomena in the suppression pool. Computational fluid dynamics (CFD) computer codes were developed to simulate the thermal-hydraulic behavior in the suppression pool. Analysis results using the PELE-IC CFD computer code were compared to test data from the MIT air blowdown experiments and from the air bubble data from the LLL one-fifth scale tests. Analyses of the LLL air bubble tests were also performed using the MAITAI CFD computer code. Ultimately the CHAMP computer code was developed to specifically analyze the air discharge experiments at the LLL one-fifth scale Mark I test facility.

3.1.3   Massachusetts Institute of Technology Mark I Gas Blowdown Tests

In the late 1970s, the NRC sponsored air blowdown testing in a scaled Mark I suppression pool test facility at the Massachusetts Institute of Technology (MIT). Air was injected through a submerged vertical 25.4 mm (1 in.) pipe into a pool of water. As with the GE and NRC tests the primary objective of the MIT tests was to support development of loading models for the suppression pool wall and submerged structures. However efforts were made to model the pool swell dynamics and perform computer simulations of the NCG and steam blowdown into the suppression pool.

3.1.4   University of California Mark I Scaled Suppression Pool Tests

The University of California small-scale testing of a Mark I suppression pool was performed in the early 1980s. The experiments injected air through submerged vertical tubes varying in diameter from 0.9 to 9.5 cm (0.35 to 3.7 in.) in a pool of water. A hydrodynamic model of the liquid vent clearing and the bubble phenomenon at the vent pipe exit was developed using the test data. The air bubble oscillation model was based on the Rayleigh bubble equation.

3.1.5   Lappeenranta University Scaled Suppression Pool Experiments

Lappeenranta University in Finland performed experiments starting about 2002 to support the understanding of noncondensable gas and steam blowdown in a scaled suppression pool test facility. These experiments were performed to support efforts related to Scandinavian BWR pressure suppression containment design behavior. Tests were performed at three different test facilities.

3.1.5.1 Condensation Pool Experiments with Noncondensable Gas

The initial condensation pool experiments investigated the formation, size, and distribution of NCG bubble in a suppression pool following a postulated LOCA. The tests were generally

scaled to Olkiluoto nuclear power plant (NPP) conditions. The Olkiluoto NPP, Units 1 and 2 pressure suppression containments (Figure 3.1-1) are ASES-Atom-type BWR containment designs which are similar in design to a Mark II containment. The effects of NCG on the performance of an ECCS pump were also examined. In some of the tests, compressed air flowed through the vent pipes into the water pool in which an ECCS strainer was located. Tests were performed using downcomer vents with inner diameters of 162.3 mm (6.39 in.) and 213.1 mm (8.39 in.). In other tests compressed air was injected directly into the intake of the operating ECCS pumps to determine the effect that NCG ingestion would have on ECCS pump behavior.
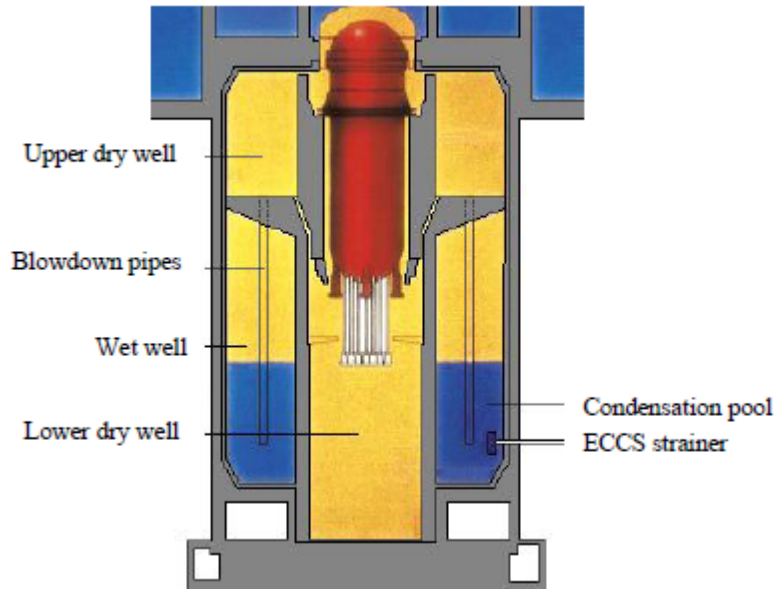
Figure 3.1-1: Schematic of the Olkiluoto Type BWR Pressure Suppression Containment (Ref. 31)

The initial air flow hit the bottom of the pool during the tests using the 162.3 mm (6.39 in.) and 213.1 mm (8.39 in.) downcomer pipes when the vent pipe was initially filled with water. The vent pipe outlets were submerged approximately 2.2 m (7.2 ft) during these tests. Because of the air impact, small air bubbles rose from the pool bottom. Pool swell was observed during which the rising air lifted a large amount of water up to the surface which was splashing strongly. Water carrying a lot of small bubbles was observed to circulate back down close to the pool wall.

Tests using the 162.3 mm (6.4 in.) downcomer pipes were run with an ECCS strainer placed in the suppression pool. The vent pipe outlets were submerged approximately 2.2 m (7.2 ft) during these tests. The top of the strainer was located 495 mm (1.6 ft) above the vent pipe exit to 505 mm (1.66 ft) below the pipe exit. During the tests when the vent pipe was initially filled with water, the initial air flow hit the bottom of the pool and contacted the ECCS pump strainer. Some of the large air bubbles, which appeared after the time of the initial gas "jet" bubbles, were also observed to reach the pump strainer. The air bubbles remained at the level of and inside the pump strainer for the first 30 seconds because backflow circulation in the pool carried small air bubbles from the upper part of the pool to the lower part.

Integral tests were performed with a pump strainer located in the pool and an operating ECCS pump. For these tests air was injected into the pool through the downcomer vents. These tests used the 162.3 mm (6.39 in.) downcomer pipes. The vent pipe outlets were submerged approximately 2.2 m (7.2 ft) during these tests. For some tests, air was sucked through the strainer into the pump at a constant flow rate when air was blown into the pool through the vent pipes. With a volumetric flow rate of 5.5 liter/second (87.2 gpm), air bubbles were not detected inside the transparent intake pipe. With a volumetric flow rate of 11 l/s (174 gpm) air bubbles were visible in the intake pipe for the first 20 seconds when air was blown through two vent pipes. The ECCS pump head and water was not observed to decline during this period.

In the pump tests, the ECCS pump was operating at a nominal speed of 2970 rpm with four different volumetric flow rates when pressurized air was injected directly into the pump intake pipe. With volumetric flow rates of 57 and 75 l/s (903 and 1,189 gpm) a 3- to 4-percent air fraction was needed before a decline in pump head and flow was observed. With smaller flows of 12.5 and 25 l/s (198 and 396 gpm) the pump head and flow started to decline after air injection was initiated and the flow totally collapsed when more than a 7-percent air fraction was present in the intake pipe. When the air injection was stopped for the 12.5 l/s case, the pump head and flow reached original values 30 seconds after the air injections was turned off. At all other flows the pump head and flow normalized in a few seconds after the air injection was turned off.

A supplemental series of tests were also performed using the 162.3 mm (6.39 in.) downcomer pipes to study the effects of velocity on the penetration of the air "jet" from the vent pipe and to study the circulation of the small air bubbles from the pool surface to the level of the ECCS pump strainer. The vent pipe outlets were submerged approximately 2.2 m (7.2 ft) during these tests. Compressed air was blown through the vent pipes during this test and the ECCS pump was operating at a constant volumetric flow rate of 11 l/s (174 gpm). A throttle valve was used to control the maximum air flow velocities. With an air flow between 15 and 32 m/s (49 and 105 ft/s) the first air "jet" hit the bottom of the pool and broke up into small bubbles which slowly rose to the surface. For these high-velocity tests a large number of small air bubbles were seen at the level of the ECCS strainer during the first 30 seconds. The air was present because of impingement of the air "jet" on the pool bottom and because of the circulation of the small air bubbles at the pool wall. Air bubbles were observed inside the strainer during the first 30 seconds but the amount was negligible after 30 seconds. When the maximum velocity was limited to 5 m/s (16 ft/s) the air "jet" didn't reach the pool bottom and only negligible amounts of air bubbles were detected inside the strainer or in the pump intake pipe even though air bubbles were noticeable at the strainer level for the first 20 seconds. The ECCS pump head and flow did not decline because of air bubbles in the pump during any of the tests.

3.1.5.2 Discharge Tests in the PPOOLEX Facility

After the previously described suppression pool experiments, which investigated NCG bubble behavior, the test facility was modified to include input from air and steam sources. This modified facility was named the POOLEX facility, which consisted of a cylinder-shaped stainless pool with an open top. The inner diameter of the pool was 2.4 m (7.87 ft), the cross-sectional area was 4.5 m^2 (48.4 ft^2) and the height was 5.0 m (16.4 ft). After completion of a series of tests, the POOLEX facility was replaced by the larger closed loop PPOOLEX test facility (Figure 3.1-.2). The PPOOLEX pressure vessel includes a wetwell compartment and a drywell compartment. The drywell and wetwell are connected by a vertical vent pipe. The main

component of the PPOOLEX facility is a 31 m³ (1,095 ft³) cylindrical test vessel, 7.45 m (24.44 ft) in height and 2.4 m (7.87 ft) in diameter. The test facility was designed for a 4 bar (58.0 psi) overpressure and a 0.5 bar (7.25 psi) under pressure.
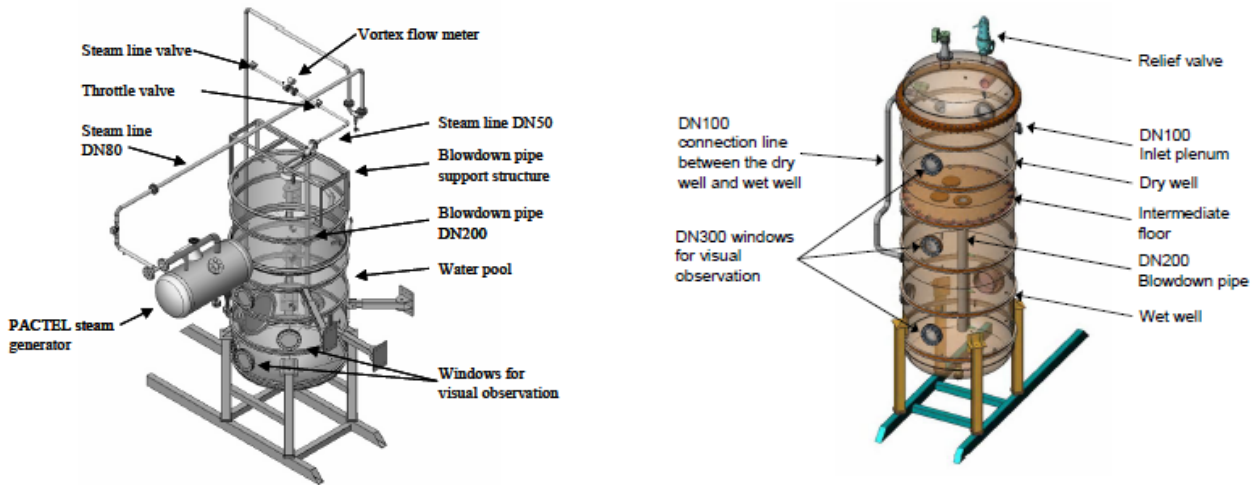
Figure 3.1-2: POOLEX (left) and PPOOLEX (right) Test Facilities (Ref. 31)

Results from two air discharge tests in the PPOOLEX test facility were simulated using the FLUENT CFD computer code. The tests were performed using downcomer vents with an inner diameter of 214.1 mm (8.43 in.). The vent pipe outlet was submerged approximately 1.05 m (3.4 ft) during these tests. The volume-of-fluid (VOF) two-phase model was used and the standard k-ε turbulence model was specified. The results obtained from the CFD simulations (Ref. 29) are in relatively good agreement with experimental results (Figure 3.1-3). Simulated pressures correspond to measurements and fluctuations because of bubble formations and break-up are captured. Generally most temperatures were simulated and the largest discrepancies could be explained by wetting thermocouples. The analytical activities concluded that the main features of downcomer air discharge experiments can be described with CFD calculations.

Additional CFD modeling efforts using different computer codes were expended to simulate pool loadings because of bubble condensation effects by simulating direct contact condensation of a steam or steam-air bubble. The analytical work concerning the steam bubble condensation process can be considered a state-of-the-art activity that requires significant additional effort. Consequently, because the interfacial heat and mass transfer relations at the bubble surface are still in development, CFD modeling of a condensing steam or steam-air bubble was not attempted at this time.
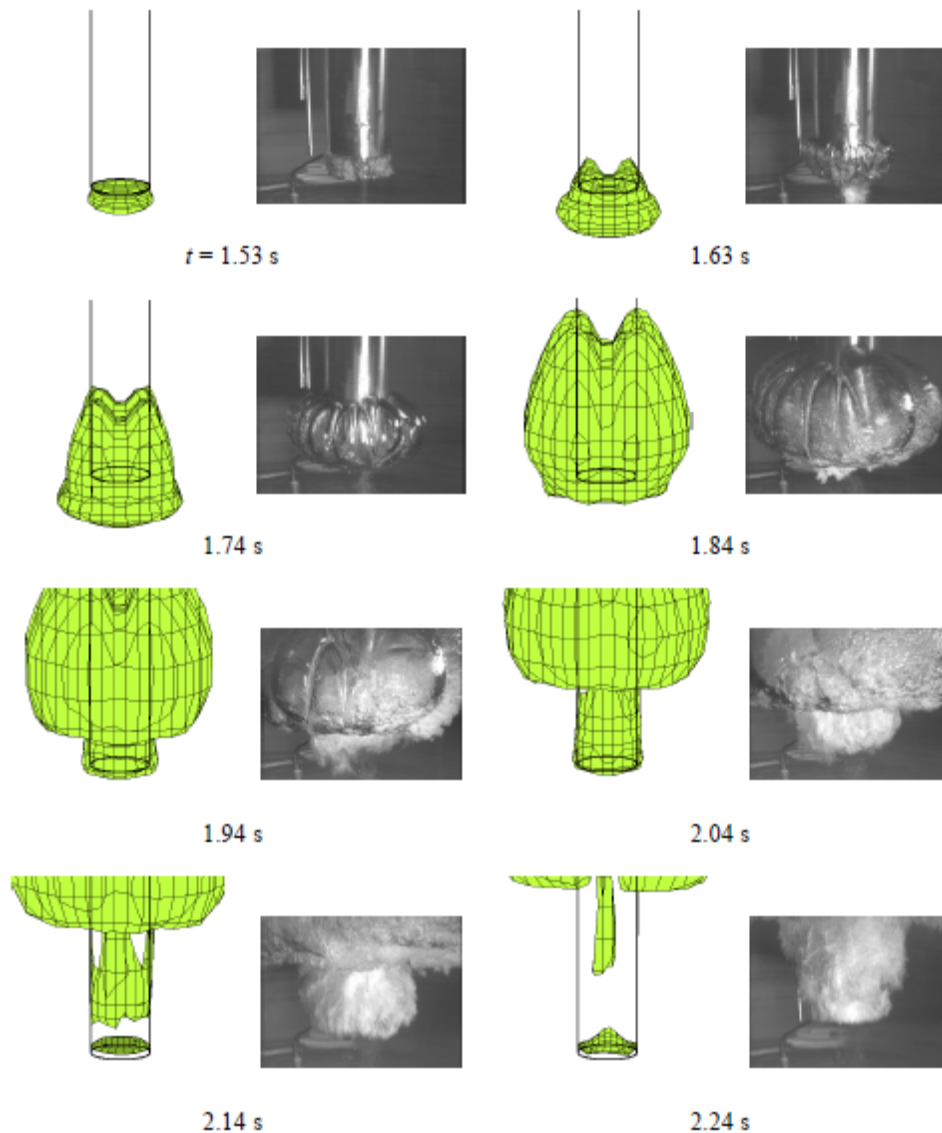
Figure 3.1-3: Vent Air Bubble Comparisons between CFD Calculation and PPOOLEX Experiment (Ref. 29)

3.1.6 Nordic Owners Group Testing for Swedish BWRs

Westinghouse Atom AB performed proprietary testing at the Lappeenranta University PPOOLEX pressure suppression test facility for the Nordic Owners Group (NOG). The NOG supported testing was performed to assess the effects that post-LOCA NCG flow from the downcomers of European BWR PS plants would have on the performance of ECCS pumps that take suction from the suppression pool. NRC staff members were allowed to review the proprietary report and accompanying videos at the Westinghouse office in Maryland on April 16, 2013, but were not permitted to make copies of the materials. The following text summarizes the document review performed by the NRC Office of Research staff.

The report summarized the testing performed at the PPOOLEX facilities for the NOG to investigate the possible suction of NCG into the ECCS intake in a BWR suppression pool following a LOCA. The test facility modeled scaled conditions for the Oskarsham and Barstuk PS containments. The downcomer pipes connecting the simulated drywell and wetwell of a BWR pressure suppression containment were modeled using four 219.1 mm (8.626 in.) diameter pipes. The top of the tank was open to atmosphere. The test facility included a simulated ECCS pump, transparent piping and a strainer screen. Flow into the ECCS pump was pumped back into the test tank. Video recordings were made of the conditions inside the test tank and inside the transparent ECCS intake piping.

Several test series were performed. NCG was injected into only one downcomer pipe for the first two test series. The ECCS pump strainer was located near the tank wall below the downcomer exit. The pump did not fail during any of these tests but, depending on test conditions, reduced flow may exist during part of the test. The pump fully recovered for all tests. Observations from the test videos showed a bubbly flow regime in the pump intake pipe for a few seconds. Additionally, for the low-strainer location, the maximum gas concentration present in the intake piping was always less than the maximum concentration present in the pool immediately outside the pump intake.

Tests were also performed during which NCG was injected into the suppression pool through all four downcomer pipes. These tests resulted in less severe conditions in the ECCS piping because the gas flow was distributed among four downcomer pipes instead of one.

Additional tests were performed using the four downcomer pipes for gas injection and with the ECCS pump inlet strainer and piping located above the downcomer exit in the suppression pool. This geometry is not typical of Mark I and II containments and was not investigated as rigorously during the NRC staff review. However, testing did show that an ECCS pump intake location above the downcomer exit resulted in larger and prolonged gas concentration in the intake piping in comparison to gas concentration conditions in the pool outside the intake. Additionally, for an intake location above the downcomer exit, the instantaneous gas concentration in the intake piping may be higher at times than that in the pool outside the intake.

Tests also studied the effects of NCG injection on the ECCS pump. One test injected air at the pump suction location. Others tested the effects of different gas injection rates on different pump flow rates. In another test series, NCG was injected directly into the ECCS pump inlet.

This testing showed that pump operation fully recovered with inlet pipe void fractions below about 8 percent. The ECCS pump may experience reduced flow depending on inlet void fraction, but the pump always recovered. At inlet void fractions above about 8 percent, the pump exhibited a large decrease in pumping capability; however, even for these conditions the pump recovered because the NCG injection duration was less than a few seconds. Typically a bubbly flow regime was observed in the inlet pipe for void fractions below about 8 percent and a stratified flow regime was observed for void fractions above about 8 percent.

A report describing a CFD analysis of the suppression pool of a NOG plant for the NCG flow phase following a LOCA was also reviewed. The CFD analysis was performed using the FLUENT code with the VOF method and a k-ε turbulence model. The general conclusion was that the CFD analysis produced a good representation of the noncondensable behavior in the suppression pool. The CFD analysis predicted a high concentration gas volume in the pool, but

tests showed a large concentration of small gas bubbles in about the same volume. Consequently, the report recommended that test results were necessary to provide confidence in CFD predictions. The CFD model also included an ECCS gas intake and piping. The pump intake was modeled using the FLUENT porous medium model.

Because the ECCS pump designs used in the NOG plants differ from those in Mark I and II plants especially with respect to pump intake location, caution should be taken in making broad conclusions from the NOG supported tests. The NOG tests provide trends in post-LOCA behavior of NCG in a suppression pool and on pump performance for the NOG design plants, but pump performance could differ for the pumps used in Mark I and II plants. Consequently specific testing of Mark I and II ECCS pumps would be necessary to fully assess the effects of NCG ingestion on those pump designs. Additionally, because the tested downcomer diameters were smaller than downcomer diameters in Mark I and II plants the NOG test results would need to be scaled to address Mark I and II conditions.

Summary and Conclusions

The following observations can be drawn from the Nordic Owners Group testing at the PPOOLEX facility. Care should be taken in extrapolating the smaller scale test results for European BWR pressure suppression designs to full-scale Mark I and II geometries.

1.   During testing the noncondensable bubble did not persist in the pool for longer than a few seconds.

2.   With the pump strainer intake below the downcomer exit, gas ingestion was observed in the pump intake pipe for several seconds; however, the tested pump always recovered after ingesting NCG although immediate pump operation and efficiency was effected by high void fraction gas flow to the pump.

These observations are consistent with the information obtained from other sources in the literature search for test data and expert opinions related to the GI-193 concerns. The observation regarding the NCG bubble duration in the pool is consistent with findings that the post-LOCA gas "exclusion zone" at the vent exit will dissipate in a few seconds and that NCG would only be present in the suppression pool for the time period necessary for the gas to rise and exit the pool surface. The observation regarding the pump recovery is consistent with the literature search finding that a centrifugal ECCS pump which operates with small inlet NCG void fraction for a few seconds can be considered capable of recovery without damage, and can operate at normal pump head and flow conditions.

In conclusion, this testing supports the current activities to assess post-LOCA noncondensable suppression pool gas concentration on ECCS pumps and suggests that the limited duration post-LOCA NCG concentration in a Mark I and II suppression pool would not have a major effect on ECCS pump operation.

3.1.7   Purdue University Mark I Scaled Air and Air/Steam Suppression Pool Tests

The NRC supported suppression pool tests at the Purdue University Multi-Dimensional Integral Test Assembly for ESBWR applications (PUMA-E) test facility to study the void fraction distribution and void penetration in a scaled Mark I suppression pool (Ref. 33). The test

apparatus was scaled for a typical Mark I BWR containment design with considerations for downcomer size, suppression pool water level, and downcomer water submergence. Instrumentation was installed to measure gas volumetric flow, void fraction, pressure and temperature. Two sets of experiments were conducted using the PUMA-E facility. Videos of the water pool were taken during the performance of these tests.

In one set of 16 tests air was injected through a 0.102 m (4 in.) downcomer pipe into the suppression pool at various air volumetric flow rates, downcomer void conditions and air velocity ramp rates. The initial air injection phase resulted in the maximum void penetration depth. During this phase the air volumetric flow rate had a minor effect on void fraction distribution and void penetration for high volumetric flow rate conditions. The later quasi-steady state phase produced less void penetration, but possessed oscillations in the void penetration. The air volumetric flow rate resulted in a larger effect on void fraction distribution and void penetration for the entire range of air flow rates. The initial downcomer void conditions were found to strongly affect the void fraction distribution and void penetration during the initial period. The air velocity ramp rates were found to have a minor effect on void fraction distribution and penetration in both phases.

In the second test set, sequential flows of air, steam-air mixtures and pure steam at various flow rates were injected in the drywell and passed though the downcomer vent into the suppression pool. Eight tests with two different downcomer sizes (0.078 m (3 in.) and 0.102 m (4 in.)) with various downcomer gas volumetric fluxes and two different initial drywell air concentrations were conducted. The initial phase of these tests produced the maximum void penetration depth. Chugging was observed at the end phase of these tests. It was observed that the void distribution and void penetration area was governed by the downcomer gas volumetric flux and the downcomer air concentration.

3.1.8   GKSS Pressure Suppression Research Program

Large-scale tests of pressure suppression systems were also performed at the GKSS test facility in Germany (Refs. 21 and 22). The German tests were performed in the 1980s and were primarily intended to study the dynamic loadings on the suppression pool boundary and on submerged structures. The German tests concentrated on testing for the Mark II and German KWU Type-69 PS systems. The tests were performed in a time frame coincident with the GE test program and one of the authors was involved with the Mark I tests funded by the NRC in the early 1980s. Consequently, most of the information from the German testing should be reflected in the GE and NRC test results. However, information regarding flow behavior in the water pool was not specifically measured.

The NRC funded testing at the GKSS facility to study the condensation behavior in a Mark II suppression pool behavior following a DBA LOCA. One of the videos from the NRC funded full-scale Mark II tests recorded the vent clearing and NCG bubble behavior in a suppression pool. Figure 3.1-4 provides video frames of the suppression pool conditions at different times following the start of the test. The video frames show two of the vent pipes submerged in the water pool. The video frames illustrate the different phases of the NCG and steam flow behavior in the water pool. The video frames depict a reflection of the initial NCG jet off the bottom surface of the pool. Because the distance of approximately 0.98 m (3.2 ft) from the vent exit and pool bottom in the test facility is smaller than the similar distances of approximately 2.44 m

(8.0 ft) and 3.7 m (12.4 ft) in a Mark I or Mark II suppression pool, the gas jet reflection may not be present in the suppression pool of a Mark I and Mark II plant.

Thermal-hydraulic measurements were not taken in the suppression pool during these tests; however, visual examination of the test video provided meaningful insights into the NCG "jet" dimensions and duration to qualitatively identify the "exclusion zone" that defines the volume of high NCG mass associated with the discharge vents. Visual examination of the video cannot support or dispel with certainty the presence of an ECCS pump safety concern, and confirmed the need for additional information to reach a definitive conclusion on the existence of a safety concern. However, information obtained from the visual examination was useful in identifying an appropriate calculational model for GI-193 assessment, and in qualitatively assessing its results.
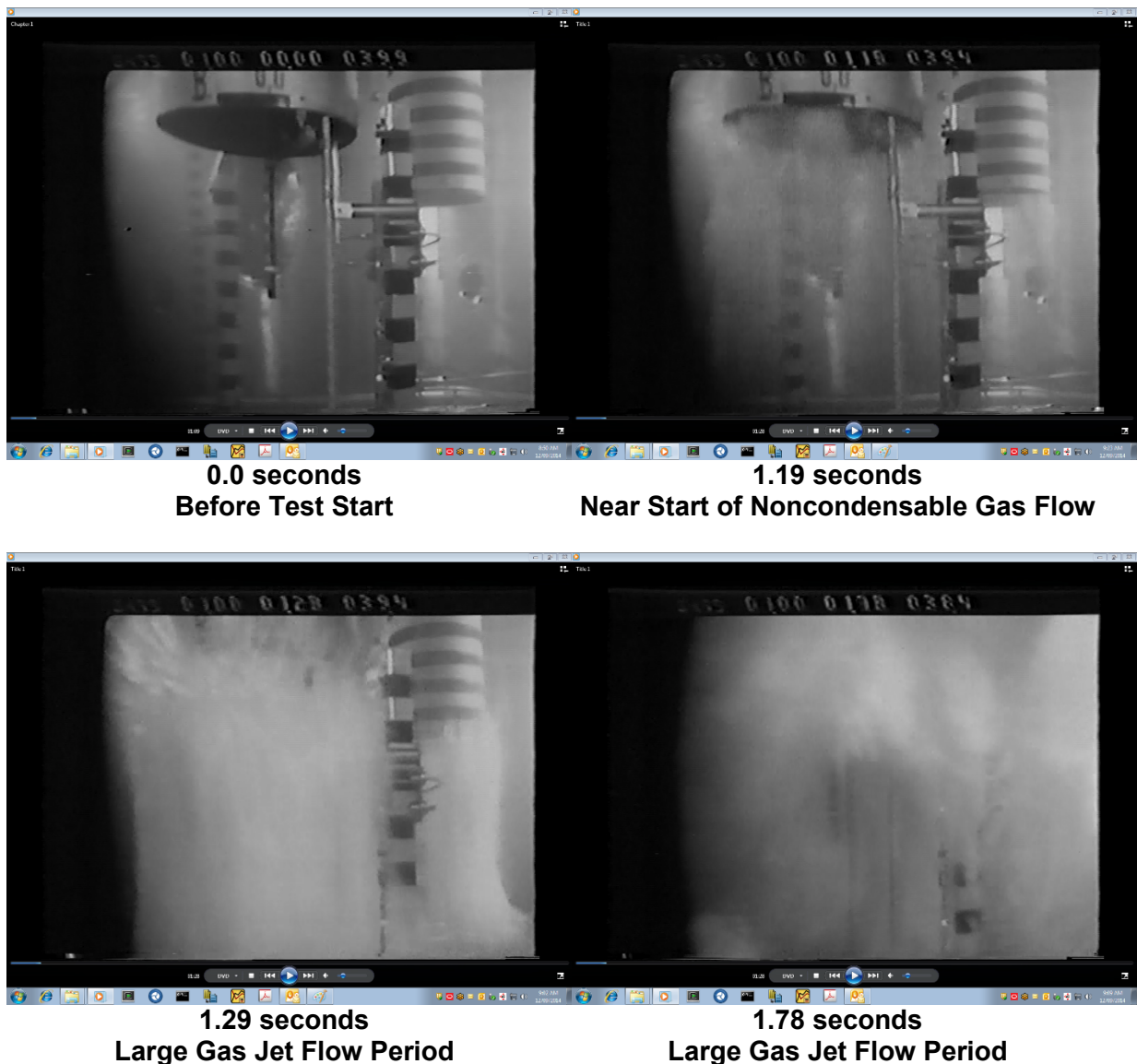
0.0 seconds
Before Test Start

1.19 seconds
Near Start of Noncondensable Gas Flow

1.29 seconds
Large Gas Jet Flow Period

1.78 seconds
Large Gas Jet Flow Period

Figure 3.1-4: Video Frames from a GKSS Full-Scale Test of Mark II Suppression Pool Behavior following a LOCA (1 of 3)

22
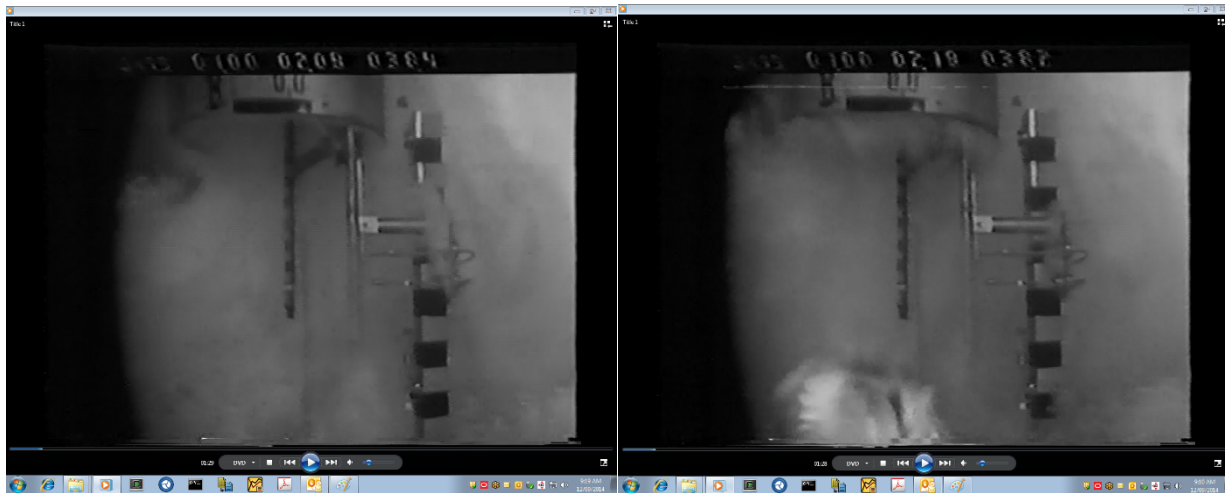
2.08 seconds
Large Gas Jet Flow Completed

2.18 seconds
Large Gas Jet Reflection off Pool Bottom
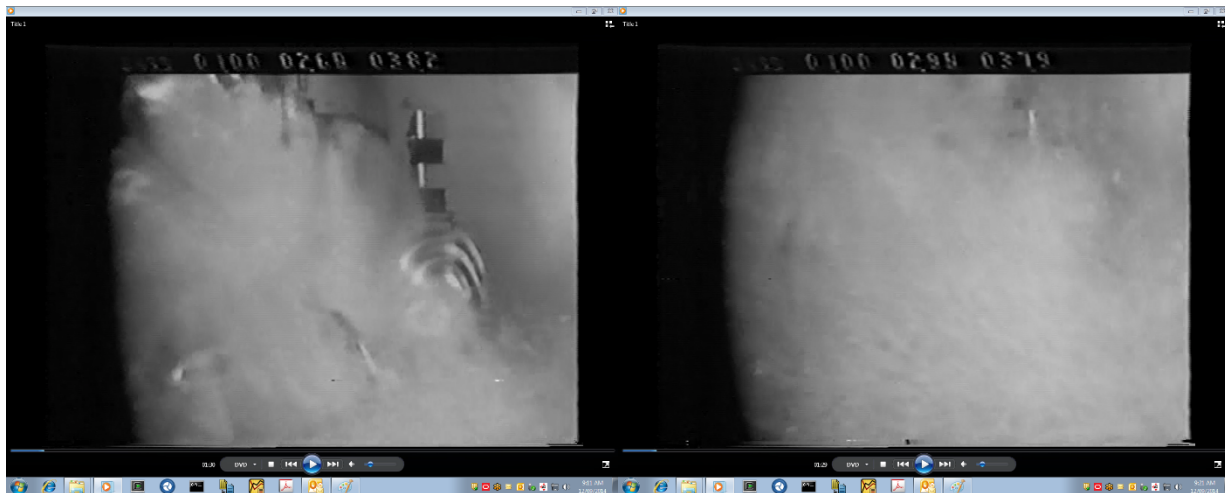
2.68 seconds
Rise of Reflected Gas Jet

2.98 seconds
Near Completion of Reflected Gas Jet Rise

Figure 3.1-4: Video Frames from a GKSS Full-Scale Test of Mark II Suppression Pool Behavior following a LOCA (2 of 3)
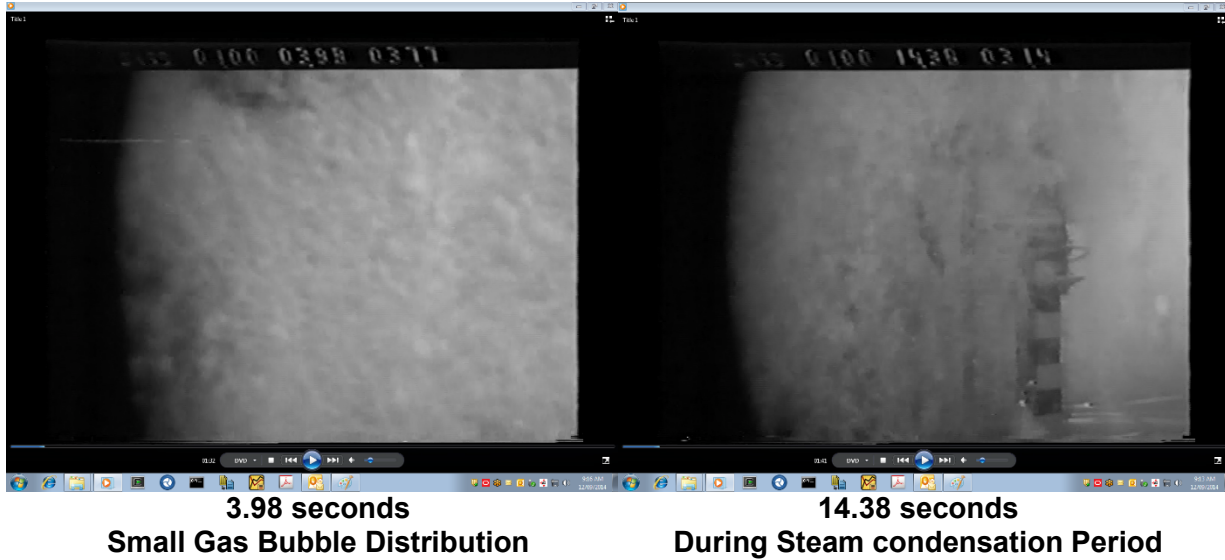
3.98 seconds
Small Gas Bubble Distribution

14.38 seconds
During Steam condensation Period

Figure 3.1-4: Video Frames from a GKSS Full-Scale Test of Mark II
Suppression Pool Behavior following a LOCA (3 of 3)

3.1.9   Marviken Test Facility Testing

A reference to recent pressure suppression test in the Marviken test facility in Sweden in 2007 (Ref. 23) was discovered. Unfortunately this recent Swedish referenced material is not publicly available; however it appears that these tests were primarily performed to verify the operation of PS systems.

3.1.10   Paul Scherrer Institute Tests

The large PANDA and LINX experimental facilities were used in the ALPHA project of the Paul Scherrer Institute (PSI) to study pressure suppression containments. The PANDA facility is a large integral scale test facility whose primary goal was to study passive containment cooling systems and the interaction between the various system components during long-term cooling. The facility has 1:1 height, 1:25 volume, and 1:25 power scaling to the General Electric Simplified BWR design. The facility was later modified to simulate the GE Economic Simplified Boiling Water Reactor (ESBWR) and the Siemens SWR-1000 design. CFD calculations were undertaken to analyze the three-dimensional drywell flows (Ref. 34).

The LINX facility has been used for separate effects tests of condensation, mixing, effect of NCG and stratification in suppression pools (Ref. 35). CFD analyses have been performed to study the behavior of bubble plumes in water pools using other published plume experiments because of the unavailability of the LINUX test data at the time the CFD analyses were being performed.

Also at PSI, Meier and colleagues (Refs. 36 and 37) conducted small-scale air and steam-air blowdown experiments with a transparent tank as part of a thesis at the Federal Institute of Technology Zurich. They observed that the length of pipe and compressibility of the gas in the piping affects the bubble size, shape and frequency at low flow rates. With high flow rates the effect of compressibility became insignificant. Two-dimensional CFD analyses modeled the joint

24

motion of gas and liquid in the water pool, including the steam bubble interface heat and mass transfer. The CFD analyses used the VOF method, which included a newly developed surface tension calculation method. Information from this PSI activity appears to have application to GI-193 and test data and videos could be used to verify developed calculation techniques for addressing the GI-193 concerns.

3.1.11 Alden Research Laboratory Testing

Alden Research Laboratory performed testing on a 1/2.4 scale model of a segment of a Mark I BWR suppression pool to study debris transport. The water volume of the tank per downcomer was scaled to the volume per downcomer pipe of a typical BWR Mark I suppression pool. Turbulent chugging associated with post-LOCA steam condensation oscillations was simulated in these tests by four 0.254 m (10 in.) diameter downcomer pipes fitted with pistons. Parametric tests were conducted to examine the type, form, and quantity of insulation debris tested; the quantity of sludge tested; and the period and amplitude of the downcomer piston chugging. The NRC has videos of some of this project's tests. This testing does not provide information useful to GI-193 assessment.

Table 3.1-1: Pressure Suppression Test Facilities

Organization/Test Facility	Downcomer ID	Reference		Test Objective
		Test	T/H Analysis	
General Electric (GE)				The primary purpose of the experiments was to quantify the loading on the suppression pool walls following a LOCA. Associated assessments used test data to develop computational methods for predicting some fluid behavior in the suppression pool.
• Mark I full-scale test program	0.6096 m (24 in.)	5	--	
• Mark I 1/4 scale pressure suppression test program	NA	7, 8		
• Mark II full-scale test program	0.5476 m (21.56 in.)	9		
• Mark III full-scale confirmatory test program	NA	6		
NRC/Lawrence Livermore Laboratory (LLL)				The primary purpose of the experiments was to quantify the loading on the suppression pool walls following a LOCA. Scaling methods were also developed. Associated assessments used test data to develop CFD models for predicting suppression pool fluid behavior.
• Mark I 1/5 scale BWR pressure suppression tests	0.1194 m (4.7 in.)	10, 11, 12	13, 14, 15, 16, 17	
MIT				Tests for air discharge in a water pool are described including scaling considerations. A CFD model was developed to analyze pool behavior following compressed air injection from a drywell through a submerged downcomer pipe.
• Air and noncondensable Mark I gas blowdown experiments	0.0254, 0.0508 and 0.0983 m (1, 2, and 3.87 in.)	18, 19	13	
University of California				These tests model bubble behavior of injected air in a pool of water. A theoretical model describing the bubble growth at the vent pipe exit was developed.
• Mark I scaled suppression pool tests	0.009 to 0.095 m (0.35 to 3.7 in.)	20	20	
GKSS Pressure Suppression Research Program	0.6 m (23.6 in.)	21, 22	--	These full-scale tests were primarily intended to study the dynamic loadings for the GE Mark II and German KWU Type-69 pressure suppression systems.
Marviken Test Facility Testing	NA	23	--	References for these recent tests at the Marviken facility are not publicly available; however it appears that these tests were primarily performed to verify the operation of pressure suppression systems.

Table 3.1-1: Pressure Suppression Test Facilities (cont.)

Organization/Test Facility	Downcomer ID	Reference		Test Objective
		Test	T/H Analysis	
Lappeenranta University • Scaled suppression pool experiments • Scaled PPOOLEX test facility air tests • Scaled PPOOLEX test facility air-steam tests	0.1623 and 0.2131 m (6.39 and 8.39 in.) 0.2141 m (8.43 in.) 0.2141 m (8.43 in.)	24, 25	-- 26, 49 27, 28, 29, 30, 31, 49	These tests measured gas bubble size in a test facility with and without an ECCS pump and strainer. Pump tests were also run with direct gas injection into the pump intake. CFD analyses predicted air bubble size and behavior for the PPOOLEX tests. CFD analyses for air-steam bubble in the PPOOLEX tests.
Lappeenranta University • Nordic Owners Group (NOG) testing for Swedish BWRs	0.2191 m (8.626 in.)	--	--	These proprietary tests were performed at the PPOOLEX facility to address the effect of air ingestion on ECCS pump behavior. NRC staff reviewed the proprietary report describing these tests.
Purdue University • Mark I scaled air and air/steam	0.078 and 0.102 m (3 and 4 in.)	33	--	These test studied air and air/steam flow through a submerged vent pipe that exits into a pool of water. Void fraction is measured in the water pool.
Paul Scherrer Institute • GE and Siemens pressure suppression system design concept tests using the PANDA test facility	NA	34, 35	--	The goal of the project was to study passive containment cooling systems and the interaction among the various system components during long-term cooling.
• Small tank tests	5 cm (1.97 in.)	36, 37	36, 37	This work involved CFD modeling of small-scale air and steam-air blowdown experiments with a transparent tank. A request has been made to gain access to the test data and videos.
Alden Research Laboratory • Mark I post-LOCA debris transport tests	0.2499 m (9.84 in.)	38	--	A $1/_{2.4}$ scale model of a segment of a Mark I BWR suppression pool was used to study debris transport. This testing does not provide information useful to GI-193 assessment.

4.   ECCS PUMP OPERATION

An important consideration in assessing the acceptable post-LOCA operation of an ECCS pump is the determination of the maximum acceptable pump inlet void fraction that will not affect pump performance and not cause damage. An additional consideration is the determination of the minimum void fraction range and related operation time from which an ECCS pump will return to acceptable operation after liquid flow is reestablished. This section presents the current knowledge regarding these topics resulting from a literature review.

4.1   ECCS Pump Timing Considerations

Figure 2.1-7 shows that ECCS pump operation could primarily be affected if the pump operates within the first few seconds following a DBA LOCA. Concerns regarding NCG ingestion by the ECCS pumps would be expected to last until the bulk of the NCG rises and exits the pool surface.

For a DBA LOCA, the ECCS low-pressure core spray (LPCS) and low-pressure core injection (LPCI) pump startup signal is typically generated at the high drywell pressure set point. A survey by the BWR Owners Group for Mark I containment designs (Ref. 4) reveals that the high-containment pressure signal can occur as early as 1 second following the start of a DBA LBLOCA. An additional 3 to 10 second pump startup delay is to be expected if a loss of offsite power is considered concurrent with the DBA LBLOCA to account for emergency diesel generator startup and ECCS pump initiation sequencing. Therefore, the earliest start time of the ECCS pumps with the availability of offsite power is about 1 second, but is about 4 seconds with an associated loss of offsite power.

DBA LBLOCA analyses are typically performed assuming the unavailability of offsite power. Consequently, it can be concluded that ECCS pump operation for DBA LBLOCA calculations will not be affected by the presence of NCG in the suppression pool coming from downcomer flow following a DBA LBLOCA for a Mark I containment because the earliest pump start time of 4 seconds is greater than the 3 second duration of the large gas bubble and large void fractions in the suppression pool.

During the initial period after receipt of a startup signal, the LPCS and LPCI pumps are operated to reach full speed. Additionally, the initial pump flow is recirculated to the suppression pool and is not injected into the core. Regardless of the availability of offsite power, the LPCS and LPCI systems are expected to pump flow into the core at about 40 and 50 seconds after appropriate valve reconfiguration. Consequently, during the first 40 to 50seconds following a LOCA, when the ECCS pumps circulate flow within the suppression pool, the effects of NCG ingestion do not affect the ability of the ECCS pumps to supply flow to the core. The primary concerns in this early time frame pertains to the possibility of incurring pump damage or, if pump damage does not occur, the ability of the ECCS pumps to recover to full operation after possible NCG ingestion during the early period.

4.2   Acceptable ECCS Pump Operation

An ECCS pump can sustain damage by over speed and vibration if excessive amounts of NCG are ingested. The following sections discuss the results of a literature search addressing

acceptable pump operation and culminate with recommended criteria for determining acceptable BWR ECCS pump operation in the presence of NCG.

4.2.1 ECCS Pump Performance in BWRs (NUREG/CR-2772)

Testing reported in NUREG/CR-2772 (Ref. 39) finds that air concentrations greater than about 3 to 5 percent by volume in a suction line of an ECCS pump can considerably lower the head-discharge curves of centrifugal pumps causing lower pump capacity at a given head.

4.2.2 Pump Performance under Air Ingesting Conditions (NUREG/CR-2792)

NUREG/CR-2792 (Ref. 40) assesses the performance of residual heat removal (RHR) and containment spray (CS) pumps during recirculation operation with sump suction following a postulated LOCA in a pressurized water reactor (PWR). The results of air/water tests on centrifugal pumps from several experimental programs were assessed to quantify the effects of air on head degradation. To apply the information in this report to BWR ECCS pumps, one must assume that conclusions developed for the assessed centrifugal pump operation tests can be applied to ECCS centrifugal pumps in BWR PS containments. Results for only three pump tests were considered applicable because the tested pump needed to meet the following requirements.

a. A pump-specific speed of 800–2000 was required. The criterion eliminated air/water performance tests for primary coolant pumps and axial flow pumps. (Note, specific pump speed is defined as $N\, Q^{\frac{1}{2}} / H^{\frac{3}{4}}$ where N is the shaft speed in rpm, Q is the volumetric flow in U.S. gpm, and H is the pump differential head in feet.)

b. The test needed to be well documented.

c. The RHR and CS pumps surveyed had impeller pump diameter up to about 0.508 m (20 in.). Data on test pumps with impeller diameters less than one-third this size were not included.

d. The test fluids were required to be air and water.

Specifically, the report notes that the performance of centrifugal pumps is known to degrade with increasing gas content. It further notes that the amount of degradation is a function of various parameters; the important ones being pump design, specific speed, flow rate, inlet pressure and fluid properties. The report states that a general guideline adhered to by the pump industry is that degradation is not a concern at normal flow rates if air ingestion levels are less than 2 percent by volume; that acceptable pump performance with air ingestion levels between 2 percent and 15 percent is dependent on pump design, and that centrifugal pump performance is fully degraded for air ingestion volumes greater than 15 percent. At low net positive suction head (NPSH) values close to the net positive suction head required by the pump (NPSHR), air ingestion will increase the degradation in performance in comparison to operation in the absence of air.

Because of a review of available test data, it is concluded that no case of severe pump degradation was observed for void fractions less than 2 percent and that degradation in performance does not occur until the pump inlet void fraction exceeds about 3 percent. Limited

test data indicated that deterioration in performance will occur until the test pumps loses prime at air volume fractions between 7 percent and 15 percent.

Discussions with pump specialists resulted in the opinion that pump inlet void fractions between 1 and 3 percent would result in negligible degradation, that air binding might occur for flows less than 50 percent of best efficiency, that pump degradation between 3 and 15 percent is dependent on individual pump design and operating conditions, and that air quantities greater than 15 percent would result in full degradation in most pumps.

The following general conclusions were reached from the studies mentioned in the report:

1.   For a wide range of operating flow rates, RHR and CS pumps should handle volumetric air quantities up to 2 percent with negligible degradation in performance.

2.   For air quantities greater than 2 percent, pump performance degradation varies substantially depending on design and operating conditions.

3.   For very low flow rates (less than 50 percent of the best efficiency point), the presence of air may cause air binding or loss of prime in the pump even at low-ingestion levels (less than 2 percent by volume). However, for low flow rates, evaluations show that the likelihood of air ingestion is low.

4.2.3   Pump Operation and Acceptable Gas Quantity (Generic Letter 2007-02)

Generic Letter 2007-02 (Ref. 41) concludes from the data in NUREG/CR-2792 (Ref. 40) that the commonly used limit of 5 percent gas into ECCS pumps may be reasonable only if a substantial flow rate can be insured. At reduced flow rates gas can accumulate with time and the pump can eventually become gas bound with gas ingestion rates that are not normally a problem at higher flow rates.

4.2.4   Lappeenranta University Pump Experiments with Noncondensable Gas

As discussed in Section 3.1.5 Lappeenranta University performed scaled suppression pool experiments with NCG. This testing includes assessments of an ECCS pump representative of the Olkiluoto BWR plant PS system, which was considered typical of the Scandinavian designs. The general observations regarding ECCS pump performance tests in the presence of NCG are listed below.

1.   In the pump tests, the ECCS pump was operating at a nominal speed of 2,970 rpm with four different volumetric flow rates when pressurized air was injected directly into the pump intake pipe. With volumetric flow rates of 57 and 75 l/s (903 and 1,189 gpm), a 3 to 4-percent air fraction was needed before a decline in pump head and flow was observed.

2.   With smaller flows of 12.5 and 25 l/s (198 and 396 gpm) the pump head and flow started to decline after air injection was initiated and the flow totally collapsed when more than a 7-percent air fraction was present in the intake pipe.

3.   When the air injection was stopped for the 12.5 l/s case, the pump head and flow reached original values after 30 seconds after the air injection was turned off. At all the

other flows the pump head and flow normalized in a few seconds after the air injection was turned off.

These integral tests demonstrated that there is a relationship between the air discharge velocities through the downcomer vents and the amount of pump air ingestion. Consequently, an assessment of NCG effects on ECCS pump behavior must include the effects of the downcomer vent air flow and the flow behavior of the gas and water in the suppression pool.

As discussed in Section 3.1.6, the Nordic Owners Group performed proprietary testing at the Lappeenranta University test facility when NCG was injected directly into the ECCS pump inlet. The testing showed that the ECCS pump with inlet pipe void fractions below about 8 percent may experience reduced flow depending on inlet void fraction, but the pump operation always fully recovered. The pump experienced a large decrease in pumping capability at inlet void fractions above 8 percent for durations of a few seconds; however, the pump always fully recovered.

It should be emphasized that these observations are typical of the Scandinavian BWR PS system pump designs and may not be totally applicable to ECCS pumps used in US Mark I, Mark II and Mark III designs.

4.2.5 BWR Owners' Group ECCS Pump Suction Void Fraction Study

Reference 42 states that "most BWR ECCS pumps are from three suppliers: Byron Jackson (now Flowserve), Sulzer, and Ingersoll (now part of Flowserve)." The reference further states that the pump types vary from single-stage centrifugal to 15-stage centrifugal pumps. This reference makes the following recommendations regarding ECCS pump operation.

1. Based on the review of pump gas intrusion data an upper limit bound of 2 percent by volume continuous suction gas void fraction is acceptable. The report notes that the acceptability of the 2 percent value is based on the test data and research compiled in NUREG/CR-2792 (Ref. 40). The report further notes that test data suggest that little to no pump degradation in pump performance occurs in the range of 0.5 percent to 5 percent with the most recurring values being 2 percent or less.

2. The report notes that NUREG/CR-2792 suggests that limited testing for multistage pumps indicates that at a given air volume pump performance degradation is less pronounced at higher inlet pressures and in multistage pumps.

3. As a guideline the report recommends that an ECCS pump will not incur damage and will recover if a 10 percent average void fraction for no greater than 5 seconds exists. It justifies this approach by referencing plant data that concluded that 3 to 5 percent air entrainment by volume over a 20 second period would not be expected to cause any significant problems.

4.2.6 University of Minnesota Centrifugal Pump Performance Tests with Air Ingestion

Reference 43 described full-scale testing to examine the effects of suspended air bubbles on the performance of a sea-water circulating centrifugal pump. The pump was a single suction, vertical discharge, horizontal suction pump. Its single-stage impeller was capable of delivering 11.356 m^3/m (3,000 gpm) at a total dynamic head or 6.895×10^4 Pa (10 psi) at 1,150 rpm. The

pump used a 0.2032 m (8 in.) diameter suction leg and 0.254 m (10 in.) diameter discharge leg. The suction pressure of about 6.895×10^3 Pa (1 psig) was used during testing. Air was injected into a vertical leg of the pump suction line through on injector nozzle.

The report states the following, "the tests established that a sudden loss of head developed across the pump which occurs between 4 and 5 percent volume concentration of air; however, the pump performance will reliably recover if the void fraction is reduced below 0.04." It should be emphasized that these observations are typical of the tested centrifugal pump and may not be totally applicable to ECCS pumps used in US Mark I, Mark II and Mark III designs

4.2.7   Expert Panel Study of Gas Accumulation on Pumps – "The Pump Roadmap"

References 44 and 45 present the results of a study performed by panel of pump experts to develop acceptance criteria for pump operation with NCG ingestion. The study resulted in the BWR pump operational criteria summarized in Table 4.1-1. The results of this activity represent the latest and best information addressing acceptable pump operation in the presence of NCG. Consequently, the criteria provided by this panel will be used as the basis for assessing acceptable BWR ECCS pump operation.

Table 4.1-1: Allowable Average Noncondensable Void Fractions to Preclude Damage to Typical BWR Pumps

Operating Condition	% Q / Q(BEP) [a, b]	Void Fraction [c]
Steady State Operation > 20 s	40%–120%	2%
Steady State Operation > 20 s	< 40% or > 120%	1%
Transient Operation	70%–120 %	10% for ≤ 5 s
Transient Operation	< 70% or > 120%	5% for ≤ 5 s

a   Q is the water volumetric flow.
b   BEP is best efficiency point.
c   Transient void fraction is averaged over the specified time span.

The BWR ECCS operational criteria developed from the information in References 44 and 45 are summarized below.

1.   Low transient flow rates (less than 70 percent of the best efficiency point) with an inlet void fraction greater than 5 percent for more than 5 seconds will result in pump damage unless pump-specific testing can show otherwise.

2.   Higher transient flow rates (between 70 percent and 120 percent of the best efficiency point) with an inlet void fraction greater than 10 percent for more than 5 seconds will result in pump damage unless pump-specific testing can show otherwise.

3.   Low flow operation (less than 40 percent of the best efficiency point) at greater than 1 percent by volume continuous suction NCG void fraction results in pump damage unless pump-specific testing can show otherwise.

4.   Full flow operation (40 percent to 120 percent of the best efficiency point) at greater than 2 percent by volume continuous suction NCG void fraction results in pump damage unless pump-specific testing can show otherwise.

ECCS pumps that operate within the void fraction conditions specified in Table 4.1-1 and within the gas void fractions indicated above in items 1 to 4 can be considered capable of recovery without damage, and will operate at normal pump head and flow conditions if the inlet void fraction is reduced to a value below 1 percent.

This criteria will be used as the basis for assessing acceptable BWR ECCS pump operation. Of course, an ECCS pump assessment would be permitted to use other operation criteria if acceptable pump-specific tests are performed that provide better operational guidance.

5.   POST-LOCA SUPPRESSION POOL ANALYSIS

Two approaches were considered for determining suppression pool void fraction distribution following a LOCA with the intent to compare the results from both approaches for verification purposes or even to pursue a synergistic analysis that combines both approaches. The first approach scaled the test results from the Lappeenranta University tests and the PUMA tests to full-scale plant geometry. The second approach used CFD calculations to define the NCG and fluid behavior in the suppression pool after verification of modeling methods using the scaled Lappeenranta University tests, the PUMA tests and qualitative verification against the Mark II full-scale test video.

5.1   Scaling of Test Data to Plant Conditions and Geometry

Scaling laws may be used to determine full-scale plant conditions from small-scale test results. Of particular interest here are test results from the Lappeenranta and Purdue Universities scaled tests because both test programs provided results related to air and air/steam bubble size and behavior in a water pool following air and air/steam flow from a submerged pipe. The PUMA tests also measured void fractions in the water pool. As previously mentioned, the Lappeenranta University scaled tests were performed using downcomer IDs of about 0.1623 m and 0.213 m (6.39 in. and 8.4 in.), and Purdue University scaled tests were performed using 0.078-m and 0.102-m (3-in. and 4-in.) ID downcomers. Because the PUMA tests provided measurements of air and air/steam bubble size and behavior as well as void fraction in the water pool, attempts were made to scale those small-scale test results to full-scale plant conditions. Data from other tests—such as the MIT tests, which used 0.0254 m, 0.0508 m and 0.0983 m (1 in., 2 in., and 3.87 in.) ID vents, the University of California tests, which used 0.009 m to 0.095 m (0.35 in. to 3.7 in.) ID vents, and the PSI tests which used 0.05 m (1.97 in.) ID vents—were not considered because these tests measured only the transient bubble size in the water pool; measurements of the void fraction distribution in the water pool are not available. For comparison, full-scale Mark I and Mark II downcomer inner diameter range from 0.5334 to 0.6096 m (21 to 24 in.).

5.1.1   Scaling Approach using Experiment Modeling

The small-scale modeling method rests on knowledge of the modeling laws which ensure that dynamic similarity exists between the model and the full-scale system. This modeling method should provide the scaling laws for predicting full-scale conditions from data derived from the small-scale model. This scaling approach was used for the pool swell process as part of the pressure suppression testing that was performed in the 1970s and 1980s. Because of the complexity of the suppression pool swell process, it would be almost impossible to achieve exact dynamic similarity. However, F.J. Moody (Ref. 3) developed a set of modeling laws that were sufficiently simple to allow convenient small-scale modeling to be applied to a large-scale geometry. These laws became the basis for the industry's small-scale tests.

The scaling method developed by A.A. Sonin and P.W. Huber (Ref. 46) for air clearing in suppression systems follows Moody's approach but includes a more rigorous consideration of the vent system's hydraulic resistance. An approach similar to the one used by used by Sonin and Huber for the pool swell problem was considered for the GI-193 scaling analysis.

The scaling analysis focused heavily on the PUMA tests because a detailed description of the scaling approach was provided in the PUMA report. Unfortunately, the primary tests of interest, the Lappeenranta University and Purdue University scaled tests, were based on much simpler scaling approaches. For example, the Purdue University tests were based on a scaling method that depended primarily on simple geometrical (e.g., length, diameter, area) ratios between the prototype and the model, and lacked the depth associated with the more rigorous and well-established approaches that are based on non-dimensional groups such as the Reynolds number and Froude number. Therefore, a more rigorous approach, such as Moody's approach, cannot be used to directly scale those test results to full-scale plant conditions. Attempts to develop a specific scaling approach that follows Moody's approach while still taking advantage of those small-scale test results were unsuccessful.

5.1.2 Scaling Approach using Downward Gas Jet Behavior

In a study of downward gas jets into a liquid by A. Emami and C. Briens (Ref. 47), the penetration length of downward nonreacting, subsonic gas jets in liquid was measured by optical methods. The effects of nozzle diameter, gas density, gas jet velocity, liquid viscosity, and liquid surface tension on jet penetration were examined. A generalized correlation to predict the penetration depth of downward gas jets was obtained. Also a simple model, using a shell momentum balance and assuming downward gas jet as a downward cone with constant angle, was introduced and validated with experimental data. All experiments were performed at room temperature and in a rectangular glass tank with dimension of 0.6 m (1.97 ft) length, 0.3 m (0.98 ft) width, and 0.4 m (1.31 ft) height which was filled up to 75 percent of its height with different liquids, such as distilled water, ethanol (95 percent), or sucrose solutions, to vary the liquid viscosity and surface tension. Helium, argon, and oil-free air were used as the gas phase. The gas mass flow rate for helium was 0.15 g/s (0.00033 lb_m/s) and for air and argon were 1.1 and 1.3 g/s (0.0024 and 0.00287 lb_m/s) , respectively. The gas was introduced into the liquid through a submerged downward stainless steel tube. Four nozzle diameters were used. The inner diameters of the nozzles were 1.07, 2.03, 2.85, and 4 mm (0.042, 0.08, 0.112, and 0.1575 in.). The length of stainless steel tube was 0.7 m (2.3 ft). Preliminary measurements were taken with a fast video camera. A photodiode cell and a horizontal laser beam were used to measure the jet penetration length. The average jet penetration length (L50%) was taken to correspond to a 50 percent probability of jet presence and a four parameter sigmoid curve, fitted to the experimental data, was used for interpolation. The span of the jet fluctuation range was taken as the differences between the distances corresponding to 10 and 90 percent jet presence probabilities (L10%–L90%).

When gas is injected to the liquid through a downward nozzle, the whole process can be described as follows: The gas flow produces a bubble, which keeps growing until the buoyancy force gets strong enough to overcome inertial forces. At this point, the bubble starts moving upward. Then the bubble detaches from the nozzle tip moving upward while covering the nozzle tube. At low gas flow rates a bubbling regime is dominant, and with increasing gas flow rate a fluctuation gas jet grows and the bubble size increases. The high-speed videos taken at different gas flow rates suggest that the cavity can be assumed as a downward cone.

This model, which is based on a momentum balance, assumes a conical shape for the downward gas jet. Momentum input comes from the gas entering the control volume at the nozzle tip. Momentum output is negligible because of the low bubble velocity leaving the control volume. The force acting on the control volume is the buoyancy force. The frictional force of the liquid on the control volume is negligible as the jet is assumed to be stationary (Figure 5.1-1).

This approach seems to be rigorous enough and is based on the appropriate nondimensional groups such as a modified Froude number. However, there are two points of concern: The first is that the nozzle diameters used in the tests were much smaller than the downcomer diameter, which may result in a different flow regime, and the second is that although the results may have accurately described the behavior of a gas jet into liquid, they may have missed the inertial effect of the initial clearing of the water column on the subsequent behavior of the gas jet. For these reasons, this alternate approach was considered inadequate for scaling the test results up to actual plant geometry and conditions.
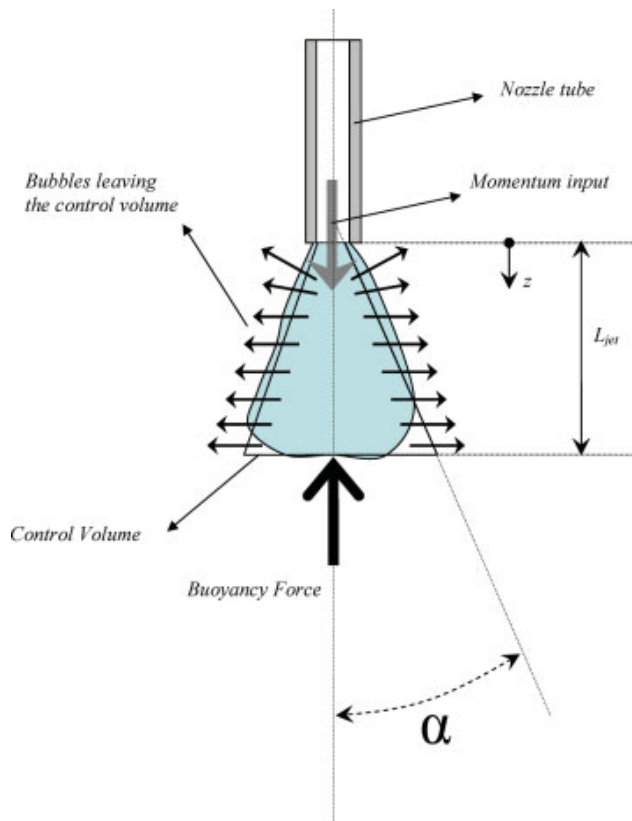
Figure 5.1-1: Model for Downward Gas Jet in Liquid

5.1.3 Assessment of Scaling Approaches Using CFD Analysis

The evaluation of the two scaling approaches described above indicated that neither approach is adequate for accurately scaling test results to full-scale plant geometry and conditions. The PUMA approach was deemed inadequate because it was overly simplified. It is based on simple geometrical (e.g. length, diameter, area) ratios and not on basic nondimensional groups such as Froude number. The scaling approach by Emami and Briens, although more rigorous, was also deemed inadequate because the nozzle diameters used in the tests were much smaller than the downcomer diameter, which may result in a different flow regime, and also because the analysis ignores the important inertial effect of the initial clearing of the water column and its effect on the initial depth of the gas jet.

The adequacy of both approaches was further investigated using CFD analysis. The investigation was performed as follows:

- One of the PUMA tests was used as a benchmark test to determine the adequacy of the CFD approach. The analysis was based on the test geometry and dimensions, as well as initial and boundary conditions. The test was simulated successfully and the CFD model was considered adequate for these type of predictions.

- An idealized full-scale CFD case was developed from the PUMA test using the PUMA scaling method. CFD analysis was performed using the idealized full-scale geometry and conditions. The scaled results and CFD results did not match. This suggested that the PUMA scaling approach was not appropriate.

- An idealized full-scale CFD case was developed from the same PUMA test using the Emami and Briens scaling method, and a CFD analysis was performed using the idealized full-scale geometry and conditions. The scaled results and CFD results did not match. This again suggested that the Emami and Briens scaling method was not appropriate for predicting the large scale behavior of the wetwell PS system.

A matrix of CFD cases was developed to further investigate the possibility of scaling the PUMA test results to actual plant conditions. The CFD runs included in this matrix were performed for various downcomer diameters (0.1 m, 0.2 m, and 0.6 m) and for various flowrates. The CFD sensitivity analysis results showed that because of distortion in the PUMA scaling approach, the PUMA test results may have fallen into a condition where the behavior of the jet was not representative of the actual jet at full-scale conditions. Therefore, it was concluded that it was not possible to scale the PUMA test results to actual plant conditions. However, it is considered appropriate to use the PUMA tests to generically benchmark the CFD methods used for performing the analysis of a downcomer jet in a full-scale plant geometry.

5.1.4 Conclusions Regarding Attempt to Scale Test Data to Plant Geometry

It was concluded that an approach to scale currently available test data for NCG behavior in a water pool to full-size geometry was not feasible. This conclusion also eliminated the option to pursue a synergistic scaling/CFD analysis effort and the ability to compare both independent results for verification purposes.

5.2 CFD Analysis of Suppression Pool

CFD analysis techniques have been used to simulate the vent clearing and NCG flow exiting a downcomer vent. The CFD technique has been used to simulate the LLL one-fifth Mark I test facility tests, the MIT scaled Mark I NCG blowdown tests, the University of California scaled Mark I tests, the scaled test results performed at Lappeenranta University, and the PSI small-scale tests. The CFD analyses for all but the Lappeenranta University and PSI analyses were performed using older CFD codes or using a CFD code specifically developed to analyze the Mark I NCG phenomenon. The CFD methods have improved since the older codes were used about twenty years ago. Recently Lappeenranta University has successfully used the CFD Fluent code to analyze the water clearing and NCG phenomena in the suppression pool. Similarly, PSI has used current CFD calculational methods to analyze its small-scale test data.

PSI has performed two-dimensional CFD analyses of air and steam-air flow into a water pool. The Lappeenranta University staff is also performing work to extend the CFD analysis to simulate the steam-noncondensable gas behavior in the suppression pool. This effort involves developing the direct condensation behavior on the bubble surface in contact with the suppression pool water. This new analysis is state-of-the-art work and is not recommended for general use at this time.

Considering the experience with CFD analyses for analyzing the vent clearing and NCG portion of the downcomer vent flow into the suppression pool following a LOCA, it is reasonable to assume that a CFD analysis could be used to analyze the initial vent clearing and NCG flow transient in a full-scale plant geometry.

CFD is being used to study the initial blast of NCG that is blown into the suppression pool following a LOCA in the containment of a Mark I BWR. This rapid blowdown of gas through a vertical downcomer pipe submerged in the suppression pool creates a large NCG region that spreads down and outward into the suppression pool. A safety concern relates to the possibility of the NCGs being pulled into the ECCS pump intakes. This could cause a significant degradation in pump performance or even pump failure. The pump intake system is submerged in the suppression pool and in some cases may be in close proximity to the downcomer pipes. The size, depth, and transient nature of the NCG region must be considered along with the intake locations, pump startup times, and pump performance characteristics to assess the potential effect of these scenarios. The present CFD analysis is focused on the issue of predicting the size, depth, and transient nature of representative gas bubbles that are blown down through a single downcomer pipe into the surrounding region of a suppression pool.

To build confidence in the modeling approach, the CFD methods are benchmarked using some related test data. The first test considered comes from the PPOOLEX test facility in Finland, which is described in Reference 49. Prior CFD analyses of these tests in Reference 26 are used as a foundation to build the current modeling approach. These prior analyses demonstrated the applicability of the VOF method for predicting the noncondensable bubble dynamics in a scaled suppression pool environment.

The second set of test data comes from the NRC-sponsored testing at the PUMA facility described in Reference 33. Three tests using air injected through a submerged 0.102 m (4 in.) downcomer pipe in a suppression pool are considered. The initial air injection period results in the maximum void penetration depth and spread. This initial phase of the blowdown is the focus for the analysis.

Full-scale test data and videos are considered from the steam-driven GKSS PS test facility in Reference 48. The facility setup and test data, however, are more focused on later stages of the blowdown event where steam condensation induced oscillation and chugging issues are of interest. Quantitative measurements of the size and depth of the initial large noncondensable bubble formed during the blowdown are not available from these tests. The videos do provide a qualitative understanding of the complexity of the initial blowdown event at full-scale conditions including the formation of many smaller bubbles that break away from the main bubble.

The verified CFD techniques were used to develop models of actual plant geometries and simulate the NCG behavior in a plant's suppression pool. This analysis could be used to define the NCG "exclusion zone" for plant geometries and to help define the void fraction at ECCS

pump strainer locations. The analysis would also help to define the time duration during which local void fraction effects at the pump strainer would be important.

5.2.1 PPOOLEX Tests

5.2.1.1 Background

The PPOOLEX facility consists of a 31 m^3 (1,095 ft^3) cylindrical tank with rounded end caps. The height and diameter are approximately 7.5 and 2.4 m (24.6 and 7.87 ft) respectively. The facility is divided into two regions by a plate that separates an upper (drywell) region from the lower (wetwell) region. A vertical blowdown pipe connects the upper and lower regions. This pipe has an inner diameter of 0.2141 m (8.43 in.) and is submerged in water that partially fills the lower wetwell region. During the tests, pressurized air is forced into the upper drywell region through an inlet plenum. The drywell region pressurization forces air down through the vertical blowdown pipe. After the water is pushed out of the lower end of the blowdown pipe, the air begins to exit and gas bubbles are formed in the wetwell region. The prediction of the size, shape, and duration of this gas region is the focus of the benchmark study. A more complete description of the test is contained in the Finnish report documenting some earlier CFD work on these tests (Ref. 26). An overview of the facility is provided in Figure 5.2.1-1 which is copied from the test report.
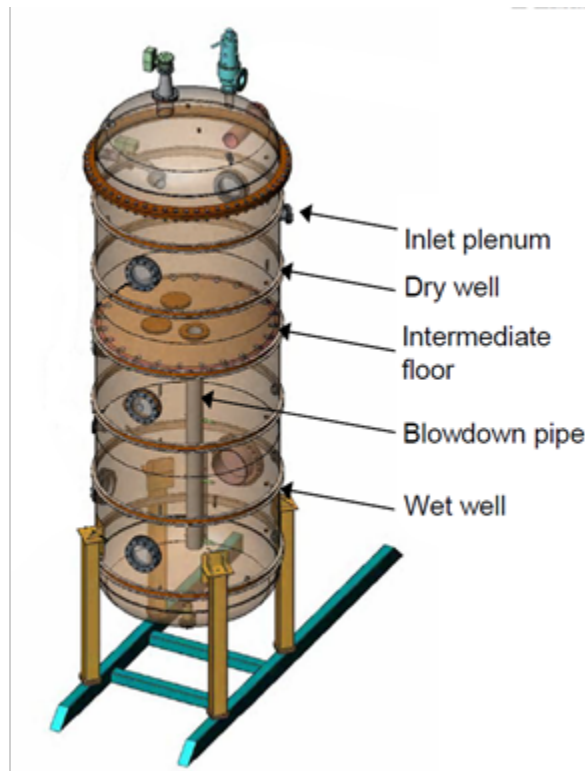
Figure 5.2.1-1: Overview of PPOOLEX Test Facility (Ref. 26)

Two tests from the PPOOLEX facility are considered for a CFD benchmark study. These tests are identified as CHAR-09-01 and test CHAR-09-03. The tests differed by the inlet plenum mass flow rates with test CHAR-09-03 having nearly three times the mass flow of test CHAR-09-01.

5.2.1.2 CFD Approach

A CFD model is created for the PPOOLEX test facility using the FLUENT v15.0 code. The model is setup using an approach similar to the one outlined in the 2008 Finnish report. That prior study also used the FLUENT code. The VOF method is used to track the interface between the air and the water as the bubble exits the blowdown pipe and rises through the wetwell. The VOF method solves a single set of momentum equations and tracks the interface between two non-mixing fluids. Each control volume in the model is filled with either one of the two fluids or is considered part of the interface. It is assumed that the interface dimensions are larger than an individual control volume and bubbles smaller than the CFD control volumes are not tracked. The method is appropriate for tracking large bubbles or interfaces in a liquid and can support compressible gases. The gas bubble is assumed to be noncondensable in this case. Table 5.2.1-1 lists the basic modeling options used.

Table 5.2.1-1: CFD Model Basic Solver Settings

Code	ANSYS/FLUENT v15.0
General	pressure based transient solver, gravity
Models	VOF Method, Implicit volume fraction scheme, energy equation
Turbulence	standard k-epsilon, standard wall functions, compressibility option
Materials	water (primary phase) air, ideal gas assumption (secondary phase)
Conditions	floating operating pressure, specified operating density = 0.0
Boundary Conditions	inlet – specified mass flow, constant temperature walls – adiabatic, no slip condition
P-V coupling	SIMPLE method
Discretization	density, momentum, energy turbulence – first order pressure – PRESTO time – second order (time step = 1/300 s)

5.2.1.3 Geometry/Mesh

The geometry is obtained from the Finnish report detailing the PPOOLEX experiments (Ref. 8). Small geometric details are omitted for this study because they are not expected to affect the gas bubble dynamics in the wetwell. The components included in the model are the main outer pressure vessel, the intermediate floor dividing the wetwell and drywell, the inlet plenum pipe, and the blowdown pipe. The dimensions and locations of these components are taken directly from the test report. All walls and surfaces are modeled with zero thickness. No solid structures are considered. Figure 5.2.1-2 illustrates the geometry used to define the CFD modeling domain. The cylindrical section of the large tank has an inner diameter of 2.38 m (93.7 in.) and the blowdown pipe has an inner diameter of 0.2141 m (8.43 in.). The blowdown pipe is slightly off the vertical axis of the cylindrical tank. Overall height of the facility is roughly 7.4 m (291 in.). The meshing refinement regions illustrated in Figure 5.2-2 are not part of the geometry. These regions are simply defined to help specify the mesh sizing in regions of interest.

Figure 5.2.1-3 illustrates the computational mesh design on a vertical plane. The mesh is created using the ANSYS meshing platform "cut cell" option which uses cubes to mesh the

entire domain. The dimensions of the cubes are successively cut in half for grid refinement. At walls, the cubes are skewed to maintain the outer wall shape. During the creation of the model several mesh designs were used and refined on an iterative basis to ensure the grid refinement regions covered the areas of interest for the air to water interface. The bulk regions of the model used cell dimensions of 0.08 m (3.15 in.) as a maximum size. The upper portion of the blowdown (downcomer) pipe was meshed using a cell size of 0.04 m (1.575 in.). The refinement regions which covered the initial water surface region, the submerged portion of the blowdown pipe and a region around this pipe were meshed with 0.01 m (0.394 in.) cells. This mesh design results in a total of 2.5 million computational volumes with the majority of these located in the mesh refinement regions.
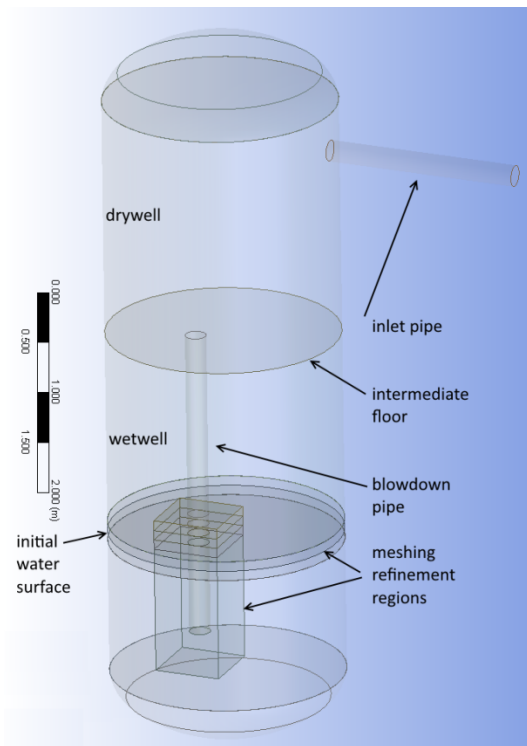
Figure 5.2.1-2: CFD PPOOLEX Geometry   Figure 5.2.1-3: PPOOLEX Computational Mesh
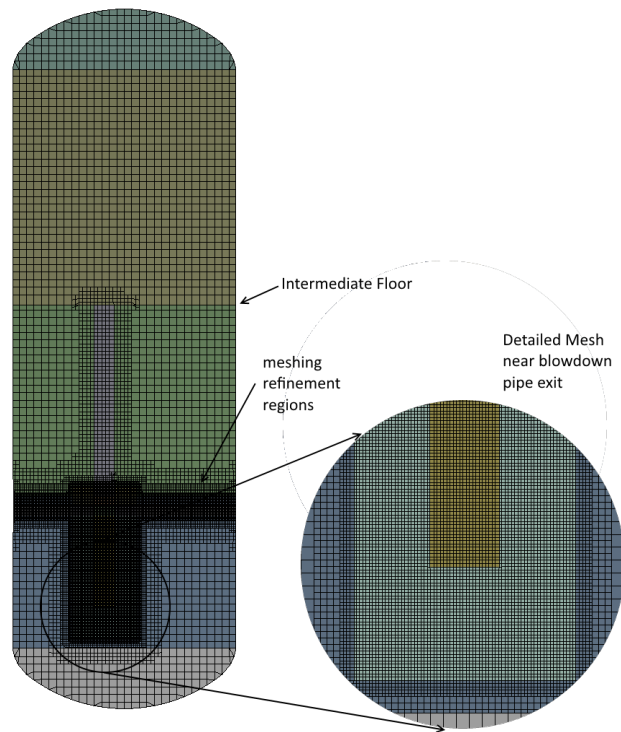
5.2.1.4 Boundary and Initial Conditions

The boundary and initial conditions are obtained from the PPOOLEX test report and the associated Finnish report documenting the prior CFD analyses. Tests 09-01 and 09-03 are considered because they span a wide range of mass flows. The interest in this study is the downward and lateral penetration of the initial gas bubble exiting the blowdown pipe. For this reason, only a short period of time is modeled and longer term effects such as wall heat transfer are not considered. Table 5.2.1-2 lists the boundary and initial conditions applied for each test. Only the mass flow of air is varied during the simulation and this is illustrated on Figure 5.2.1-4.

Table 5.2.1-2: Boundary and Initial Conditions for PPOOLEX Predictions

Condition	Test 09-01	Test 09-03
wall heat transfer	adiabatic	adiabatic
initial water temperature	297.1 °K (75.11 °F)	296.3 °K (73.67 °F)
initial air temperature	297.1 °K (75.11 °F)	296.3 °K (73.67 °F)
initial pressure	103,390 Pa (14.995 psi)	103,890 Pa (15.068 psi)
initial velocities	0.0	0.0
inlet air temperature	297.1 °K (75.11 °F)	297.1 °K (75.11 °F)
inlet mass flow	time-dependent table	time-dependent table
inlet turbulence estimation	5% intensity Hydraulic diameter 0.2 m (0.656 ft)	5% intensity Hydraulic diameter 0.2 m (0.656 ft)
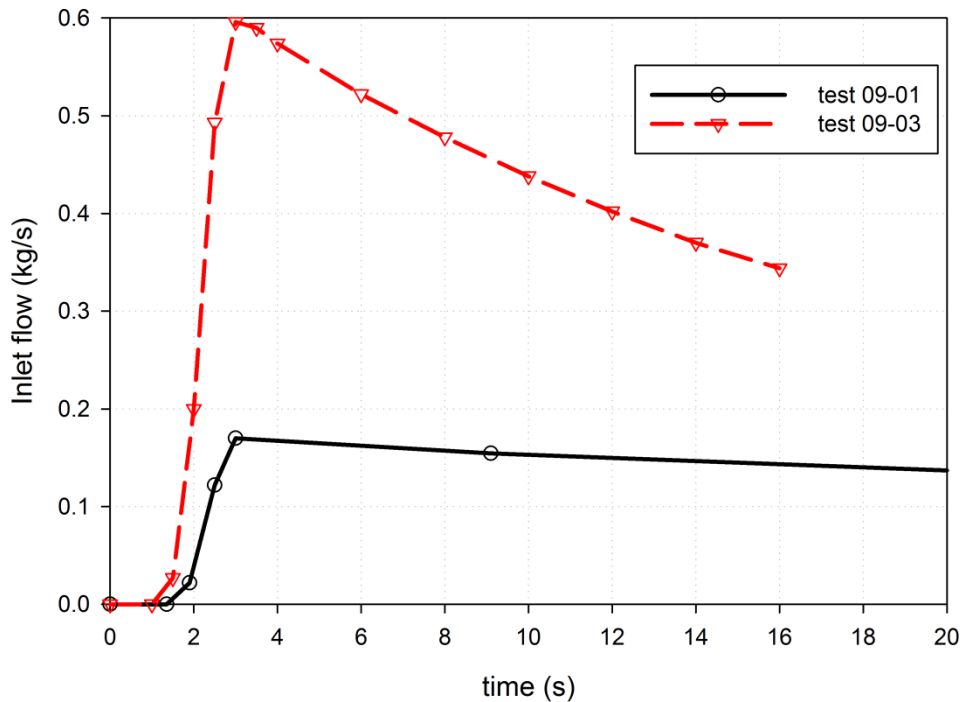
Figure 5.2.1-4: Mass Flow at Inlet for PPOOLEX Tests

5.2.1.5 Results

Only limited data are available from the PPOOLEX tests. Pressures and temperatures were measured, and there is video of the bubbles around the downcomer exit. The focus of this study is the penetration of the gas bubble into the wetwell liquid. Both depth and width of the gas bubble are of interest. Comparisons are made between the CFD predictions and the video to qualitatively compare the CFD predictions of bubble size and duration. Quantitative comparisons of predicted system pressures are used to demonstrate that the overall CFD boundary conditions and predicted system response are in line with the test. Temperature comparisons are not included because the duration of the first bubble is relatively short and

temperature variations are minimal. It is noted that initial temperatures are established to match the test data.

Figure 5.2.1-5 shows contour plots that highlight the predicted bubble size and location compared to test video frames at the same time intervals for test 09-01. The first frame is selected to correspond to the time when the bubble first starts to leave the blowdown pipe which is 10 seconds for test 09-01. Six video frames are shown alongside the CFD predictions. The original video frame rate is approximately $1/30^{th}$ of a second and every fourth video frame is shown. Simulation time is indicated on each set of figures. The qualitative results indicate that the CFD predictions adequately predict the bubble size, shape and duration. These results illustrate the first bubble that exits the blowdown pipe after the initiation of the mass flow. The simulation is carried out further to simulate the release of several more large bubbles into the wetwell region. The predictions matched the frequency of bubble formation for the duration of the simulation considered. This is a good indication that the boundary conditions for the CFD model are a good representation of the test conditions.
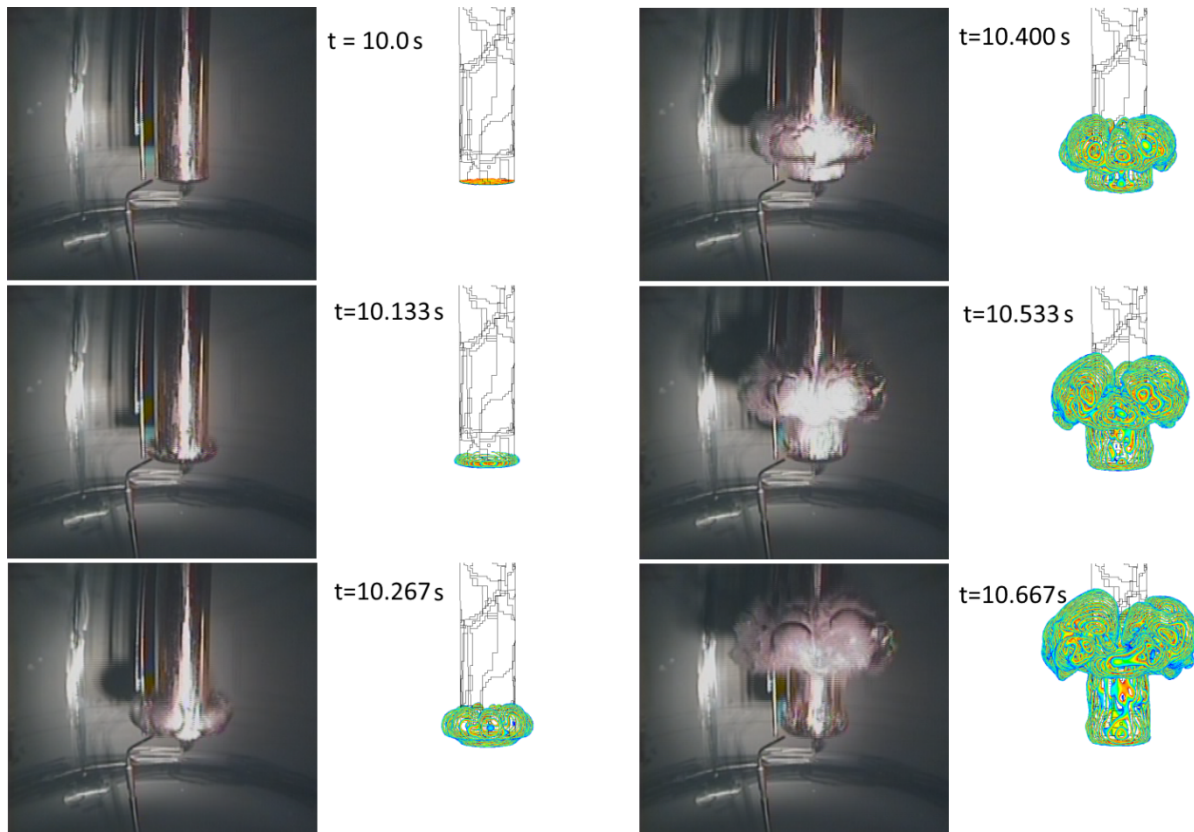
Figure 5.2.1-5: Comparison of Predicted Bubble Size and Location for Test 09-01

Pressures are monitored in the CFD prediction and compared to the test data for points in the drywell and wetwell. Figure 5.2.1-6 shows a comparison with three of the measured test pressures during the first 20 seconds of test 09-01. Pressures are considered in the upper drywell, the airspace in the wetwell, and a point submerged in the wetwell. The pressurization in the upper drywell (P1101) is well predicted by the CFD code. The initiation of the pressure rise and the total pressure rise are a good indication that the inlet boundary mass flow is properly

accounted for. The wetwell pressure (P04) is also predicted well. The initiation of the pressure rise around 10.0 seconds corresponds to the time when the gas bubble begins to emerge from the blowdown pipe. The rate of pressure rise after 10 seconds is a good indication that the mass flow of air exiting the blowdown pipe is accurately predicted. The predictions show a small upward bias in the pressure which remains consistent throughout the test. This could be the result of a reduced pressure at the start of the test (slight vacuum), which was not accounted for or a simple bias in the measurement. Overall the predictions do a good job of following the pressure from the experiment. A third comparison is made for the pressure measured near the exit of the blowdown pipe (P05). This pressure rise is similar to the dry measurement (P04) in the wetwell region but includes the hydrostatic pressure of the water above it. The predictions match the test data. The pressure response predictions indicate that the CFD model is setup correctly to model the incoming mass flow and that the timing and mass flow rates for gas entering the wetwell region is accurately represented.
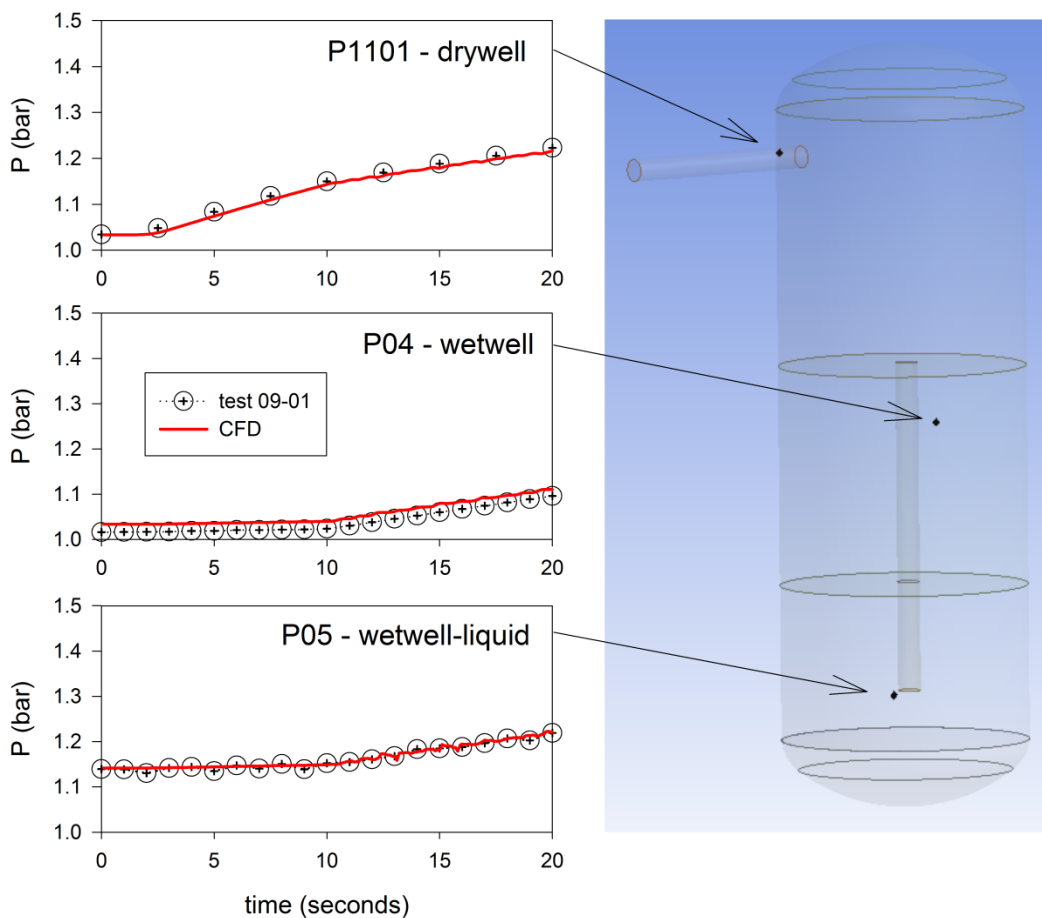
Figure 5.2.1-6: Comparisons of Predicted and Measured Pressures, Test 09-01

Test 09-03 has a mass flow rate that is approximately 300 percent higher than the mass flow in test 09-01. A similar CFD modeling approach is used for test 09-03 and similar results are obtained. Figure 5.2.1-7 shows contour plots that highlight the surface of the gas bubble exiting from the blowdown pipe compared to images taken from the test video. Once again, the CFD model does a good job of predicting the size, shape, and timing of the gas bubble blown down

45

into the wetwell region. There appears to be a slight tendency for the CFD model to predict the bubble to rise faster than the test video indicates but the difference is minor. The parameters of interest, depth and width of the bubble, are qualitatively well predicted as observed from the comparison with the video.
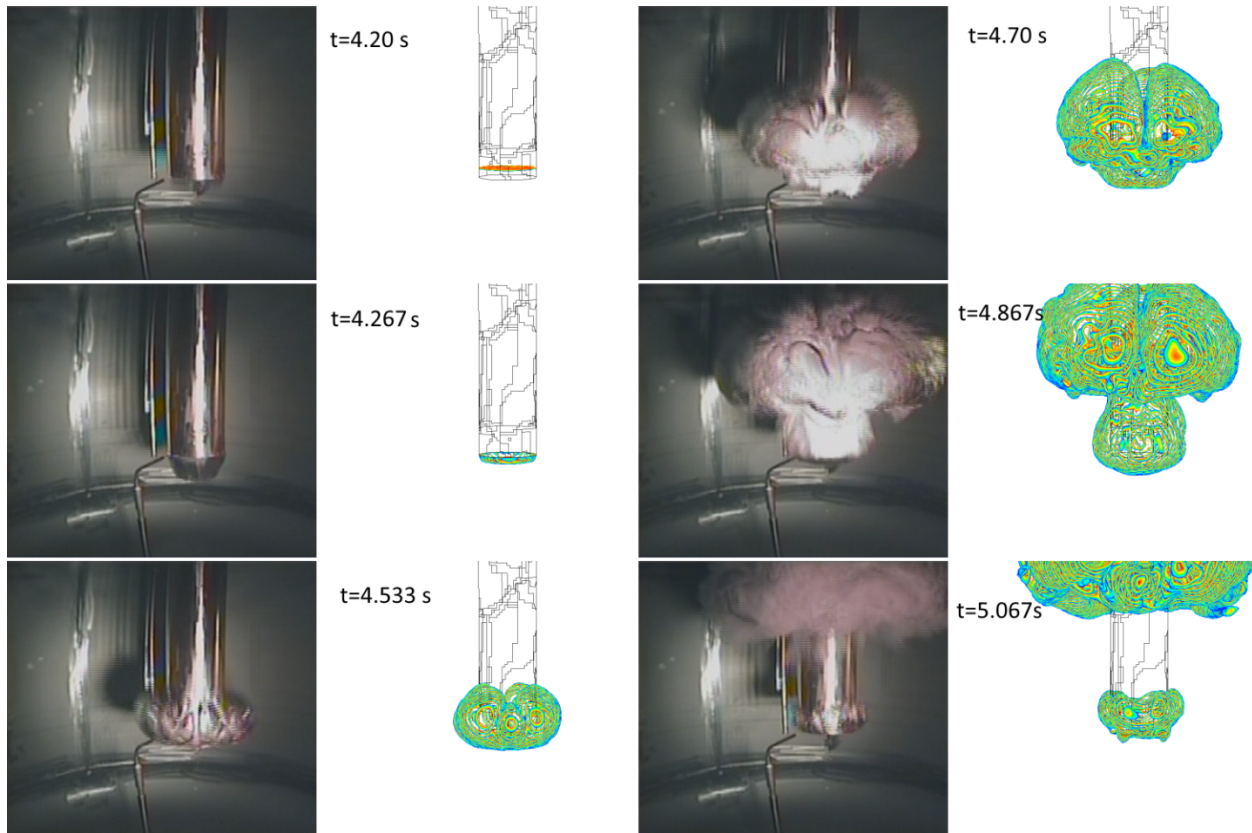
Figure 5.2.1-7: Comparison of Predicted Bubble Size and Location for Test 09-03

Pressures are monitored in the CFD prediction and compared to the measured test data for points in the drywell and wetwell. Figure 5.2.1-8 shows a comparison with three of the measured test pressures during the first 8 seconds of test 09-03. Pressures are considered in the upper drywell, the airspace in the wetwell, and a point submerged in the wetwell. The prediction of the pressurization in the upper drywell (P1101) matches the data very well. The trend for the wetwell pressure (P04) is also predicted well but there appears to be a slight shift in the initial pressure value and the timing for the start of the pressure rise. It is suspected that there is uncertainty in the timing of the rapidly changing boundary condition for the inlet mass flow during the initial phase of the transient and this could account for the difference in pressure rise time. The rate of the pressure increase is similar between the test and the predictions. The initiation of the wetwell pressure rise at around 4 seconds corresponds to the time when the gas bubble emerges from the blowdown pipe. A third comparison is made for the pressure measured near the exit of the blowdown pipe (P05). This pressure prediction also shows a slight delay in the pressure response compared to the test data but the rate of pressure rise is similar. Overall, the pressure response predictions indicate that the CFD model is doing a reasonable job of accounting for the incoming mass flow for the purposes of determining the bubble dynamics in the wetwell.
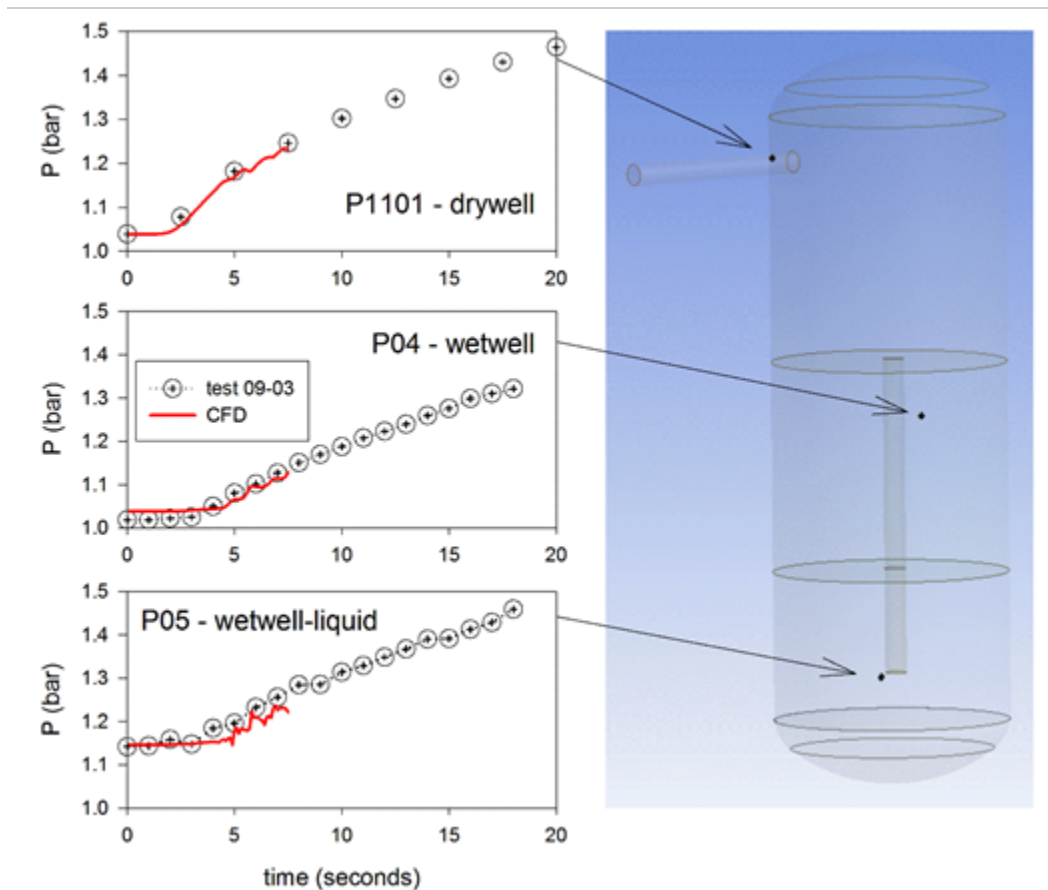
Figure 5.2.1-8: Comparisons of Predicted and Measured Pressures, Test 09-03

5.2.1.6 Conclusions

These PPOOLEX tests provide a valuable data set for benchmarking the capabilities of a CFD code to predict the general size and shape of NCG bubbles exiting from a submerged blowdown pipe. The VOF method used in the FLUENT code does an adequate job of predicting the overall bubble size, shape, and rise time based on the qualitative comparisons made with test videos. Pressures within the system are well predicted, which is a good indication that the CFD code is accurately representing the mass flows into and through the system.

One limitation of these tests is the minimal penetration depth of the gas bubble. The NCG exits the pipe and quickly turns upward towards the surface. Penetration depths are not measured directly but are estimated at 0.2 L/d (length to pipe diameter) and 0.5 L/d below the pipe outlet from the video for tests 09-01 and 09-03 respectively. This bubble depth is small compared to prototypical penetration depths at full-scale conditions where bubble penetration depths of several pipe diameters are expected. In addition, the NCG bubble remains well defined with little or no bubble break up. The limited penetration depth and bubble break up is not prototypical for a large-break reactor accident scenario.

5.2.2 PUMA Tests

5.2.2.1 Background

Building upon the lessons learned from the PPOOLEX modeling effort, a second test series from the PUMA test facility is modeled. The NRC sponsored this test program, and multiple blowdown tests are available for consideration. A few select tests from the steady-state test series are chosen for modeling to provide a wide range of conditions. Some scaling is included in the test report as the basis for the pipe sizing and water depth. Details of the test program, facility, and scaling analysis are found in the NUREG/CR-7186 (Ref. 33) documenting the testing.

Figure 5.2.2-1, which comes from the test report, illustrates some of the key dimensions of the test vessel. The 2.74 m (107.9 in.) ID vessel is a little over 3 m (118.1 in.) high. The initial water level for the tests is 1.05 m (41.3 in.) as measured from the inside base of the tank. The downcomer pipe is 0.102 m (4 in.) in diameter and is submerged 0.37 m (14.6 in.) (roughly 3.6 pipe diameters). A larger vent pipe, which is unused for these tests, is in place on the center line of the facility. The downcomer pipe is offset 0.68 m (26.8 in.) from the center of the tank to provide space for the bubble to expand.
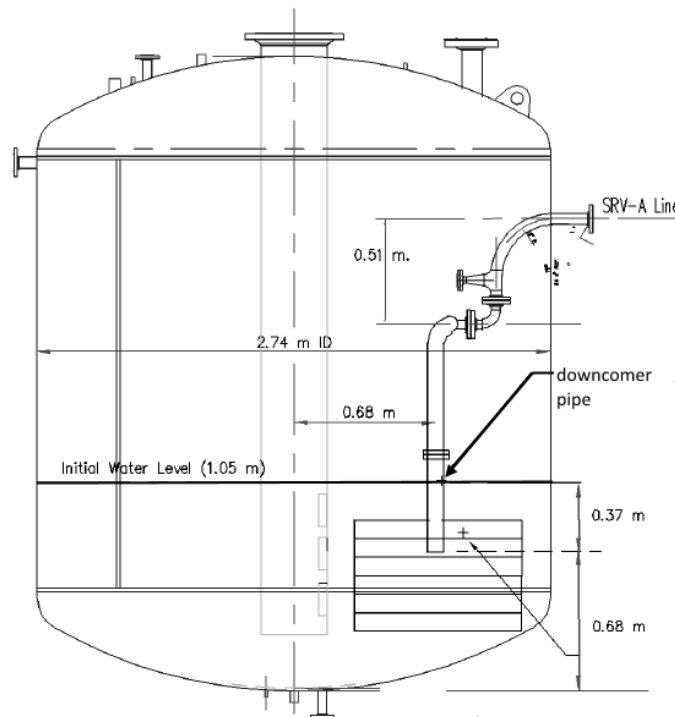
Figure 5.2.2-1: Overview of PUMA Vessel Used for Tests

There is a support structure built around the pipe exit to hold instrumentation for measuring the void fraction. Although the instrumentation probes are small, the support structure is relatively large, and there is a concern that this structure will break up the incoming air bubble as it expands out of the downcomer pipe. This is a qualitative observation only. Figure 5.2.2-2 shows

48

three frames of a test video before, during, and after the first bubble emerges from the pipe. The support structure is clearly shown in the figure, and it clearly interacts with the bubbles at various elevations.
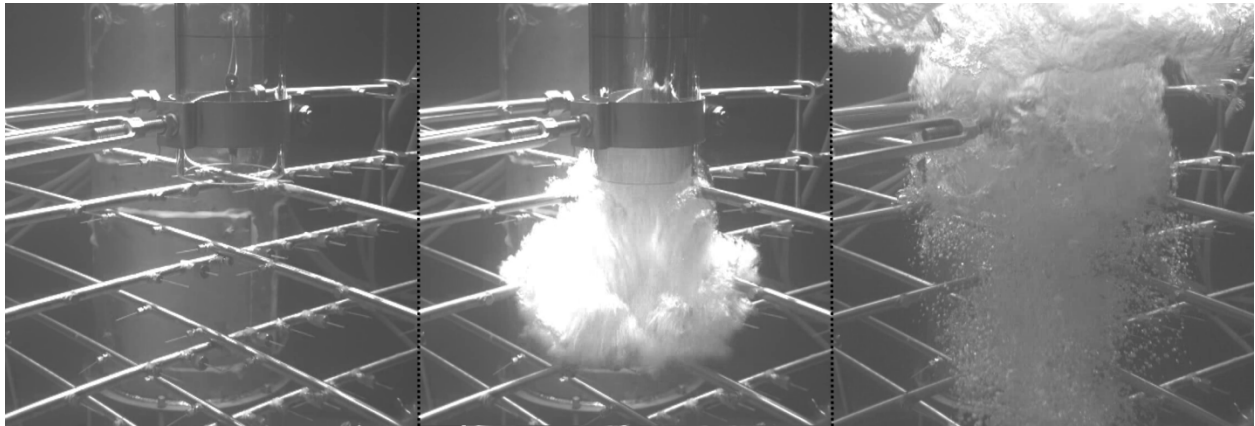
Figure 5.2.2-2: Video Frames Showing Downcomer Pipe and Instrumentation Supports

Support rods are placed below the downcomer exit directly in the path of the gas bubble as shown in the middle image of Figure 5.2.2-2. Dimensions and precise locations are not available for the support rods but the size of each rod appears to be around 8–10 percent of the downcomer diameter. The two rods crossing directly under the downcomer exit create a flow obstruction that is expected to add turbulence to the incoming flow and potentially affect the bubble dynamics. The PUMA tests showed a significant amount of small bubbles breaking away from the main bubble when compared to the PPOOLEX tests, which showed no significant void fraction away from the main bubble (see Figures 5.2.1-5 and 5.2.1-7). The right side of Figure 5.2.2-2 shows the region below the downcomer exit after the initial large bubble has risen. A cloud of small bubbles is left behind by the large rising bubble. These bubbles are observed to slowly rise back to the surface.

The observations of the small bubbles in the PUMA test are only qualitative. No direct measurements of these bubbles are included in the test report. They are noted here because the origin of the small bubbles is not clear. Although no small bubbles are observed in the PPOOLEX tests, the PUMA tests appear to be more dynamic based on the significantly larger bubble penetration depth. The deeper penetration of the main bubble (several pipe diameters) and the more dynamic nature (higher turbulence) of the PUMA tests is expected to result in more small bubbles. The support rods are noted as a possible source of additional turbulence and bubble break up. This observation is made to help understand the results and potential uncertainties in the results.

5.2.2.2 CFD Approach

The CFD model is created for the PUMA test facility using the FLUENT v15.0 code. The model is setup using the same VOF modeling approach applied successfully to the PPOOLEX tests outlined above. As before, the gas is noncondensable and only the initial bubbles are considered. See Table 5.2.1-1 for a list of the basic modeling options.

5.2.2.3 Geometry/Mesh

The geometry is obtained from the NUREG/CR-7186 report (Ref. 33), which details the PUMA facility experiments. Small geometric features are omitted to simplify the mesh design. The components included in the model are the main outer pressure vessel, the central vertical vent pipe (which is not used for these tests), and the downcomer (blowdown) pipe. The dimensions and locations of these components are taken from the NUREG/CR-7186 report. All walls and surfaces are modeled as zero thickness walls. No solid structures are considered. Small flanges, and other supporting structures, such as the instrumentation support rods near the downcomer exit, are not included in the model. The piping upstream of the vertical downcomer pipe is also simplified.

Figure 5.2.2-3 illustrates the geometry used for the CFD model. The vertical downcomer (blowdown) pipe is modeled in the position identified by the drawings. The test report identifies a 0.0508 m (2 in.) line that connects the 0.102 m (4 in.) downcomer pipe to the pressure vessel that supplies the gas for the test. The inlet boundary condition is established at the approximate location of the mass flow measurement on the 2 in. line. A horizontal length of 0.3048 m (12 in.) is used for the 0.0508 m (2 in.) line in the model to represent the flow path and volume between the mass flow measurement location and the entrance to the vertical downcomer pipe. Valves and elbows are not included in the CFD model of the inlet piping. The mesh is created using the same cubic mesh design (ANSYS cut-cell option) used for the PPOOLEX models. This approach uses a cubic mesh array with mesh refinements made by reducing the cube dimensions successively by one half. Hanging nodes (non-conformal mesh design) on the plane of the transition are a result of this approach. Transition regions are setup away from areas of interest to create a uniform mesh in the areas of interest. The main area of interest is the region below and around the downcomer exit. Other regions for refinement include piping and the water surface. Figure 5.2.2-4 shows a mesh cross section on a vertical plane of the model which includes the central vertical vent as well as the downcomer pipe. The mesh consists of 2.96 million cells.
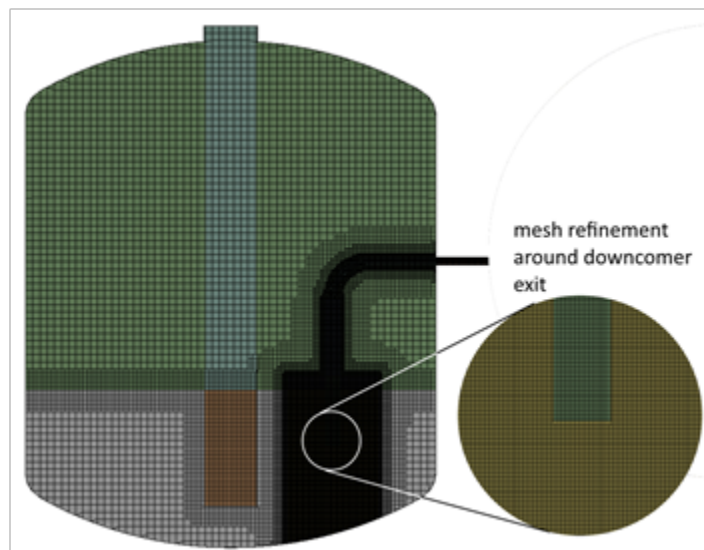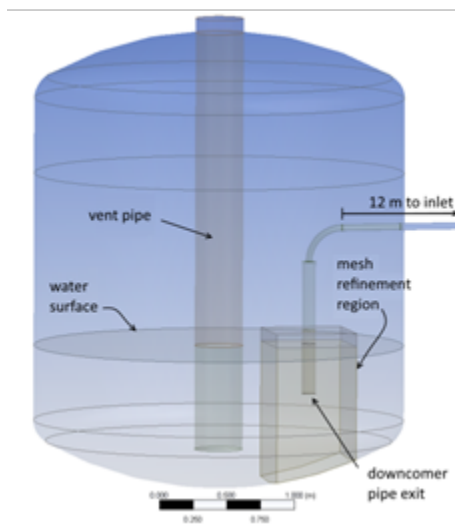
Figure 5.2.2-3: CFD PUMA Geometry   Figure 5.2.2-4: PUMA Computational Mesh

5.2.2.4 Boundary and Initial Conditions

Boundary and initial conditions are obtained from the PUMA test report. PUMA tests labeled as "steady state" test A1, A2, and A3 are considered because they provide a range of mass flow rates. The interest in this study is the downward and lateral penetration of the initial gas bubble exiting the blowdown pipe. For this reason, only a short period of time is modeled and longer term effects, such as wall heat transfer, are not considered important. Table 5.2.2-1 lists the boundary and initial conditions for the CFD simulations. Only the mass flow of air into the inlet pipe is variable. These flow rates are plotted in Figure 5.2.2-5.

Table 5.2.2-1: Boundary and Initial Conditions for PUMA Models

Condition	A1	A2	A3
wall	adiabatic	adiabatic	adiabatic
initial water temperature	296.4 K (73.85 °F)	296.2 K (73.49 °F)	297.3 K (75.47 °F)
initial air temperature	296.4 K (73.85 °F)	296.2 K (73.49 °F)	297.3 K (75.47 °F)
initial pressure	102,440 Pa (14.858 psi)	102,440 Pa (14.858 psi)	102,470 Pa (14.862 psi)
initial velocities	0.0	0.0	0.0
inlet air temperature	288 °K (58.73 °F)	288 °K (58.73 °F)	288 °K (58.73 °F)
inlet mass flow	time-dependent	time-dependent	time-dependent
inlet turbulence estimation	5% intensity; hydraulic diameter 0.05 m (0.164 ft)	5% intensity; hydraulic diameter 0.05 m (0.164 ft)	5% intensity; hydraulic diameter 0.05 m (0.164 ft)
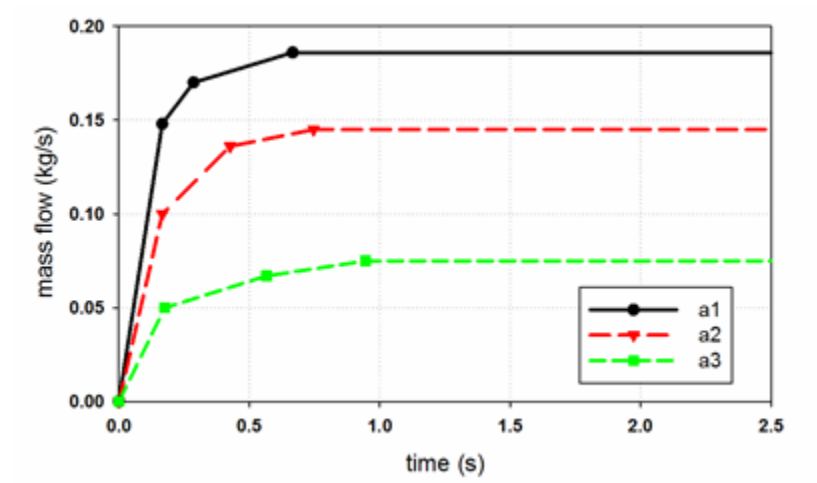
Figure 5.2.2-5: Mass Flows at the Inlet Pipe Boundary for the PUMA Tests

5.2.2.5 Results

The PUMA testing involved limited measurement locations and a high-speed video that captured bubbles emerging from the downcomer pipe. A qualitative comparison is made for each of the tests with the video. Figures 5.2.2-6, 5.2.2-7, and 5.2.2-8 show selected snapshots in time for tests A1, A2, and A3 respectively. Each test is compared to contour plots of void fraction from the CFD predictions at equivalent times. The contour plots show the void fraction

in a range from 0.4 to 0.6 which highlights the interface region between liquid and gas in the prediction. Times shown on the figures are from the CFD simulation. The test video times did not correspond to the actual test times. The time scale on the video was shifted so that the timing of the first emergence of gas from the downcomer pipe was identical for the CFD prediction and the test video.
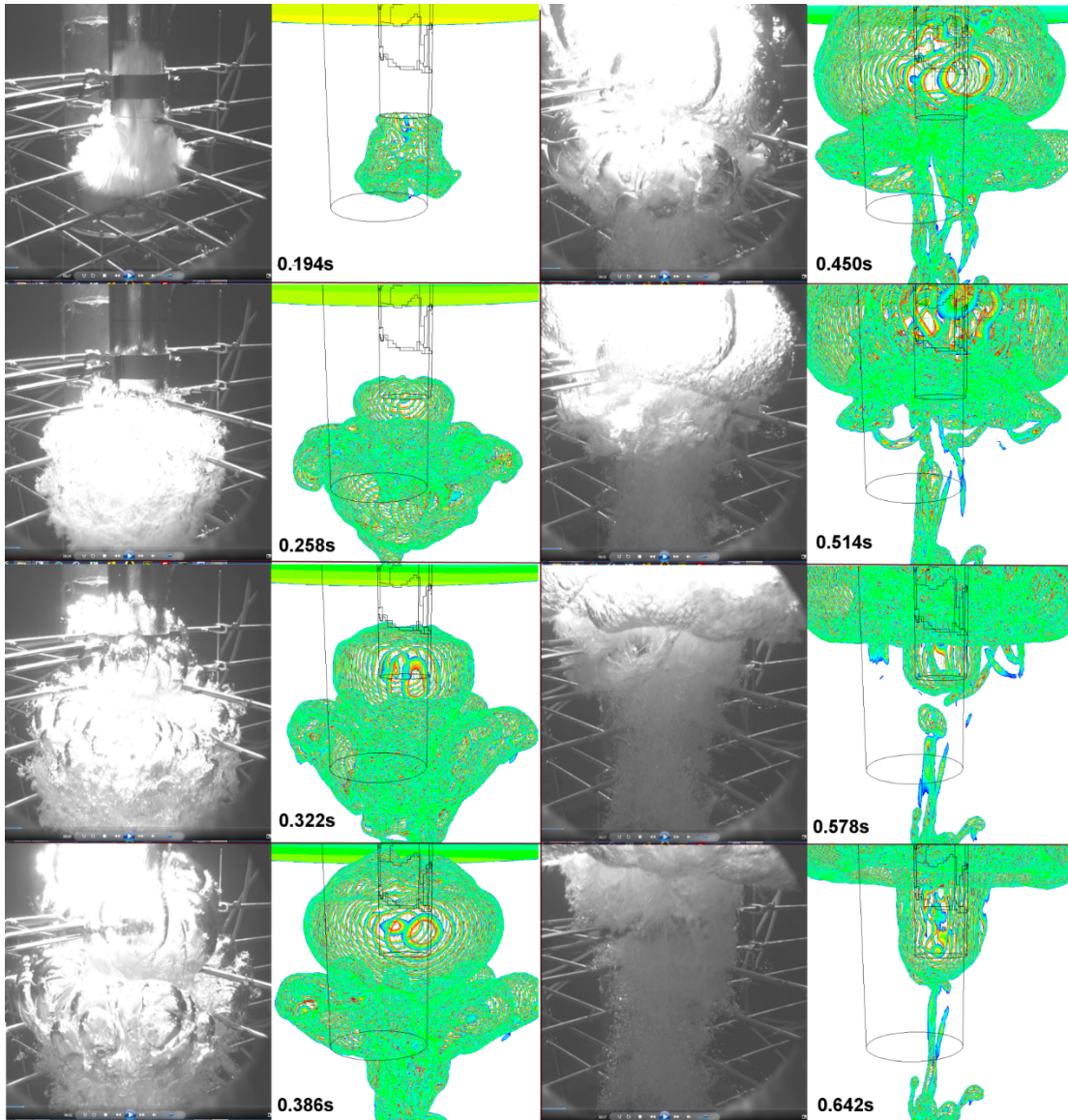
Figure 5.2.2-6: Comparison of Test Video and CFD Predictions for Test A1
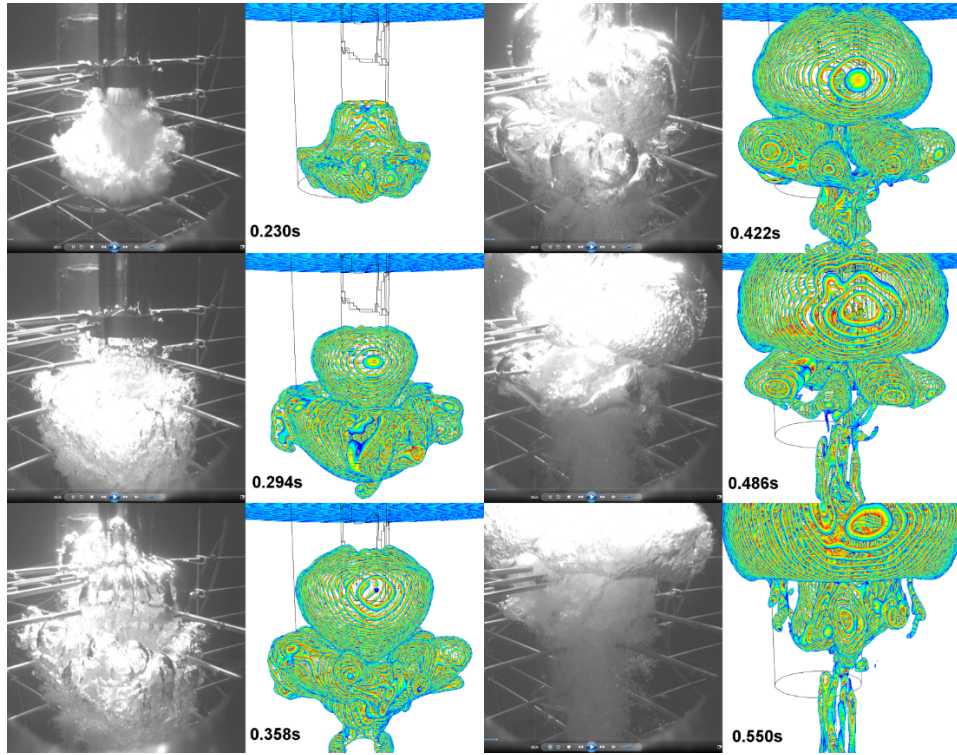
Figure 5.2.2-7: Comparison of Test Video and CFD Predictions for Test A2
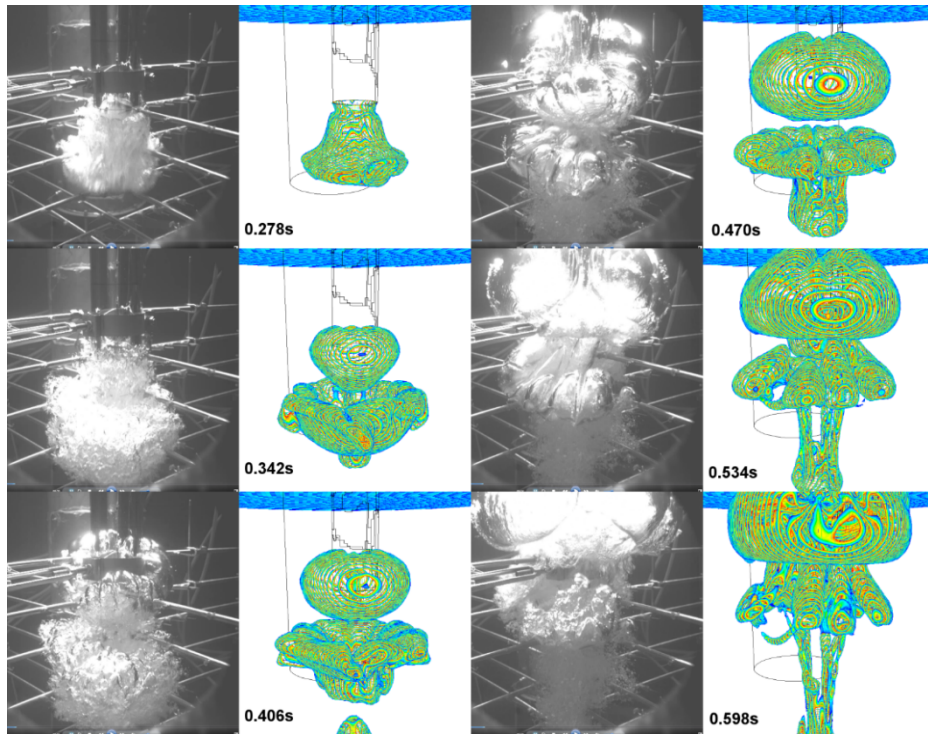
Figure 5.2.2-8: Comparison of Test Video and CFD Predictions for Test A3

53

The video comparisons show the dynamic bubble response and demonstrate how quickly the first large bubbles expand down into the pool and then rises again towards the surface. In just a little over 0.3 seconds, the main bubble exits the downcomer pipe, plunges nearly three pipe diameters into the pool, and then rises up past the downcomer pipe exit. As illustrated by the video images, when the main bubble rises up towards the surface, it leaves behind a trail of smaller bubbles which rise more slowly. These smaller bubbles are also affected by any overall fluid motion in the pool.

The tests generally show an initial large bubble forming and then, after a slight pause, another large bubble forms above the first. The entire region is generally connected and begins to rise quickly with the upper bubble still expanding as gas exits the downcomer pipe. The initial bubble follows the second bubble upward and is broken down as it joins the first leaving behind a smaller set of bubbles in its wake.

The CFD predictions qualitatively match the test video. The same general behavior is observed with an initial bubble penetrating down approximately 3 pipe diameters and then another large bubble forming above it just below the downcomer exit. As the bubbles rise, there is a small amount of gas left in the wake. The CFD predictions using the VOF method are not able to predict the cloud of small bubbles observed in the tests because of the resolution of the computational grid. It is encouraging, however, that an overall similar behavior is predicted.

The depth, spread, general structure, and timing of the bubbles are well predicted based on the comparisons with test videos. Details of the bubbles outer structure are slightly different, and this is not surprising given the uncertainty in the rapidly changing blowdown boundary conditions and the absence of the support structures in the CFD model. Another important factor in the bubble dynamic behavior is the piping upstream of the downcomer exit. Sensitivity studies show that changing the pipe length has an effect on the bubble dynamics. It appears that as the bubble begins to form and exit the pipe, the pressure drops in the piping and the mass flow exiting the pipe is dependent upon the total volume of pipe upstream of the exit as well as any flow restrictions. The final predictions are made with a simplified piping system that approximates the upstream length and volume to the mass flow measurement location, which serves as the inlet boundary condition.

The video comparisons show qualitatively that the CFD predictions do a reasonable job of predicting the bubble dynamics and structure. Quantitative comparisons of bubble dynamics are also made using the available data. The test included void fraction measurements at a few selected locations. These measurements, however, do not provide the resolution needed to quantify the bubble. The test report also included a quantitative reading of the bubble penetration depth obtained by scaling results off of the video frame. These measurements are compared to similar measurements made from the CFD predictions. Figure 5.2.2-9 shows the penetration depth for tests A1, A2, and A3 as a function of time. The CFD predictions are read from contour plots similar to the example shown from test A2 in the middle plot on Figure 5.2.2-9. A grid array is overlaid on the image showing L/d lines. All data are reported in the normalized L/d scale.
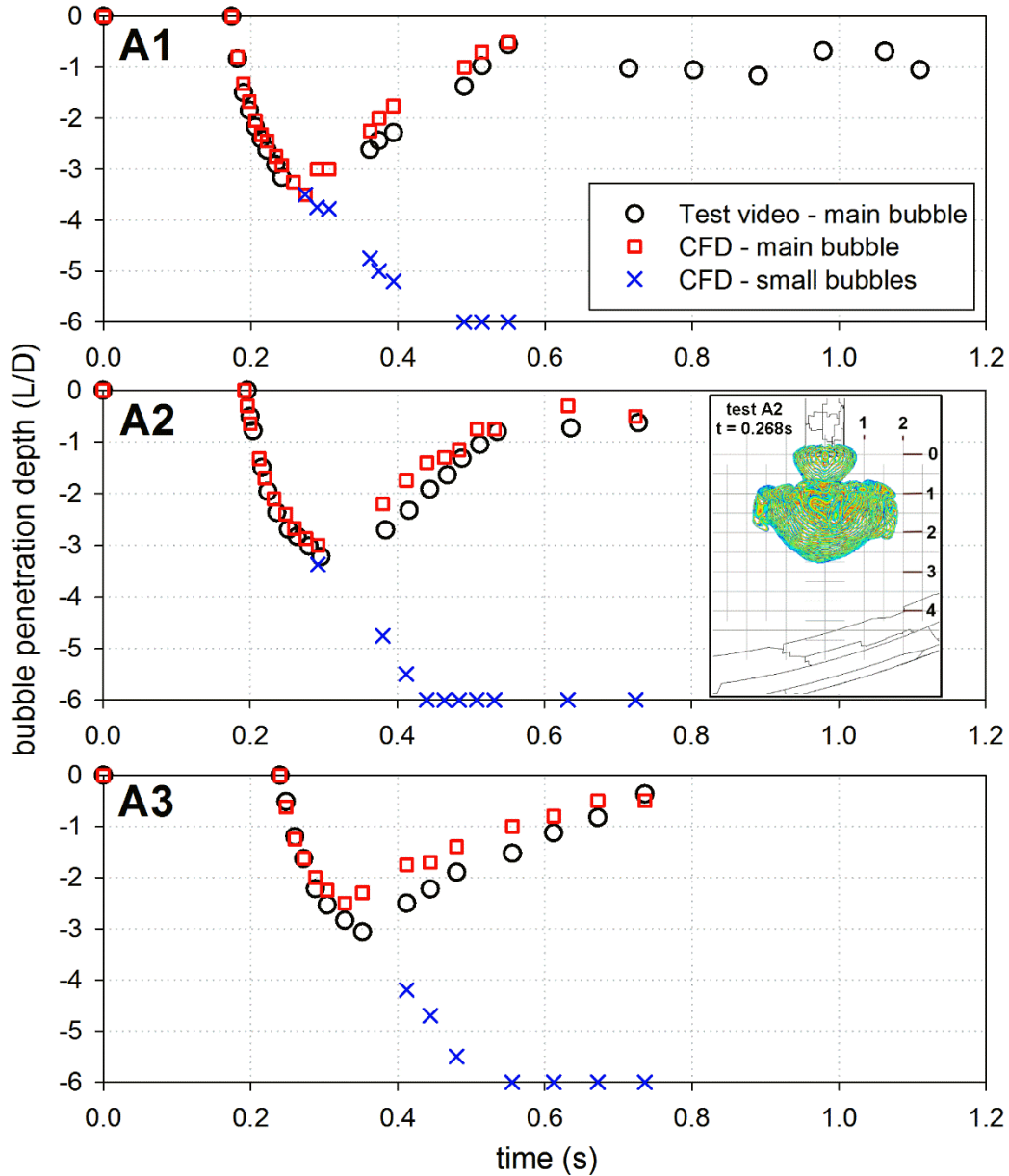
Figure 5.2.2-9: Penetration Depth vs Time Comparisons for PUMA Tests

The results in Figure 5.2.2-9 indicate that the CFD model does a good job of predicting the main bubble penetration depth and rise time. Several observations should be made to help qualify the results. The PUMA test data readings from the video only focused on the main bubble region. The small bubbles that appear in the wake behind the rising large bubble are not considered in the test report. Another consideration is that scaling depth from video frame images can result in some measurement uncertainty. A complication is the identification of the lower edge of the main bubble when there is an attached wake of smaller bubbles. During this time, there is uncertainty in the precise location of the lower interface of the main bubble. The video field of

view is also an issue. The vantage point is above the lowest point of the main bubble and a direct view of the lower edge of the main bubble may be obstructed by the bulging sides of the bubble region. In addition, the facility view port window blocks off visibility for anything below approximately -3.2 L/d. It appears from the videos of these tests that the main bubble does not penetrate further below this depth. Observations of smaller bubbles below this depth, however, are not possible. There is also no instrumentation at these lower levels.

The CFD predictions do a good job of predicting the bubble penetration depth. This is especially true while the bubble is descending and only the main bubble is present. During the period when the main bubble is rising, the location of the lower edge is difficult to determine from the CFD predictions. This is because of the difficulty in identifying the interface between the main bubble and the attached wake. The observations made when the bubble penetration depth is growing are generally more accurate than the predictions associated with the period of time when the bubble is rising with an attached wake.

The CFD method used does not resolve small bubbles that break away from the main bubble but does predict a small contiguous region that detaches from the main bubble in a manner similar to the test observations. This region not only forms in the wake of the large bubble but also continues downward during the initial penetration forming a small amount of NCG that penetrates towards the floor of the pool (at L/d = -6). This region is tracked in the CFD results and plotted in Figure 5.2.2-9 as the "small-bubbles." These small bubbles do not emerge from the main bubble until it begins to rise. The smaller bubbles do not rise quickly and are affected by the global liquid flow patterns in the pool.

An interesting result is the relative consistency of the bubble penetration depth for all three tests. The different mass flow rates for each test do not affect the penetration depth, which is just over 3 pipe diameters for each test. The bubble duration is also similar for each test. Within 0.4 to 0.5 seconds, the bubble exits the downcomer pipe, penetrates downward 3 L/d, and rises up past the downcomer exit. In all three tests considered the predicted small bubble region extended to the floor of the facility at L/d = -6.

The width of the NCG region is similar for all three tests. Tests A1 and A2 extend outward approximately 2.25 L/d at the maximum point below the downcomer exit. Test A3 extends outward approximately 2 L/d at the maximum spread while the main bubble is below the downcomer exit. The test results include bubble spread measured at one fixed elevation with limited instrumentation. These limited instruments do not capture the maximum bubble spread which is observed at a different elevation. Direct comparisons with the test data are not attempted.

5.2.2.6 Conclusions

These PUMA tests provide benchmark test data for assessing the capabilities of a CFD code to predict the general size and shape of NCG bubbles emerging from a submerged blowdown pipe. The VOF method used in the FLUENT code does an adequate job of predicting the overall bubble size, shape, and rise time based on the comparisons made with test data. The good comparisons suggest that the applied CFD approach is adequate for predicting bubble penetration depths and rise times.

One limitation of these tests is the structural blockages associated with the instrument support rods. These rods potentially influence the bubble shape and break up characteristics. Another

limitation is the lack of measurements for the small bubbles that break away from the main bubble and the lack of visibility for bubbles approximately 3.2 L/d (and deeper) below the downcomer exit. Penetration depths for all three tests (three different mass flow rates) are similar at just over -3 L/d.

5.2.3 Full-Scale Simulations

5.2.3.1 Background

The methods used to simulate the two small-scale test programs are applied to a full-scale scenario based upon MELCOR predictions of a postulated large-break LOCA (recirculation line break scenario considered) in a BWR Mark I design discussed in Section 2 and Reference 2. The MELCOR analysis provides the drywell and wetwell initial conditions, the predicted drywell and wetwell transient pressures and temperatures, as well as the predicted mass flow rates through the downcomer vent system into the wetwell region (see Figures 2.1-4, 2.1-5, 2.1-6 and 2.1-7). These values are used, along with a simplified representation of a BWR suppression chamber geometry to make predictions of the NCG bubble penetration depth and duration after exiting the blowdown pipe. The BWR Mark I geometry is used because it represents one of the smaller wetwell (suppression chamber) regions with some designs having pump strainer screens in close proximity to the downcomer pipe.

The large-break LOCA scenario is considered for this analysis because it is predicted to develop the highest drywell pressures. The boundary conditions used as well as flow paths, flow areas, and volumes are representative of a typical BWR design. These values could be different for other Mark I BWR designs. Figure 5.2.3-1 shows an overview of a Mark 1 BWR containment. The area of interest for this study is the suppression chamber.
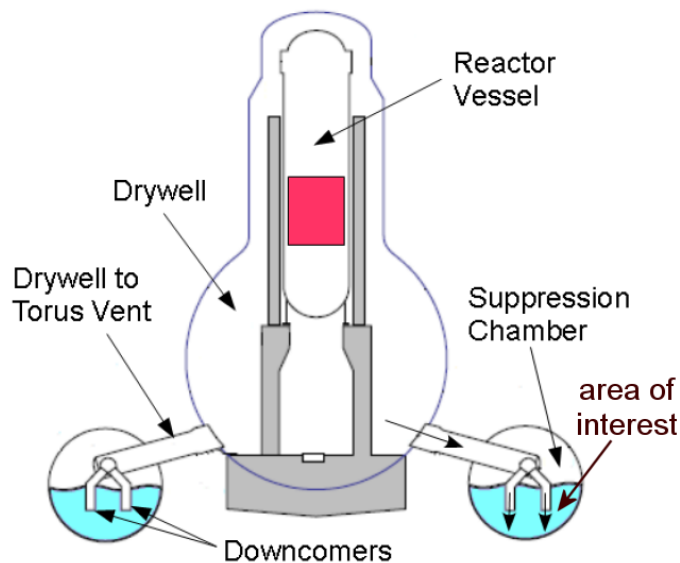
Figure 5.2.3-1: Generic BWR Mark I Containment Layout

5.2.3.2 CFD Approach

An initial CFD model is created for the full-scale simulations using the modeling approach demonstrated for the scaled test facilities above. The basic solver settings are outlined in Table 5.2.1-1. It is assumed that the downcomers and drywell to torus vent piping will be initially filled with liquid below the suppression pool water level and with NCG above the water column. Consequently, after the liquid is expelled from the downcomer, the subsequent vent flow is assumed to be 100 percent NCG. The assumption of 100 percent NCG is expected to provide a conservative prediction of the size and duration of the NCG bubble in the suppression pool.

In comparison, for the MELCOR predictions shown in Figure 2.1-7, the initial flow from the drywell to wetwell is a mixture of steam, water droplets, and NCG. As shown if Figure 2.1-8, the initial vent flow is calculated to contain a maximum NCG mass fraction of about 73 percent. The mass fraction of NCG in the vent flow is predicted to rapidly drop below 10 percent after 2 seconds following the start of the LOCA.

It is suspected that many small bubbles may break away from the main bubble during the initial blowdown phase under full-scale conditions. This is based on qualitative insights gained from video recordings of full-scale tests. Bubbles smaller than the CFD control volumes are not tracked with the VOF method. This modeling limitation poses some additional uncertainties for these full-scale predictions. In addition to the VOF method outlined above, a Eulerian-based two-phase CFD approach is applied to add further insights to the analysis. This approach allows interpenetrating fluids and has the capability to track the void fractions associated with any small bubbles that break away from the main bubble. The Eulerian approach, however, is far less robust than the VOF methods, and no data are readily available to benchmark this approach. The Eulerian results serve as only an indication of the potential bubble behavior and significant work is needed in this area to build further confidence in the Eulerian approach under these conditions.

5.2.3.3 Geometry/Mesh

A simplified geometry is developed based upon information obtained from several sources. Volumes and flow areas from the MELCOR model are used as a basis. The model is based on a torus geometry with a major diameter of 32.61 m (107 ft) and a cross-sectional diameter of 8.53 m (28 ft). The total number of downcomer pipes is 80 and each downcomer pipe has an inner diameter of 0.59 m (23.2 in.). The downcomers are assumed to be arranged in 40 pairs and spread evenly around the torus.

For the CFD model, a section of the torus equal to $1/40^{th}$ of the total is assumed to be cylindrical (straight) and this section contains a pair of downcomer pipes. The small cylindrical section is 2.56 m (8.4 ft) in length and its volume is equal to $1/40^{th}$ of the full torus volume. To further reduce the size of the computational domain, a symmetry plane is assumed between the two downcomer pipes so that only ½ of this region (or about $1/80^{th}$ of the torus region) is modeled. Figure 5.2.3-2 illustrates the CFD model domain for the full-scale simulation. The model consists of the symmetrical half section of an 8.52 m (27.95 ft) inner diameter cylinder (representing the torus) with a length of 2.56 m (8.4 ft). The downcomer pipe has an inner diameter of 0.59 m (23.2 in.) and a total length, from inlet boundary to exit, of 20 m (65.62 ft). The 20-m length is selected to create a volume upstream of the downcomer exit that is consistent with $1/80^{th}$ of the volume of the drywell to torus vent piping system based upon the MELCOR model. The geometry is broken up into a few volumes to make creating initial

conditions easier. The lower volumes, with an upper level 3.86 m (12.66 ft) from the base of the domain, are initially filled with water. The downcomer pipe exit is 1.0 m (3.28 ft) below the water surface (or 2.86 m (9.38 ft) above the base of the domain).

The mesh design is similar to that used for the benchmark studies above. The ANSYS Fluent cut-cell mesh design uses cubic meshes with refinement regions created by successively dividing each edge of the cubes in half for each level of refinement. These refinement transition regions are created away from the expected bubble domain. Figure 5.2.3-3 illustrates a cross section of the computational mesh on a vertical plane through the downcomer pipe. Mesh sizes range from 0.02 m (0.787 in.) in the most refined region up to 0.32 m (12.6 in.) for the largest cells above the water surface. The total number of cells is 3.3 million.
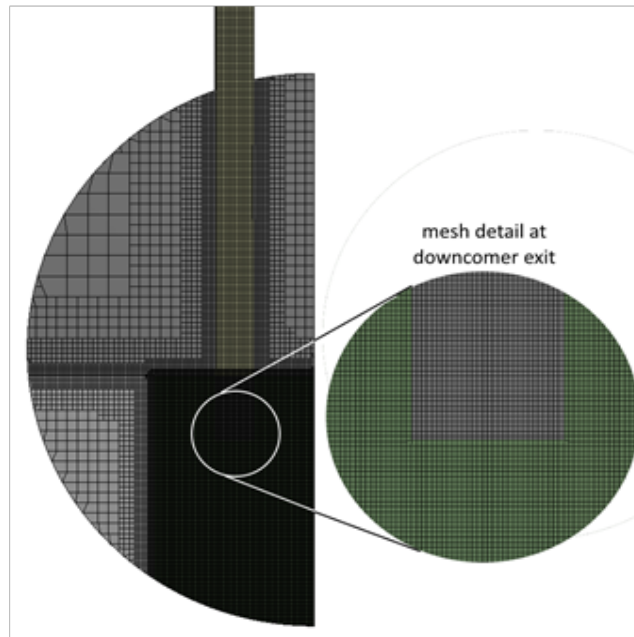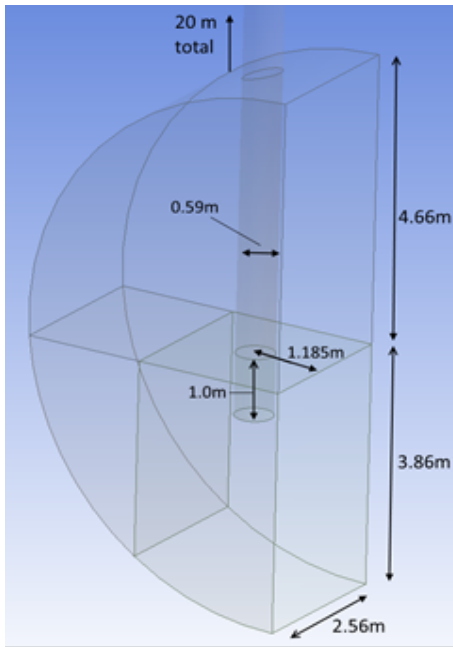
Figure 5.2.3-2: CFD Torus Section Model   Figure 5.2.3-3: CFD Torus Section Mesh

5.2.3.4 Boundary and Initial Conditions

The boundary and initial conditions are based on predictions from a MELCOR code simulation of a recirculation line break. The MELCOR predictions provide the basis for the initial temperatures of the liquid and gas spaces, the initial system pressure, and the time-dependent mass flow from the drywell to the vent pipes. The mass flow prediction from MELCOR includes the total mass flow from the drywell into the vent piping system which includes 80 downcomer pipes. Because only one downcomer pipe is modeled with CFD, the inlet mass flow condition is set to $1/80^{th}$ of the MELCOR value (Figure 2.1-6). For the CFD analysis, the initial gas in the drywell, vent piping system, and wetwell gas space is assumed to be NCG. The drywell and vent system gas is assumed to make up the gas blown down into the suppression pool. Because the focus is on the initial gas bubble, only noncondensables (air in this case) are considered. Table 5.2.3-1 lists the boundary and initial conditions applied to the CFD model. Only the mass flow of air into the inlet pipe is varied with time during the simulation. The assumption that all of the initial flow is composed entirely of air is expected to lead to a

conservative prediction of the depth and size of the initial NCG bubbles in the suppression pool. Figure 5.2.3-4 illustrates the time-dependent mass flow into the inlet pipe boundary condition. MELCOR predictions (Figure 2.1-6) have provided the total mass flow of gases, including steam, and the CFD boundary condition assumes this entire flow is composed of air which will be pushed out of the pipe in front of the steam. All walls are considered to be adiabatic because potential heat losses are considered minimal during the short duration of the initial blowdown.

Table 5.2.3-1: Boundary and Initial Conditions for Torus Model

Boundary Condition	Value
wall heat transfer	adiabatic
initial water temperature	330.4 °K (135.05 °F)
initial air temperature	330.4 °K (135.05 °F)
initial pressure	111690 Pa (16.2 psi)
initial velocities	0.0
inlet air temperature	330.4 °K (135.05 °F)
inlet mass flow	time-dependent table
inlet turbulence estimation	5% intensity, Hydraulic diameter 0.6 m (1.97 ft)
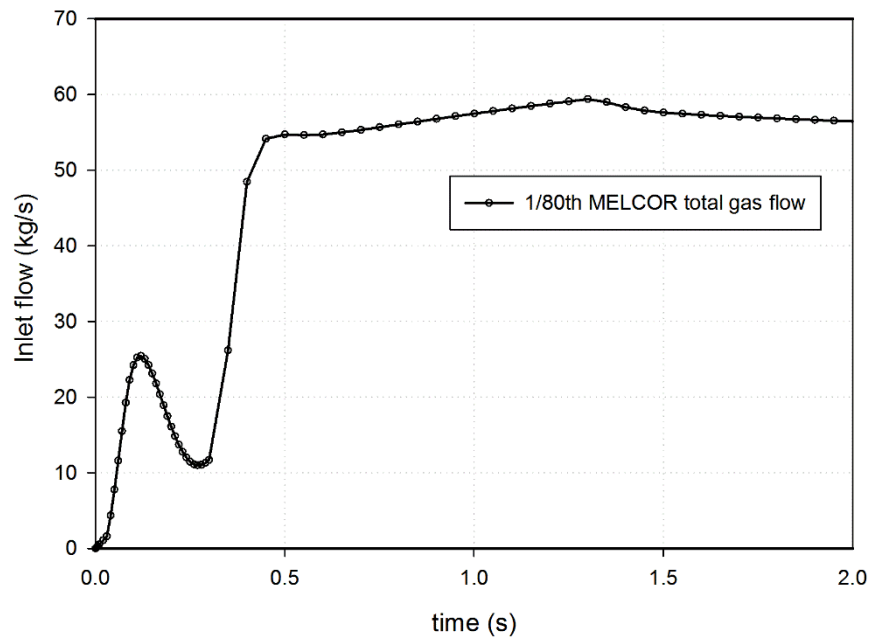
Figure 5.2.3-4: Mass Flows at Inlet for Full-Scale Simulation

5.2.3.5 Results

The focus of this study is the penetration of the gas bubble into the wetwell liquid. Both depth and width of the gas bubble are of interest. Before considering the bubble dynamics, a series of sensitivity studies are completed to ensure that the modeling is consistent with our expectations based upon the MELCOR predictions. All indications are that the CFD predictions are consistent with expectations of torus pressure and vent mass flow when compared to the MELCOR

predictions. The fluid clears from the downcomer pipe in approximately 0.3 seconds in both codes. The pressure rise in the wetwell (suppression chamber) is also consistent with the MELCOR analysis. These qualitative comparisons build confidence in the overall setup of the CFD model domain and boundary conditions. Matching the pressure rise in the suppression pool helps ensure that the mass flow out of the downcomer pipe is consistent with the MELCOR model. Several sensitivity studies are completed on the mesh size, turbulence models, interfacial tracking methods, time step size, and downcomer pipe pressure drop to ensure that the final predictions are not sensitive to these parameters. Temperature comparisons are not included because the duration of the first bubble is relatively short and temperature variations are minimal. It is noted that initial temperatures are established to match the MELCOR modeling.

Figure 5.2.3-5 shows contour plots of void fraction in the suppression pool at various times for the VOF method predictions. The contour plots are clipped between 0.1 and 0.9 to remove all of the pure gas or liquid regions. This view shows only the interface transition between water and gas and highlights these surfaces. The water surface and the expanding gas bubble surface are clearly highlighted. Grid lines are overlaid in the region around the downcomer exit to help quantify the size and depth of the gas bubble. These grid lines are centered on the pipe exit and spaced at a distance of ½ the downcomer pipe diameter ($\frac{1}{2}$ D = 0.295 m (0.968 ft)).

Figure 5.2.3-5: Contour Plots of Time-Dependent Bubble Interface (VOF Method)

61
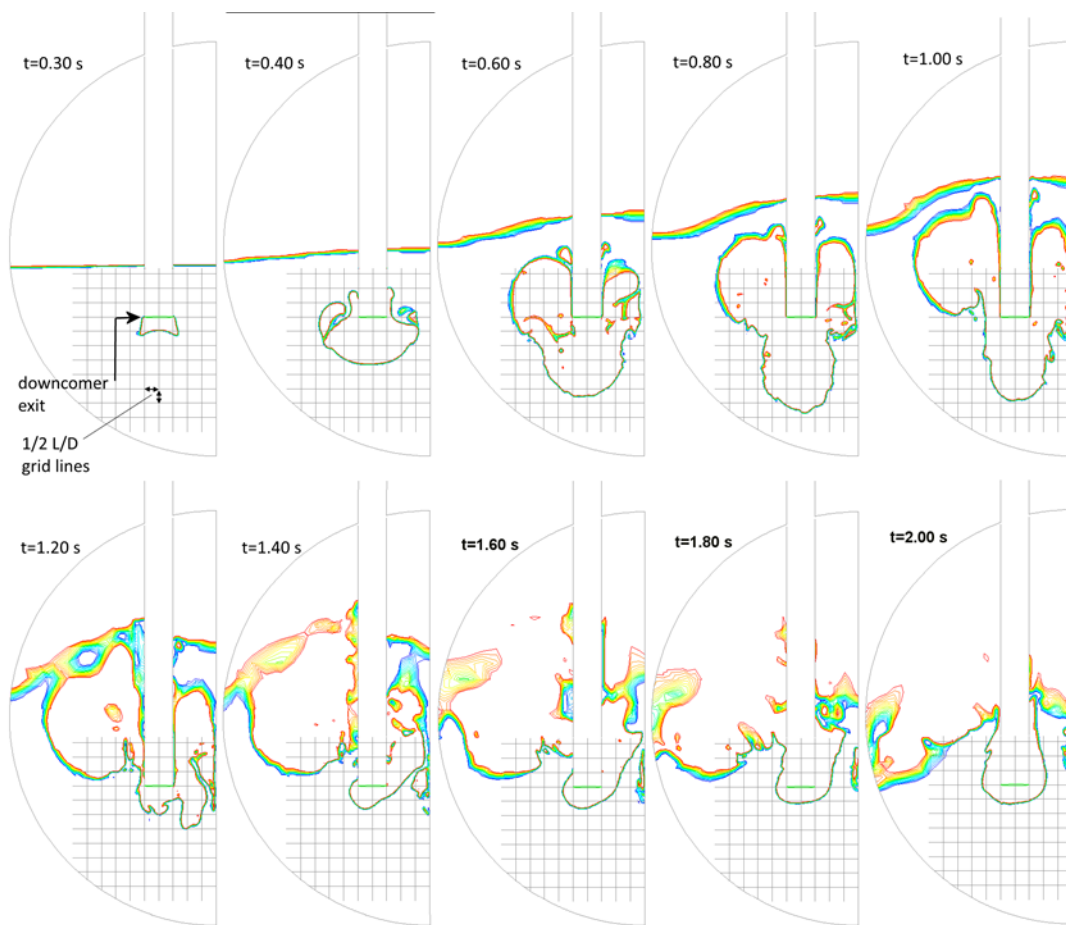
The results in Figure 5.2.3-5 show that the water is cleared from the downcomer pipe approximately 0.3 s after the initiation of the large-break scenario. This is consistent with the MELCOR predictions. The gas bubble penetrates deep into the pool as it follows the path of the initial water slug that shoots out of the downcomer pipe. The peak penetration depth of nearly 3.5 diameters is reached about 0.5 seconds later at a time of 0.8 s. From there, it takes less than 0.5 seconds more for the main bubble to rise back up toward the pipe outlet. The mass flow exiting from the pipe outlet beyond this time only reaches a depth below the exit of approximately 0.5 to 1 diameter. This penetration depth could decrease further as the gas concentration changes over to steam and condensation begins. The effect of steam and condensation is not considered in these cases.

It should be emphasized that these predictions for gas bubble behavior are conservative because the CFD analysis assumes that the downcomer vent flow is composed entirely of NCG. As previously discussed and shown of Figures 2.1-7 and 2.1-8, the NCG fraction of the total downcomer flow during the first 2 seconds following a LOCA is substantially less than the steam and water flow exiting the downcomer.

The Eulerian approach is applied to consider the effect of small bubbles that are expected to break away from the main bubble. This two-phase CFD approach relies on a series of interfacial terms that can affect the final results. Validation of these terms for this project is beyond the scope of the current effort and the ANSYS/FLUENT default values are used to show the methods potential. Results are reported as predicted but it is important to note that the uncertainty in this method has not been established for this problem. Results should be treated as a qualitative estimation of the small bubble behavior. Table 5.2.3-2 lists the basis solver settings used for the Euler based simulations. Second order differencing methods were found to be unstable so a first order approach was adopted.

Table 5.2.3-2: Eulerian Multi-Phase CFD Model Basic Solver Settings

Code	ANSYS/FLUENT v15.0
General	pressure based transient solver, gravity
Models	Eulerian Multiphase with VOF option, explicit volume fraction scheme, energy equation, assumed small bubble diameter = 0.005 m (0.197 in.)
Turbulence	standard k-epsilon, standard wall functions, compressibility option, Mixture turbulence option
Materials	Water air, ideal gas assumption
Conditions	floating operating pressure, specified operating density = 1.1777 kg/m^3 (0.0735 lb$_m$/ft^3)
Boundary Conditions	inlet – specified mass flow- time-dependent, constant temperature walls – adiabatic, no slip condition
P-V coupling	Phase Coupled SIMPLE
Discretization	density, momentum, turbulence, energy, time – first order volume fraction - compressive

Eulerian multiphase predictions are illustrated in Figure 5.2.3-6. The results are plotted at times that correspond to the times used in Figure 5.2.3-5 for the VOF approach. The figures show

contour plots of void fraction clipped between 0.01 and 0.99 to remove regions where there is less than 1 percent air or water. This view clearly shows the extent of the penetration of gas into the suppression pool. Grid lines are overlaid in the region around the downcomer exit to help quantify the size and depth of the gas bubbles. These grid lines are centered on the pipe exit and spaced at a distance of ½ the downcomer pipe diameter ($^1/_2$ D = 0.295 m (0.968 ft)). The color bar on the left of the figure shows the scale used to map void fraction to color.

The void fraction contours in Figure 5.2.3-6 show that the Eulerian method predictions of the main bubble region (void > 0.99) are similar to those from the VOF method. The main bubble exits the blowdown pipe at around 0.3 seconds and extends to a maximum depth of around 3.5 pipe diameters 0.5 seconds later at 0.8 s. From there, it takes less than 0.5 seconds for the main bubble to rise back up towards the pipe outlet. The gas flow exiting from the pipe outlet beyond this time penetrates downward less than 1 diameter. The Euler results do not show significant void away from the main bubble until after 0.8 seconds when the main bubble stops expanding downward and begins to rise quickly back towards the surface. At this time, a small void fraction representing bubbles that break away from the main bubble remains at the full penetration depth. This gas region rises much more slowly than the large bubble.
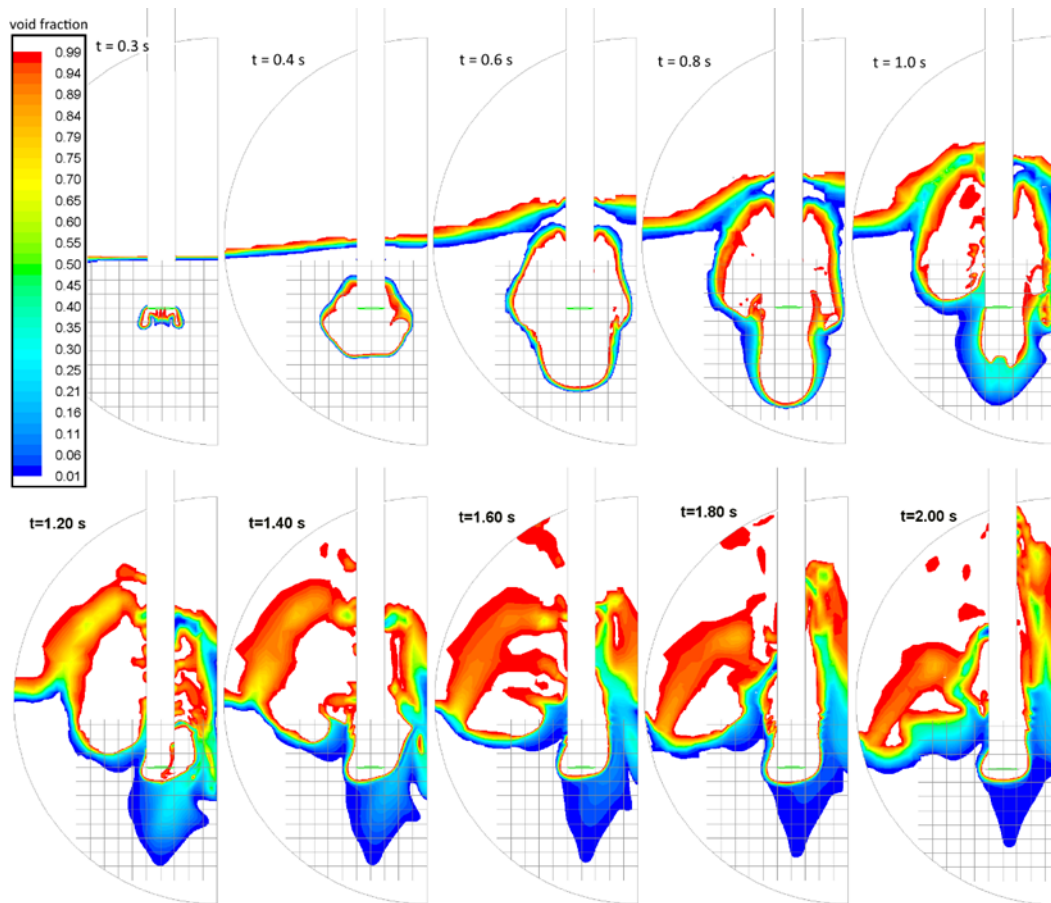
Figure 5.2.3-6: Contour Plots of Time-Dependent Void Fraction (Eulerian Method)

To quantify the penetration depth predictions, a graph of the maximum penetration depth as a function of time is created for both the VOF and Eulerian multiphase predictions. Figure 5.2.3-7

shows the maximum penetration as a function of time for the VOF and Eulerian multiphase approaches. The VOF results are taken from results such as those in Figure 5.2.3-5 and represent the maximum penetration of gas into the water below the downcomer exit. For the Eulerian multiphase predictions, several specific void fractions are considered. The results in Figure 5.2.3-7 show the depth of the Eulerian predictions with a minimum void fraction of 1 percent. Values of 2 percent and 15 percent are also considered in Figure 5.2.3-7 to provide additional insights.

The results for the penetration depth show that maximum penetration is reached around 0.8 seconds after the initiation of the transient. After that time, the main bubble rises quickly and recedes back to a depth of less than 1 diameter below the pipe exit at around 1.3 seconds. This represents the maximum penetration depth of the gases exiting the downcomer pipe at that time. In a prototypical scenario, steam flow is expected to follow shortly after the initial burst of NCGs and the bubble dynamics would change as the steam condenses.
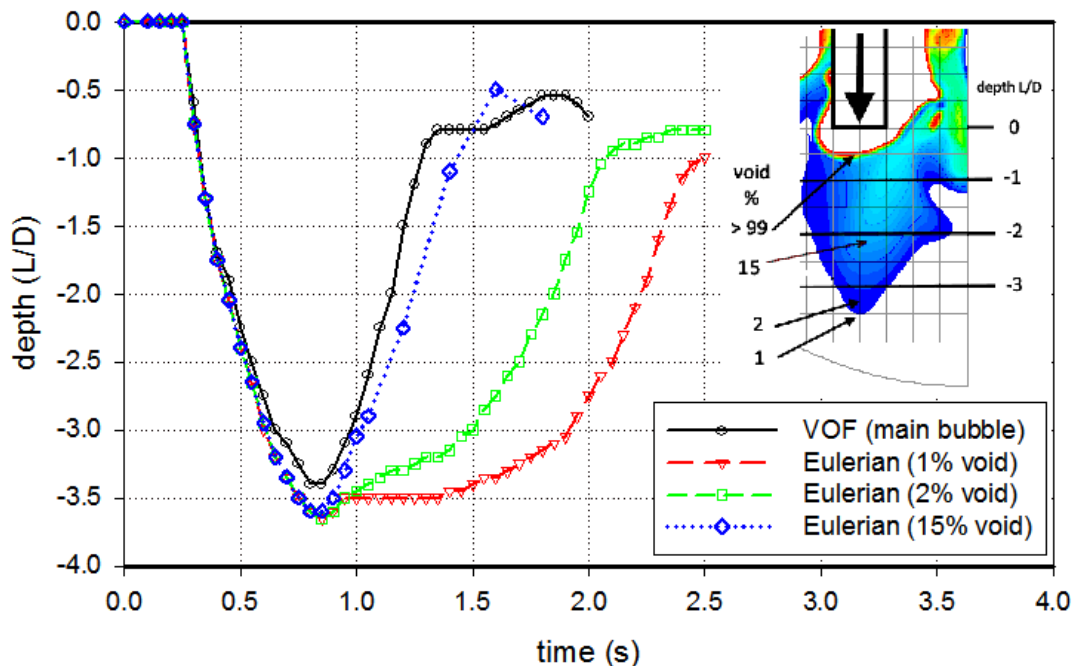
Figure 5.2.3-7: Time-Dependent Maximum Penetration Depth

The Eulerian-based predictions provide insights into how the smaller bubbles respond. As expected, these do not rise as fast as the main bubble and they will be affected by global flow patterns in the liquid region. A region with a void fraction of 1 percent is predicted to remain at a depth of 3.5 diameters for a short time and then rises to the level just below the downcomer exit by 2.5 seconds. The 15 percent and 2 percent regions are predicted to rise more quickly and reach the upper location at approximately 1.5 and 2.1 seconds respectively. The Eulerian predictions are very similar to the VOF predictions while the main bubble is expanding down into the suppression pool (up until 0.8 seconds). There is a slight amount of additional penetration in the Eulerian results during this initial blowdown time which may be partially explained by the use of first order differencing in the Eulerian model (first order methods are used for stability in the Eulerian case). Although the VOF and Eulerian models used the same boundary and initial

64

conditions, these are different approaches with different modeling options. After the initial downward penetration, the Eulerian results become more interesting. As the main bubble rises up, there is a wake of smaller bubbles left behind. These predictions provide some insights into the magnitude and void fraction of this wake region.

The lateral spread of the main bubble is another consideration. The width or spread is different at various depths and changes with time. To quantify this spread, fixed depths of 1, 2, and 3 L/d below the downcomer exit are considered. The maximum radial spread in the plane of the images considered (see Figure 5.2.3-6) for the three depths considered are plotted as a function of time in Figure 5.2.3-8. The distance is normalized in terms of downcomer diameter and measured from the center of the downcomer pipe. When the bubble is nonsymmetric, the larger radial measurement is recorded on the plot. Grid lines overlaid on the contour plots showing the bubble interface are used to determine the bubble width as illustrated in the example on the right side of Figure 5.2.3-8. The maximum radius of the main bubble in this figure is approximately 1.9 pipe diameters and occurs at a depth below the exit of 1 pipe diameter. It is noted that the bubble is wider above this level but these higher elevations are not considered.
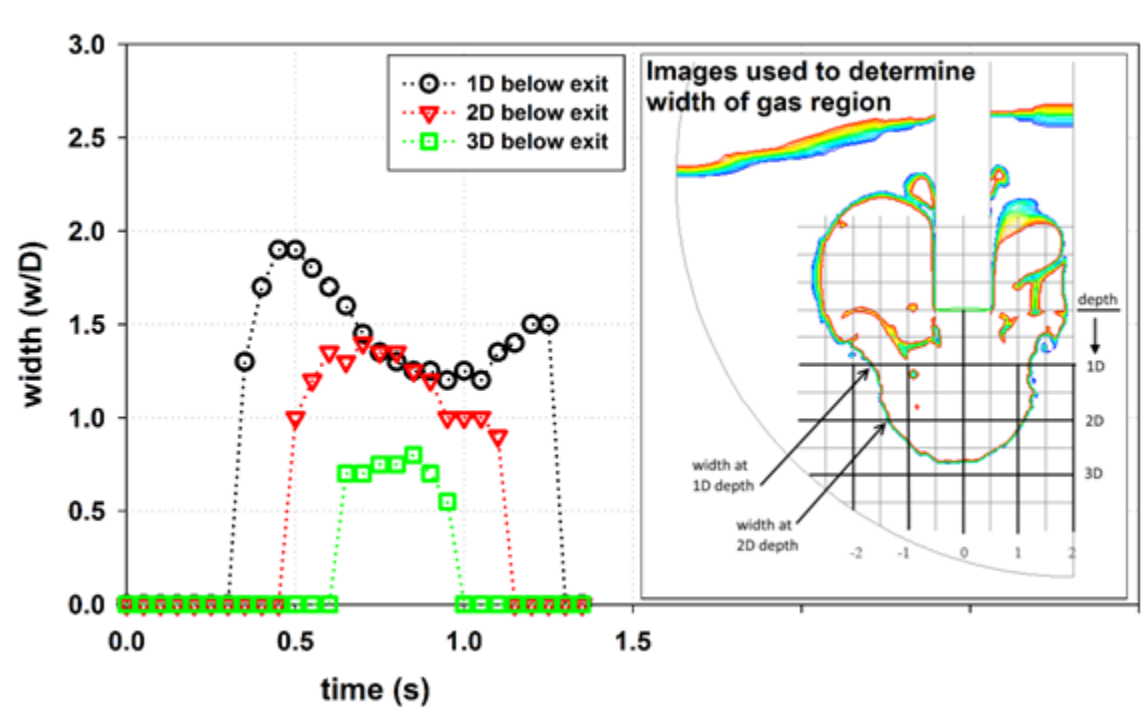
Figure 5.2.3-8: Time-Dependent Radial Width of Main Bubble

The predictions indicate that the initial blowdown and rise of the main bubble occurs relatively quickly. Results indicate that within 2.5 seconds, the void fraction below the downcomer exit region is reduced to less than 1 percent. The results for the small bubble residence times inferred from Figure 5.2.3-7 have an unknown degree of uncertainty, however, because of the modeling approach. The physics of the bubble breakup and bubble formation in the wake of the main bubble has not been validated. In addition, the smaller bubbles are expected to be affected by larger flow patterns in the suppression pool which are likely to be plant-specific and not accounted for in this simplified model domain. Condensation events, which are also expected to occur once the NCGs clear, will also cause flow disturbances resulting in additional

mixing of the smaller bubbles. These and other limitations of the approach should be considered before applying these results in a quantitative manner.

As previously discussed, small gas bubbles can break away from the large gas bubble when it is present in the suppression pool. The small gas bubbles can remain in the suppression pool for a longer time than the large bubble because they are more affected by turbulence and circulation currents which can lengthen the time to rise and exit the pool. After the exit of the large gas bubble, the void fraction in the suppression pool is primarily the result of small bubbles.
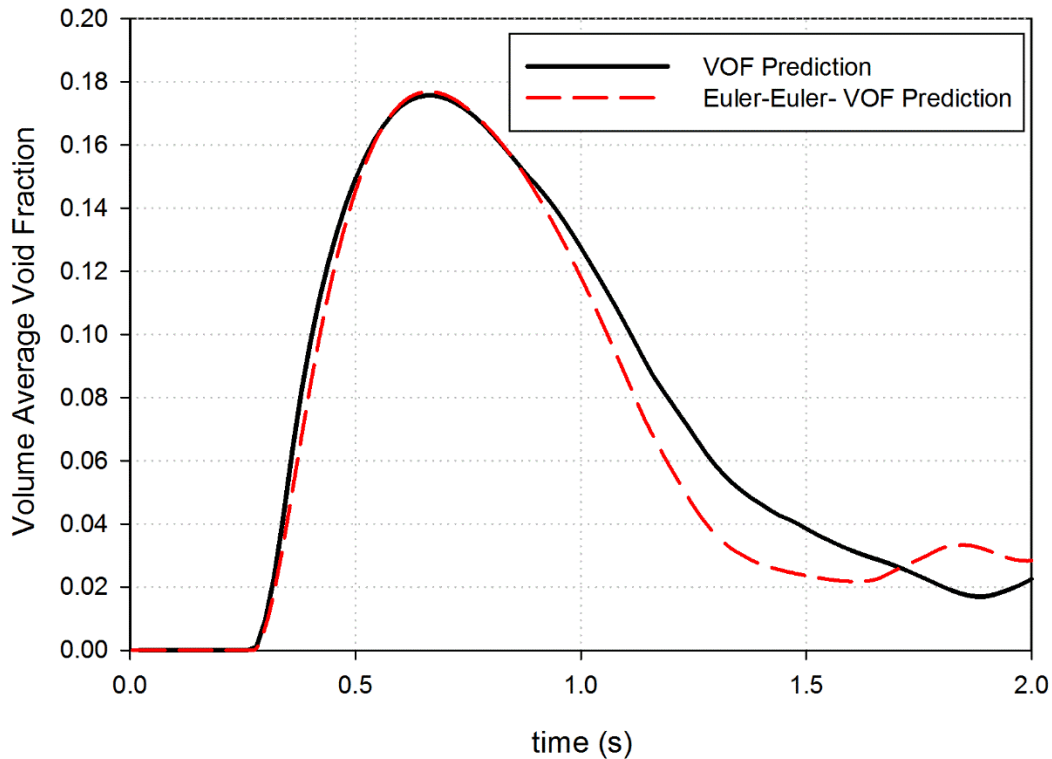
Figure 5.2.3-9: Average Pool Void Fraction below the Downcomer Exit Using the VOF and Euler Methods

The average void fraction in the volume below the downcomer exit is of interest after the departure of the large gas bubble. This void fraction, which primarily results from the presence of small bubbles, provides an estimate of the void fraction that can enter the pump inlet strainers which are located below the downcomer exit in most plants. The VOF method only tracks gas bubbles that are larger than the computational grid size. To assess the magnitude of the suppression pool void fraction after the large bubble exit, the average void fraction for the volume below the downcomer exit is calculated for the VOF analysis. This average void fraction is plotted on Figure 5.2.3-9. At 2 seconds, the predicted void fraction value of about 0.02 (2 percent) is mainly attributed to the large bubble that is formed at the exit of the downcomer pipe and is not associated with any distributed small bubbles. Consequently, the average void fraction in the suppression pool below the downcomer exit is expected to be less than 0.02 (2 percent) after 2 seconds after the LOCA start.

In contrast to the VOF method, the Eulerian method tracks void fractions associated with small gas bubbles that break away from the large bubble. Predictions using the Eulerian method provide an approximation of the void fraction in the suppression pool outside of the large gas bubble and in the suppression pool after the rise and exit of the large gas bubble. Figure 5.2.3-9 includes the average void fraction in the suppression pool below the downcomer exit predicted by the Eulerian method. At 2 seconds, the predictions are approximately 0.03 (3 percent). Most of this void fraction results from the remaining large gas bubble that continues to exit from the downcomer.

After 2 seconds the void fraction in the volume below the downcomer exit is expected to continually fall because the small NCG bubbles will rise and exit the pool and the NCG flow entering the pool from the downcomer drops off quickly. As shown on Figures 2.1-7 and 2.1-8, the MELCOR analysis predicts that the NCG flow rapidly drops and by 2 seconds consists of only about 8 percent of the total downcomer flow. However, as previously stated, in the CFD calculation the downcomer vent flow is conservatively assumed to be composed entirely of NCG. Additionally, using the NCG flow assumed for the CFD analysis (Figure 5.2.3-4), all the NCG initially present in the drywell is deposited in the wetwell by about 1.4 seconds. However, the CFD analyses conservatively continues gas flow after that time. Consequently, the values for void fraction below the downcomer exit shown in Figure 5.2.3-9 represent conservative estimates of the expected values.

The VOF plot on Figure 5.2.3-9 only uses the large bubble volume to calculate the average void fraction below the downcomer exit because the VOF method only calculates the behavior of the large bubble in the suppression pool. In contrast, the Euler plot uses both the large and small bubbles volumes to calculate the average void fraction below the downcomer exit because the Euler method calculates the behavior of the large gas bubble as well as any small bubbles. Because the large bubble volume is consistent between the Euler and VOF approaches, the average small bubble void fraction in the fluid region outside the large bubble is approximately the difference between the average void fractions for the region below the downcomer exit calculated by the Euler and VOF analyses. Consequently, the average void fraction at a strainer located below the downcomer exit and outside of the large bubble will be 0.01 (1 percent) or less for times greater than about 2 seconds. This calculation demonstrates that the void fraction in the suppression pool water outside the large bubble at 2 seconds is smaller than indicated on Figure 5.2.3-9. A void fraction of 1 percent would result in acceptable pump operation using the BWR ECCS pump operation criteria described in Section 4.2.7.

5.2.3.6 Conclusions

A full-scale simulation using a simplified representation of a single downcomer pipe and conservative boundary conditions from a MELCOR analysis provides valuable insights into the bubble dynamics associated with a full-scale blowdown event. The main bubble penetrates approximately 3.5 pipe diameters below the downcomer exit and then rises back past the downcomer pipe exit within 1.5 seconds. Smaller bubbles, which are predicted to break away from the large main bubble, rise more slowly. These smaller bubbles are predicted to rise up past the downcomer exit approximately 2.5 seconds after the start of the scenario. Both a VOF and Eulerian approach are used to predict the bubble penetration depth. The Eulerian predictions provide results for a range of void fractions (i.e. for the small bubbles) but are not benchmarked and only serve as an indication of the small bubble behavior. The width of the main bubble is also considered and is limited to about 1.9 pipe diameters for depths more than

1 pipe diameter below the downcomer exit. Other phenomena which could further enhance, mix, or distribute the NCG region, such as plant-specific features, flow fields caused by pump suction, or strong condensation events, should be considered on a case-by-case basis.

6.   ASSESSMENT APPROACH FOR ECCS PUMP OPERATION IN BWR PRESSURE SUPPRESSION CONTAINMENT SYSTEMS

This section summarizes the recommendations for addressing the GI-193 concerns resulting from the review of available, applicable references and the results of the analyses presented in this report. The work to address a GI-193 concern for a particular plant can be divided into two activities. The first activity involves the determination of a time-dependent "exclusion zone" and a time-dependent void fraction distribution in the suppression pool following a LOCA. The analyses presented in Section 5.2.3 provide the information necessary to define a suppression pool "exclusion zone" within which a pump strainer and inlet should not be located, and a noncondensable void fraction distribution in the suppression pool. The second activity involves the determination of the ECCS pump start times and operation, and the void fraction criteria for acceptable ECCS pump operation. The void fraction criteria is used in conjunction with the information developed from the first activity to determine whether a safety concern exists in a particular plant.

Assuming the void fraction at the strainer location is representative of the void fraction at the pump inlet, the assessment of ECCS pump operation following a LOCA consists of several steps:

1.   Determine the post-LOCA NCG "exclusion zone" in the suppression pool.

2.   Determine the void fraction in the pool water outside the "exclusion zone."

3.   Determine the location of the ECCS pump strainer in relation to the "exclusion zone."

4.   Determine the acceptability of ECCS pump performance if NCG is present at the pump strainers.

5.   If the assessment determines that the ECCS pump operation would be affected, the final step would be the determination of the course of action to correct the condition.

This approach does not include several phenomena that could affect the determination of pump behavior such as gas penetration into the pump strainers, gas transport through the piping to the pump inlet, NCGs transport in the pool toward the pump strainers caused by suction flows, and possible NCGs coming out of solution at the pump location in the suppression pool. These items will be discussed later in this section.

Using the results of the analysis results presented in Section 5.2.3 and the results of the literature search information presented in Section 3, the following sections discuss the method to define the "exclusion zone" and void fractions in a Mark I suppression pool following a DBA LOCA. The following sections will also provide information on the ECCS pump timing and acceptable operation as related to the time-dependent suppression pool void fraction conditions. This information will be used in a procedural method to determine the acceptability of ECCS pump operation following a DBA LOCA.

6.1 Post-LOCA Suppression Pool Behavior

As indicated in Table 2.1-1 and Figure 2.1-7, the vent flow and suppression pool conditions following a LOCA can be divided into four phases: (1) the downcomer vent solid water clearing phase, (2) a large NCG bubble or "jet" phase, (3) a small NCG bubble phase, and (4) an all steam flow phase that results in suppression pool steam condensation oscillation and chugging. The following sections describe the suppression pool phenomena occurring in each phase and identify the phase that presents the major concern for NCG ingestion into the ECCS pump suction. Figure 6.1-1 illustrates the timing of the suppression pool conditions and pump operation using information discussed in Sections 2, 4 and 5. The high-containment pressure signal occurs about 1 second following the start of a DBA LOCA. An additional minimum 3-second pump startup delay is applied with loss of offsite power to account for emergency diesel generator startup and ECCS pump initiation sequencing.
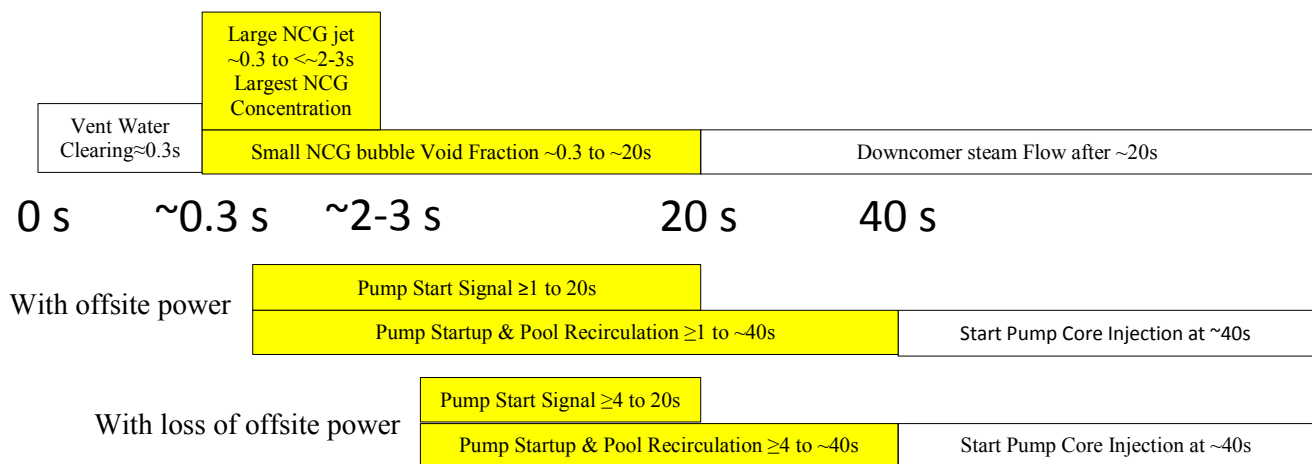
Figure 6.1-1: Downcomer Flow/Suppression Pool Conditions and ECCS Pump Operation Comparison

6.1.1 Downcomer Vent Water Clearing

A water column exists in the downcomer vent before the start of a LOCA. As the drywell pressure increases following a LOCA the water column is pushed into the suppression pool because of the increased pressure differential between the drywell and wetwell. As discussed in Sections 2 and 5.2, the water clearing phase lasts about 0.3 seconds for a DBA LOCA, but can take longer for smaller break sizes.

6.1.2 Noncondensable Gas Flow and Bubble Behavior

The NCG flow behavior can be divided into two phases, a large gas bubble phase followed by a longer small gas bubble phase. After the completion of vent water clearing, the noncondensable gas-steam mixture in the drywell begins to flow out of the vent and into the suppression pool. As shown on Figure 2.1-7, the initial flow in this phase contains a significant amount of NCG. This initial large gas "jet" can penetrate a significant depth into the pool as it follows the initial water "jet" downward. The amount of NCG in the vent flow decreases quickly and reaches very small levels after 2–3 seconds for a DBA LOCA. The size of the initial large NCG "jet" can define an

70

"exclusion zone" volume at the vent exit which possesses a large fraction of NCG. The ECCS strainer and pump suction should not extend into the "exclusion zone" during ECCS pump operation. After 2–3 seconds the size of the NCG volume decreases as the initial large gas bubble rises and exits the top of the suppression pool. After the large NCG bubble exits, small gas bubbles can still flow into the suppression pool water; however the volume and penetration of this gas flow is significantly less than the initial large gas "jet." The average suppression pool void fraction is expected to significantly decrease to low levels by about 10 seconds, but, much lower levels of NCG void fractions levels may last in the suppression pool to about 30–40 seconds.

6.1.3   Condensation Oscillation and Chugging

After the NCG flow reaches very low levels, the bulk of the flow exiting the vent is a steam-water mixture. Initially this flow rate can be significant but will decrease as the vent flow decreases following the LOCA. High steam flow results in steady condensation. Decreasing steam flow can produce oscillating bubbles at the vent exit resulting from steam condensation at the bubble surface. This phenomenon is called condensation oscillation. At even lower steam flow conditions, the exiting steam flow can create a bubble that fully condenses rapidly or collapses at the vent exit causing backflow of water into the vent pipe. This "chugging" phenomenon can occur in a cyclical fashion consisting of steam bubble formation and full collapse.

The steam condensation mode, which generally exists at times later than 10 seconds after a DBA LOCA, is not expected to impair ECCS pump operation because the fraction of NCG exiting the vent and entering the suppression pool is small and because any steam in the suppression pool is expected to condense before entering the ECCS pump inlet.

6.2   <u>Other Considerations Regarding Suppression Pool Conditions</u>

Additional concerns were considered in the development of the logic for assessing acceptable ECCS pump performance following a LOCA. The effect of initial dissolved NCG in the suppression pool was determined to have a secondary or negligible effect on pool void fraction. Additionally, it was considered conservative to use the pool void fraction outside the pump inlet strainer in this assessment because consideration of NCG behavior in the intake line to the ECCS pump would generally result in a lower void fraction at the pump inlet.

6.2.1   Consideration of Dissolved Noncondensable Gas in the Suppression Pool

The suppression pool water contains dissolved NCG. This section assesses whether significant levels of NCG in the suppression pool can come out of solution following a LOCA and affect the pool void fraction.

The maximum saturated equilibrium amount of dissolved gas that a water pool can contain is dependent on the pool temperature and pressure. Following downcomer vent discharge after a large double-ended guillotine break LOCA, local heat up of the suppression pool could result in some of the dissolved gas coming out of solution as bubbles if the equilibrium NCG concentration at the elevated temperature and pressure is less than the equilibrium gas concentration at the initial steady-state conditions before the LOCA. Because of the following calculations, the inclusion of the initial dissolved gas in the suppression pool is not considered an important criterion for determining void fraction distribution in the suppression pool.

Additionally, it was concluded that the dissolved air present in the suppression pool water is not expected to significantly affect the void fraction distribution calculated by a CFD analysis in the suppression pool for the initial 1- to 2-second period following a large-break LOCA.

Information from a typical Mark I plant can be used as the basis for determining increase in pool void fraction resulting from a LOCA. Typical Mark I containment design parameters are as follows:

Drywell net free volume	4,785.5 m^3 (169,000 ft^3)
Max. suppression pool water volume at high water level	3,454.7 m^3 (122,000 ft^3)
Min. suppression chamber free volume at high water level	3,780.3 m^3 (133,500 ft^3)
Drywell and suppression chamber pressure	1.034×10^4 Pa$_g$ (1.5 psig)
Drywell temperature	330.37 °K (135 °F)
Suppression chamber atmosphere and pool temperature	308.15 °K (95 °F)
Peak short term suppression chamber pressure following a LOCA	1.896×10^5 Pa$_g$ (27.5 psig)
Peak short term suppression pool temperature following a LOCA	329.26 °K (133 °F)

Using information for equilibrium air concentration in water from References 52 and 53, the equilibrium concentration of air in water can be estimated. The equilibrium air concentration in water
at 308.15 °K (95 °F) and 1.034×10^4 Pa$_g$ (1.5 psig)
is about 0.0192 kg$_{air}$/m$^3_{mixture}$ (1.2×10^{-3} lb$_{mair}$/ft$^3_{mixture}$)
at 288.71 °K (60 °F) and 1.034×10^4 Pa$_g$ (1.5 psig)
is about 0.0256 kg$_{air}$/m$^3_{mixture}$ (1.6×10^{-3} lb$_{mair}$/ft$^3_{mixture}$)
at 329.26 °K (133 °F) and 1.896×10^5 Pa$_g$ (27.5 psig)
is about 0.0216 kg$_{air}$/m$^3_{mixture}$ (1.35×10^{-3} lb$_{mair}$/ft$^3_{mixture}$)

Lower Limit Calculation
With the suppression pool initially at its maximum steady-state operating temperature of 308.15 degrees K (95 degrees F), it is concluded that the dissolved air in the suppression pool will remain dissolved because the equilibrium air concentration at the peak short-term post-LOCA pressure and temperature condition (329.26 degrees K (133 degrees F) and 1.896×10^5 Pa$_g$ (27.5 psig)) is larger than the steady-state conditions before the LOCA.

Upper Limit Calculation

If the suppression pool is initially assumed to be at 288.71 °K (60 °F) and the air dissolved in the suppression pool water comes out of solution at the peak short term conditions following a LOCA, the resulting air mass released by the suppression pool water can be estimated as:

$$(1.6 \times 10^{-3} - 1.35 \times 10^{-3}) \text{ lb}_{mair}/\text{ft}^3_{mixture} \times 122{,}000 \text{ ft}^3 = 30.5 \text{ lb}_{mair} \text{ (13.8 kg}_{air})$$

The density of air at 313.15 °K (104 °F) is 1.089 kg/m^3 (0.068 lb$_m$/ft^3) and at 333.15 °K (140 °F) is 1.025 kg/m^3 (0.064 lb$_m$/ft^3).

Consequently, the average void fraction in the suppression pool at 333.15 degrees K (140 degrees F) resulting from the release of dissolved air can be estimated as:

$$30.5 \text{ lb}_m \text{ / } 0.064 \text{ lb}_m/\text{ft}^3 \text{ / } 122{,}000 \text{ ft}^3 = 0.0039 = 0.39\%$$

This value is the upper limit on void fraction increase in the suppression pool caused by the instantaneous release of dissolved air in the pool water for the short-term period following a LOCA. This upper limit void fraction increase is small compared to the expected large void fraction distribution in the suppression pool during the first 2 seconds following a large-break LOCA. A pool void fraction increase of 0.39 percent would not affect the conclusions regarding ECCS pump operation resulting from the larger pool void fraction increase caused by downcomer air flow following a LBLOCA. Additionally, even for this upper limit case scenario, the void fraction in the suppression pool is not expected to rise immediately to the maximum value because dissolved air is not released instantaneously from a water mixture but takes some time to be released (Ref. 50).

Therefore, it is concluded that the dissolved air present in the suppression pool water is not expected to significantly affect the void fraction distribution calculated by a CFD analysis in the suppression pool for the initial 1- to 2-second period following a large-break LOCA.

6.2.2 Consideration of Noncondensable Gas Transport to and Accumulation at the ECCS Pump Inlet before Pump Startup

This concern relates to the potential for the NCG to flow through the ECCS pump inlet strainer before pump startup, remain in the dead-ended pipe region downstream of the strainer, and enter the pump as it starts. This concern, which is dependent on the design of the pump inlet strainer and the geometry of the pump intake line, was judged to be insignificant for the reasons discussed in the following paragraphs.

As previously indicated NCG from the drywell can enter the suppression pool only after the downcomer vents are cleared of water. As shown on Figure 6.1-1, vent clearing is completed at about 0.3 seconds following the start of the DBA LOCA. Calculations indicate that NCG starts flowing into the suppression pool at about 0.3 seconds and forms a large gas bubble that lasts to about 2–3 seconds when the large gas bubble exits the pool. As indicated by the plant survey performed by the BWR Owners Group, the earliest time for the start of the ECCS pumps is about 1 second assuming the availability of offsite power and at about 4 seconds assuming the loss of offsite power. Consequently, the earliest time frame during which NCG can flow from a large gas bubble into a dead-ended intake pipe is the time period between 0.3 seconds and 1 or 4 seconds when the pump starts following a DBA LOCA. NCG flow from small bubbles in the suppression pool will exist from about 0.3 seconds to about 20 seconds following a DBA LOCA.

The possibility for gas to enter the pipe intake before pump startup is dependent on the local pool void fraction conditions at the pipe intake strainer. Consequently, the time and location dependent void fraction at a specific strainer location in the suppression pool can be determined from Figures 5.2.3-5 and 5.2.3-6. The postulated NCG flow from the suppression pool through the intake strainer could be greater if the strainer is located in a region with a larger pool void fraction.

Before pump startup, NCG flow from the suppression pool to the intake pipe is unlikely because the gas must flow from the pool through an intake strainer, which has a large flow resistance to enter the intake pipe. Additionally, the incompressible water in the pipe must flow backwards from the pipe through the high flow resistance strainer into the suppression pool to make room for the incoming gas flow. Consequently countercurrent gas-liquid flow must be present in the strainer and intake pipe for gas to accumulate in the intake pipe. The presence of countercurrent flow in the intake strainer and intake pipe would further increase the flow resistance for additional gas to enter the intake pipe.

Additional resistance to gas flow into the intake pipe can exist because of the surface tension effects in the small holes that may be present in the intake strainer. To permit gas flow through the small holes, a sufficient pressure differential must exist across the small holes in the intake strainer to overcome the capillary surface tension force represented by the following equation.

$$\Delta p = 2\,\sigma\,/\,r$$

where p is the pressure force required to overcome the capillary surface tension force
      σ is the surface tension, and
      r is the radius of curvature of the intake strainer holes, typically the equivalent hole radius.

It is highly unlikely that the flow conditions described above would exist to allow gas to flow through the inlet trainer and into the inlet pipe, and for countercurrent gas-liquid flow to occur across an inlet strainer connected to a dead ended pipe.

In the unlikely case that gas does flow through the inlet strainer, the small holes in the inlet strainer will break up any large pool gas bubble into smaller gas bubbles because the bubble size in the intake pipe will be limited to the size of the strainer holes. This behavior will result in a smaller pipe void fraction after mixing with the water volume in the intake pipe. Additionally, the smaller bubbles in the intake pipe would need more time than available to coalesce into a larger bubble before the ECCS pumps start.

Additionally, each ECCS pump is connected to a header which is fed by several strainer pipes. Consequently, any two-phase, low void fraction flow in an individual intake pipe will mix with water coming from other intake lines in the header that feeds the pump reducing the void fraction before entering the pump.

6.2.3 Consideration of Noncondensable Gas Transport in the Inlet Piping during Pump Operation

The developed assessment procedure conservatively uses the void fraction at the strainer inlet for its assessment and does not account for the void fraction decrease resulting from the pressure drop that can exist between the strainer inlet and pump inlet during ECCS pump operation. The void fraction decrease from the strainer inlet to the pump inlet is dependent upon the piping geometry (e.g. length and diameter), the pump operation characteristics (Refs. 50 and 51), and the flow resistances and fluid characteristics of the inlet line as described in Section 6.2.2. A time-dependent pool void fraction at the strainer inlet can be estimated by determining whether the strainer inlet is located inside or outside the "exclusion zone"; however, the void fraction change from the strainer to the pump inlet can only be calculated using plant-specific design information. Consequently, the determination of the void fraction at the pump inlet is beyond the scope of the GI-193 activities, but may be included in a calculation using plant-specific design information. Alternatively, it is conservative to assume that the void fraction at the strainer inlet is representative of the void fraction at the pump inlet.

6.3 Determination of ECCS Pump Strainer Location in a Suppression Pool

The location of the ECCS pump strainer relative to the downcomer vents in the suppression pool of a BWR PS containment is plant dependent. Consequently the assessment of the acceptability of an ECCS pump strainer location must be determined on a plant-specific basis.

6.4 ECCS Pump Operation

The assessment of ECCS pump behavior must consider the NCG distribution in the suppression pool. The CFD analysis results can be used to define the "exclusion zone" and the gas void fraction in the suppression pool outside the "exclusion zone." The pump strainer and intake should be located outside the gas "exclusion zone" during ECCS pump operation. The gas void fraction concentration outside the "exclusion zone" is important to define the gas void fraction entering the pump strainer and intake.

ECCS pump operation should be considered to be acceptable if the gas void fraction at the pump intake is determined to be less than the void fraction at which pump degradation would be expected. If the local pool void fraction falls above the void fraction at which pump degradation would be expected, an assessment must be made as to whether the pump operation would recover after the NCG exits the pool. This assessment should consider the pump start time, pump speed, and flow rate, operating duration and the duration of the elevated void fraction at the pump inlet.

6.4.1 ECCS Pump Timing Considerations

Section 4.1 discusses the post-LOCA startup timing considerations for the ECCS pumps. Each plant should perform a plant-specific assessment to determine the ECCS pump startup times with and without the availability of offsite power. The plant-specific assessment should also specify the pump speed during the period when flow is recirculated in the suppression pool and the time when pump flow is reconfigured to provide core injection.

As mentioned in Section 4.1, a typical minimum start-up time for the LPCS and LPCI pumps is about 1 second with offsite power available and about 4 seconds without the availability of offsite power. During the initial period the LPCS and LPCI pumps are operated to reach full speed. Additionally, between startup and 40 to 50 seconds the ECCS pump flow is recirculated to the suppression pool and is not injected into the core. Regardless of the availability of offsite power, the LPCS and LPCI systems are expected to start pump flow into the core at about 40 to 50 seconds after the appropriate valve reconfiguration.

As discussed in Section 5.2.3 and illustrated in Figure 6.1-1, ECCS pump operation could primarily be affected if a pump operates within the first 2 seconds following a DBA LOCA. However, lower levels of NCG can last to about 30–40 seconds because of the time necessary for the bulk of the gas to rise and exit the pool surface. Figure 6.1-1 shows the relationship between the downcomer flows described in Section 5.2.3 and the ECCS pump operations as described in Section 4.

6.4.2   ECCS Pump Acceptable Operation Criteria

An ECCS pump can sustain damage caused by over speed and vibration if gas is ingested. The acceptable ECCS pump operating range for NCG inlet void fraction was discussed in Section 4. Section 4 also discussed the ability of the ECCS pump to recover especially if only a small amount of gas is ingested. As discussed in Section 4, the BWR ECCS pump operational criteria were developed and provided in References 44 and 45. The BWR ECCS operational criteria are summarized in Table 4.1-1.

The BWR ECCS operational criteria presented in Section 4 are summarized below.

1.   Low transient flow rates (less than 70 percent of the best efficiency point) with an inlet void fraction greater than 5 percent for more than 5 seconds will result in pump damage unless pump-specific testing can show otherwise.

2.   Higher transient flow rates (between 70 percent and 120 percent of the best efficiency point) with an inlet void fraction greater than 10 percent for more than 5 seconds will result in pump damage unless pump-specific testing can show otherwise.

3.   Low flow operation (less than 40 percent of the best efficiency point) at greater than 1 percent by volume continuous suction NCG void fraction results in pump damage unless pump-specific testing can show otherwise.

4.   Full flow operation (40 percent to 120 percent of the best efficiency point) at greater than 2 percent by volume continuous suction NCG void fraction results in pump damage unless pump-specific testing can show otherwise.

ECCS pumps that operate within the void fraction conditions specified in Table 4.1-1 and within the gas void fractions indicated above in items 1 to 4 can be considered capable of recovery without damage, and will operate at normal pump head and flow conditions if the inlet void fraction is reduced to a value below 1 percent.

An ECCS pump assessment would be permitted to use other operation criteria if acceptable pump-specific tests are performed that provide better operational guidance.

6.5   Procedure for Performing a GI-193 Plant Assessment

The assessment of the ECCS pump behavior must consider the NCG distribution in the suppression pool. If a pump starts before the large gas bubble exits the suppression pool, the pump strainer and intake should be located outside the transient gas "exclusion zone" defined by the large gas bubble. However, the gas void fraction concentration outside of the "exclusion zone" is also important to define the gas void fraction entering a pump strainer and intake located outside the "exclusion zone." The results from CFD methods described in Section 5.2.3 could be used to define the gas void fraction in the suppression pool outside the "exclusion zone" defined by the large NCG bubble. If the gas void fraction at the pump intake is determined to be less than the void fraction at which pump degradation would be expected, the ECCS pump operation should be considered to be acceptable. (This assumes that pump suction does not move the gas bubble if the pumps starts outside of but in close proximity to the gas region.)

If the local pool void fraction falls above the void fraction at which pump degradation would be expected, an assessment must be made as to whether the pump operation would recover without damage after the NCG exits the pool. This assessment should consider the pump start time, pump speed and flow rate, operating duration and the duration of the elevated void fraction at the pump inlet.

Section 6.4.1 discusses the post-LOCA startup timing considerations for the ECCS pumps. Each plant should perform a plant-specific assessment to determine the ECCS pump startup times with and without the availability of offsite power. The plant-specific assessment should also specify the pump speed during the period when flow is recirculated in the suppression pool and the time when pump flow is reconfigured to provide core injection.

After pump startup, the criteria for acceptable pump operation will be determined using the flow logic presented in Figure 6.5-1 which provides a logic stream for the procedure to assess the post-LOCA operation of the ECCS pumps. The procedure proposes that the ECCS pump operation be assessed using the maximum and transient NCG void fraction at the strainer location using the graphs contained in Figures 5.2.3-5, 5.2.3-6, 5.2.3-7 and 5.2.3-8. Additionally, Section 5.2.3.5 and Figure 5.2.3-9 suggest that the void fraction at a strainer located below the downcomer exit and outside of the large bubble will be 0.01 (1 percent) or less for times greater than about 2 seconds. This assessment approach is proposed because of the short duration of the large NCG large bubble which is less than 3 seconds. For this assessment it is assumed that the "exclusion zone" for the large NCG bubble is defined by the boundary where the pool void fraction exceeds 10 percent. This assumption is consistent with the ECCS pump acceptable operation criteria listed in Section 6.4.1. Other void fraction criteria are also consistent with the information listed in Section 6.4.2.

The assessment procedure presented in Figure 6.5-1 was developed using information for a Mark I containment. Because of similar vertical downcomer geometry, the results of this study can be conservatively applied to a Mark II containment design, which possesses a larger suppression chamber. A Mark III design includes a horizontal vent pipe orientation and the ECCS pump inlets are located significantly further from the vent exits. Consequently, the ECCS pumps in a Mark III design are expected to be less affected by NCG because lower void fractions are expected at their inlets.

Figure 6.5-1 includes an option to perform ECCS pump-specific testing if the application of the flow logic determines that the timing and void fraction criteria results in pump failure including the inability to recover. This testing option would provide the actual operability assessment of a particular ECCS pump.

For this assessment, ECCS pump performance during operation with void fraction conditions at the pump inlet was considered from a general, not plant-specific perspective. A review of Figure 6.5-1 reveals that an ECCS pump start time greater than about 2–3 seconds may be sufficient to conclude that pump operation is unaffected. This assessment supports the technical conclusion that delayed ECCS pump flow initiation beyond 3 seconds, plus a possible safety factor, following a DBA LOCA initiation will adequately protect the ECCS pumps from damage.

Similarly, consideration of the void fraction at the strainer location may be sufficient to conclude that pump operation is unaffected. This assessment approach assumes that the void fraction at the strainer location is transferred unchanged through the strainer and piping to the pump inlet. This is a conservative assumption with regards to the determination of acceptable pump operation. The assessment includes the option to refine the pump operation assessment by using calculations to determine the void fraction at the pump inlet. Other studies and tests have demonstrated that the void fraction at the strainer location could be substantially different after traveling a distance through a pipe to the pump inlet. Consequently, calculational methods outlined in Reference 44 can be used to estimate the gas transport in the pipe from the strainer to the pump inlet to determine the actual void fraction at the pump inlet. Additionally, a defensible method would need to be developed to calculate the transport of NCG from the large bubble or small bubbles in the suppression pool, through the strainer and into the pipe downstream of the strainer. Of course, the method used to perform this calculation (e.g. a thermal-hydraulic computer code) must be verified against applicable test data before it could be used in this application.

Another approach to determine the void fraction at the pump inlet would be to include the strainer inlet and piping leading to the ECCS pump in the full CFD model used to predict the NCG bubble behavior. This model would include details of the pump strainer and piping along with the time-dependent pump suction flow at the end of the piping. This approach would not only estimate the void fraction in the piping approaching the pump inlet, but would also predict the interactions between the size and location of the NCG bubble and the calculated suppression pool flow field and void fraction distribution that includes the effect of the pump suction. Of course, the CFD method used to perform this calculation must be verified against applicable test data before it could be used in this application.

6.6   Possible Corrective Actions

If an ECCS pump assessment concludes that a pump would fail and not recover, the plant operator must determine what corrective action would be necessary. Four possible corrective actions could be considered.

1.   The ECCS start time could be delayed to ensure that the pump would start after elevated gas void fraction conditions are reduced in the suppression pool at the elevation of the pump strainer and intake.

2.   The location of the ECCS pump strainer and intake could be moved to eliminate or minimize the gas void fraction concern at the pump strainer and intake.

3.   Closing off a specific pump strainer is also an option if other strainer intakes provide sufficient flow into a common header feeding a pump.

4.   As previously mentioned, the licensee may also choose to perform a more detailed plant-specific analysis which models the strainer and downcomer locations, and explicitly calculates the voiding at the ECCS pump inlet.
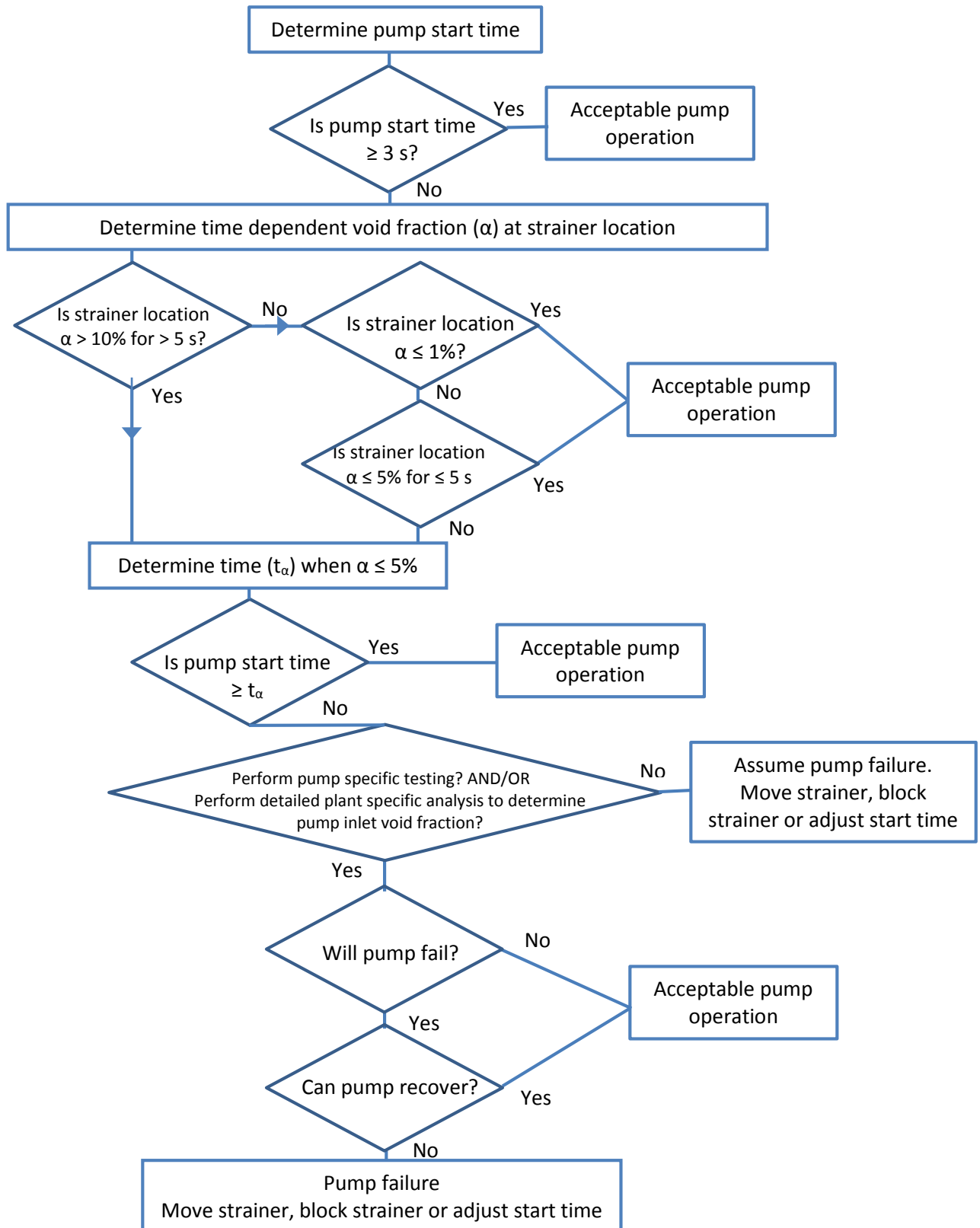
Figure 6.5-1: Approach for Assessing Effects of Noncondensable Gas on ECCS Pump Operation

6.7   Sample Calculation for Performing a GI-193 Plant Assessment

To illustrate the application of the plant assessment procedure, assessments are made for strainer locations at four points. The depth position is measured as the ratio of length over pipe diameter (L/d) from the bottom of the downcomer. The radial position is measured as L/d lengths measured from the downcomer centerline. The suppression pool void fractions are measured off Figure 5.2.3-6. Table 6.7-1 provides the void fraction measurements for these four locations. The maximum void fraction is highlighted in bold characters. Figures 6.7-1 and 6.7-2 plot the measured void fractions.

Table 6.7-1: Suppression Pool Void Fraction Sample Cases for GI-193 Assessment

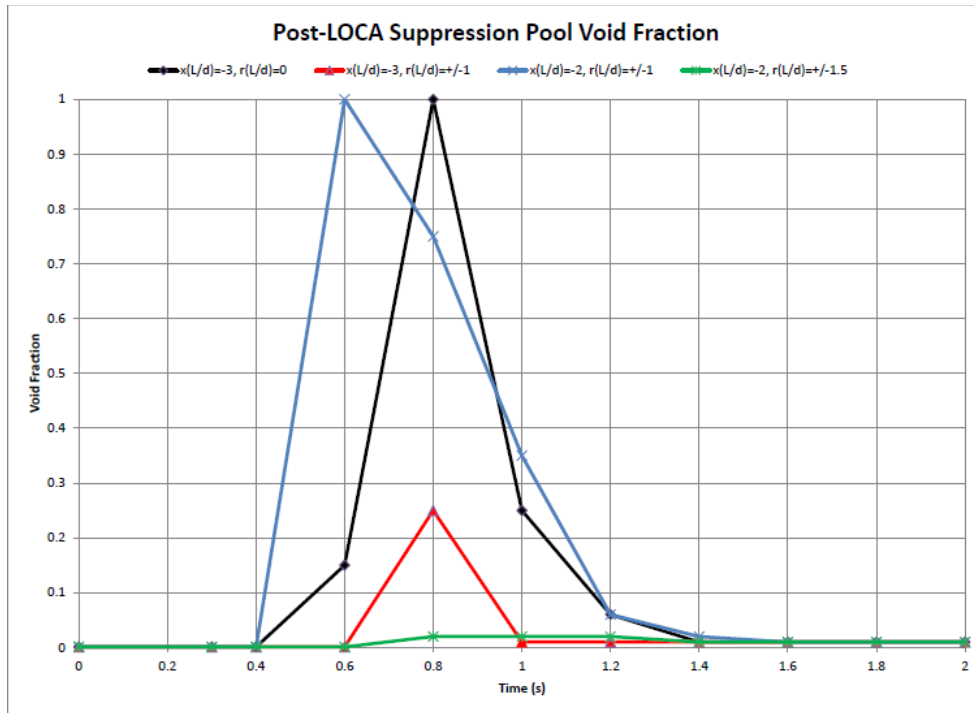| Time (s)	Case 1		Case 2		Case 3		Case 4	
	x (L/d) 3	r (L/d) 0	x (L/d) 3	r (L/d) ±1	x (L/d) 2	r (L/d) ±1	x (L/d) 2	r (L/d) ±1.5
0.0	0.0		0.0		0.0		0.0	
0.3	0.0		0.0		0.0		0.0	
0.4	0.0		0.0		0.0		0.0	
0.6	0.15		0.0		**1.0**		0.0	
0.8	**1.0**		**0.25**		0.75		**0.02**	
1.0	0.25		≤0.01		0.35		**0.02**	
1.2	0.06		≤0.01		0.06		**0.02**	
1.4	0.01		≤0.01		0.02		≤0.01	
1.6	0.01		≤0.01		≤0.01		≤0.01	
1.8	0.01		≤0.01		≤0.01		≤0.01	
2.0	≤0.01		≤0.01		≤0.01		≤0.01	

Figure 6.7-1: Plot of Suppression Pool Void Fraction Sample Cases for GI-193 Assessment
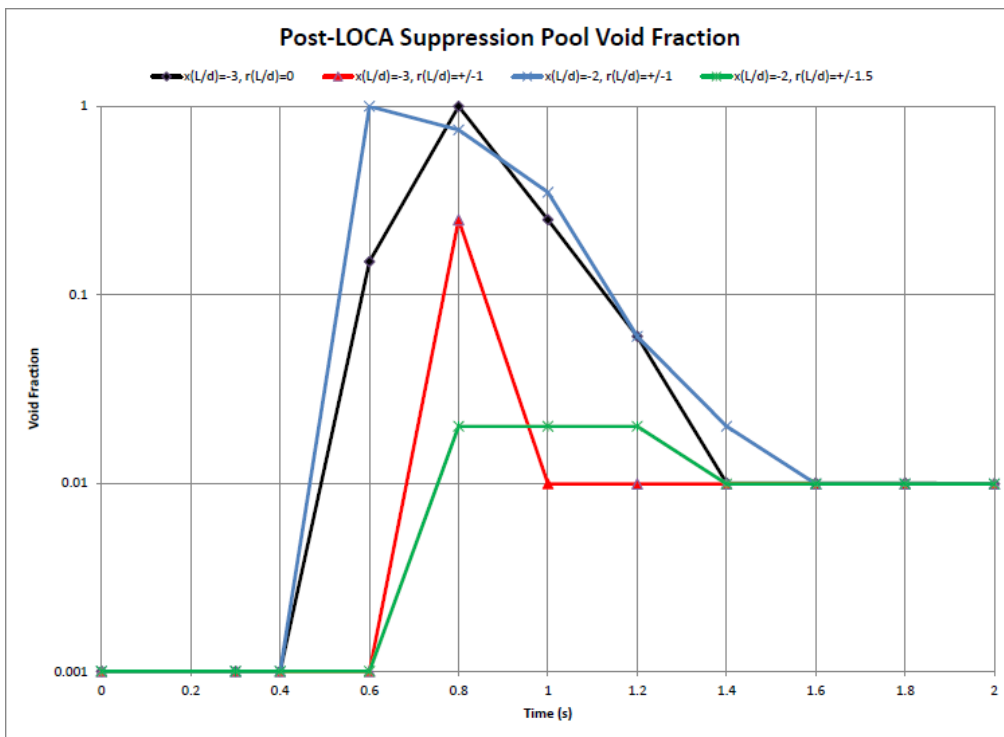

Figure 6.7-2: Log Plot of Suppression Pool Void Fraction Sample Cases for GI-193 Assessment

82

Case 1—This case reaches a maximum void fraction of 100 percent at the strainer location and remains above 5 percent for about 0.7 seconds. The assessment procedure indicates that this case would result in pump failure if the pump start time is less than about 1.3 seconds because the void fraction drops below 5 percent between 1.2 and 1.3 seconds. The void fraction is less than 5 percent after about 1.4 seconds; therefore the ECCS pump would be expected to operate acceptably if it starts after 1.3 seconds. Pump-specific test can be performed to ascertain if pump performance is acceptable if the start time is less than 1.3 seconds.

Case 2—This case reaches a maximum void fraction of about 25 percent at the strainer location and remains above 5 percent for about 0.2 seconds. The assessment procedure indicates that this case would result in pump failure if the pump start time is less than about 0.9 seconds. However, because no plant is expected to have an ECCS pump start time less than 1.0 seconds, this strainer location would result in acceptable ECCS pump performance.

Case 3—This case reaches a maximum void fraction of 100 percent at the strainer location and remains above 5 percent for about 0.8 seconds. The assessment procedure indicates that this case would result in ECCS pump failure if the pump start time is less than about 1.3 seconds. The void fraction falls to about 5 percent at less than 1.3 seconds; therefore the ECCS pump would operate acceptably if it starts after about 1.3 seconds. Pump-specific test can be performed to ascertain if pump performance is acceptable if the start time is less than 1.3 seconds.

Case 4—This case reaches a maximum void fraction of about 2 percent at the strainer location and remains at that value for about 0.6 seconds between 0.6 and 1.4 seconds. The void fraction falls below 2 percent between 1.2 and 1.3 seconds and falls below 1 percent at less than 1.3 seconds. The ECCS pump is expected to operate acceptably or recover from failure because the void fraction at the strainer does not exceed 5 percent for more than 5 seconds and quickly falls below 1 percent.

7. SUMMARY AND CONCLUSIONS

This report describes a method to perform a plant-specific assessment to determine whether an ECCS pump will operate acceptably following a DBA LOCA in a Mark I pressure suppression pool using the analyses results and criteria presented in this report. The development of an assessment method is summarized in Section 6. The assessment approach uses the ECCS pump strainer location, the ECCS pump operation criteria, the post-LOCA ECCS pump startup and full operation timing information, and the pool void fraction information at the pump strainer to make its determination. It should be noted that the plant operators will be responsible for applying the methodology and criteria to their specific plant geometry to complete an assessment for a particular plant.

The work to address GI-193 for a particular plant can be divided into several activities. The first activity presented in this report defined the transient penetration and duration of the large noncondensable gas bubble "exclusion zone" in a Mark I suppression pool following a DBA LOCA. The analyses also provide the time and location dependent void fraction in the suppression pool water outside of the large gas bubble. The second activity defined the acceptable void fraction criteria for ECCS pump operation obtained from literature review. The void fraction criteria would be used in conjunction with the information developed from the first activity to determine whether a safety concern exists in a particular plant.

7.1 Determination of Suppression Pool Exclusion Zone and Void Fraction Distribution Assessment Method

As mentioned in Section 5.1, all attempts to develop a scaling approach using small-scale test data to determine a NCG "exclusion zone" and void fraction distribution for post-LOCA downcomer venting in a full-scale suppression pool proved unattainable. However, a CFD analysis approach was used successfully to address the GI-193 concerns. CFD analyses of the water pool for two test facilities were performed to obtain the large gas bubble size and the surrounding void fraction distribution using data at different downcomer pipe diameters. Data from the following facilities provided the necessary test data:

1.   the Lappeenranta University PPOOLEX tests
2.   the Purdue University (PUMA) tests

A CFD model and analysis was applied to a full-scale plant geometry using the modeling techniques developed to analyze the test facilities. The full plant CFD analysis predictions were qualitatively compared to the videos and data from the GE full-scale Mark II tests.

7.2 Acceptable ECCS Pump Operation Criteria

The acceptable BWR ECCS pump operational criteria presented in Section 4 are summarized below.

1.   Low transient flow rates (less than 70 percent of the best efficiency point) with an inlet void fraction greater than 5 percent for more than 5 seconds will result in pump damage unless pump-specific testing can show otherwise.

2. Higher transient flow rates (between 70 percent and 120 percent of the best efficiency point) with an inlet void fraction greater than 10 percent for more than 5 seconds will result in pump damage unless pump-specific testing can show otherwise.

3. Low flow operation (less than 40 percent of the best efficiency point) at greater than 1 percent by volume continuous suction NCG void fraction results in pump damage unless pump-specific testing can show otherwise.

4. Full flow operation (40 percent to 120 percent of the best efficiency point) at greater than 2 percent by volume continuous suction NCG void fraction results in pump damage unless pump-specific testing can show otherwise.

ECCS pumps which operate within the void fraction conditions specified in Table 4.1-1 and within the gas void fractions indicated above in items 1 to 4 can be considered capable of recovery without damage, and will operate at normal pump head and flow conditions if the inlet void fraction is reduced to a value below 1 percent.

An ECCS pump assessment would be permitted to use other operation criteria if acceptable pump-specific tests are performed that provide better operational guidance.

The method outlined in this report is limited by the assumptions used to develop the criteria. For instance the assumptions regarding the ECCS pump start times is based on the survey information present in Reference 4. The pump operation acceptance criteria were obtained from the literature search and testing information described in Reference 44. The CFD approach used to predict the location and duration of the NCG phase is also limited to the simplified cases considered. Other phenomena such as suppression pool structures or flow patterns which could further enhance, mix, or distribute the NCG region should be considered on a case-by-case basis.

The analyses used to develop the criteria were developed for a DBA LBLOCA in the suppression pool of a Mark I containment using the information provided in Reference 2. The DBA LOCA results in the most severe NCG conditions in a suppression pool because it provides the largest and fastest break flowrates that result in the largest gas flow into the suppression pool in the shortest time. A Mark I containment results in the most limiting NCG suppression pool conditions because of its smaller size and smallest downcomer vent submergence when compared to the larger Mark II and Mark III suppression pool designs. Additionally, the ECCS pump strainers are generally located closest to the downcomers in a Mark I design. Because of similar vertical downcomer geometry, the results of this study can be conservatively applied to a Mark II containment design, which possesses a larger suppression chamber. A Mark III design includes a horizontal vent pipe orientation and the ECCS pump inlets are located significantly further from the vent exits. Consequently, the ECCS pumps in a Mark III design are expected to be less affected by NCG because lower void fractions are expected at their inlets.

8. REFERENCES

1. U. S. Nuclear Regulatory Commission, Memo from Farouk Eltawila to Carl Paperiello, "Task Action Plan for Resolving Generic Safety Issue 193, BWR ECCS Suction Concerns," May 24, 2004 (Agencywide Documents Access and Management System (ADAMS) Accession No. ML041450208).

2. Notafrancesco, A., H. Esmalli, B. Lee and J.L. Tills, "Application of the MELCOR Code to Design Basis BWR Containment Analysis," U.S. Nuclear Regulatory Commission, Office of Nuclear Regulatory Research, RES/FSTB 2011-01, May 2011 (ADAMS Accession No. ML111570060).

3. Lahey, R.T. and Moody, F.J., *The Thermal Hydraulics of a Boiling Water Reactor – Second Edition*, American Nuclear Society, 1993.

4. Fleischer, L., "Assessment of NEC Generic Issue #193 Prepared for Generic Issue #193 Committee of the BWR Owners' Group," General Electric Hitachi Nuclear Energy, NEDC-33526-P Rev. 1, October 2009.

5. "Mark-I Containment Program, Full-Scale Test Program, Final Report," General Electric, NEDE-24539-P, April 1979.

6. "Mark-III Confirmatory Test Program, Full Scale Condensation and Stratification Phenomena Test Series 5707," General Electric, NEDE-21853-P, August 1978.

7. "1/4 Scale Test Report, Loads on Submerged Structures due to LOCA Air Bubbles and Water Jets," General Electric, NEDE-23817-P, September 1978.

8. "Mark-I Containment Program, ¼ Scale Pressure Suppression Pool Swell Test Program: LDR Load Tests," General Electric, NEDE-23545-P, December 1978.

9. "Condensation Oscillation Test Program Final Test Report," General Electric, NEDE-24811-P, May 1980.

10. McCauley, E.W, et al., "Extended Analysis of Data from the 1/5-Scale Mark I Boiling Water Reactor Pressure Suppression Experiment," U.S. Nuclear Regulatory Commission, NUREG/CR-0761, September 1979 (ADAMS Accession No. ML072710074).

11. Pitts, J.H. and E.W. McCauley, "A 1/5 Scale Experiment of a Mark I Boiling Water Reactor Pressure-Suppression System under Hypothetical LOCA Loads," Lawrence Livermore Laboratory, UCRL-79143, July 1977.

12. Lai, W. and E.W. McCauley, "Air Scaling and Modeling Studies for the 1/5-Scale Mark I Boiling Water Reactor Pressure-Suppression Experiment," Lawrence Livermore Laboratory, UCRL-52383, January 1978.

13. Norris, D.M. et al., "Computer Calculations of Air and Steam Blowdown Suppression," *Nuclear Engineering and Design*, Vol. 59, pp. 301-313, 1980.

14. McCauley, E.W. et al, "The Analysis of BWR Pressure Suppression Pool Dynamics," Lawrence Livermore Laboratory, UCRL-78694, August 1976.

15. Glenn, L.A. and W.H. McMaster, "BWR Pool Dynamics in a Loss of Coolant Accident of the Air Venting Phase," Lawrence Livermore Laboratory, UCRL-52435, March 1978.

16. Edwards, L.L. "Computer Simulations of a 1/5-Scale Experiment of a Mark I Boiling Water Reactor Pressure-Suppression System under Hypothetical LOCA Conditions," Lawrence Livermore Laboratory, UCID-17782, May 1978.

17. Edwards, L.L., et al., "CHAMP: A Coupled HEMP and Multifield Eulerian Program for Fluid Flow Simulations," Lawrence Livermore Laboratory, UCRL-52444, April 1978.

18. Anderson, W.G., P.W. Huber and A.A. Sonin, "Modeling of Pool Swell Dynamics," U.S. Nuclear Regulatory Commission, NUREG-0288, March 1977.

19. Huber, P.W., et al., "Considerations in Small-Scale Modeling of Pool Swell in BWR Containments," U.S. Nuclear Regulatory Commission, NUREG/CR-1143, November 1979 (ADAMS Accession No. ML073520012).

20. Chen, C. and Dhir, V.K., "Hydrodynamics of a Bubble Formed at a Vent Pipe Exit," International Journal of Multiphase Flow, Vol. 8 No. 2, pp.147-163, 1982.

21. Aust, E., G.F. Schultheiss, D. Seeliger, and E.W. McCauley, "Experimental Results About Dynamic Load Mitigation for BWR Pressure Suppression Containments under LOCA Conditions," 7th International Conference on SMiRT, Chicago, Illinois, 1983.

22. Aust, E. and D. Seeliger, "Pool Dynamics and Dynamic Loads in Pressure Suppression Containment Systems," Transactions of the American Nuclear Society, Vol. 41, pp. 696–699, 1982.

23. Wikdahl, C.E., "*Marvikenreaktorn - ett industripolitiskt utvecklingsprojekt i otakt med tiden,*" SKI Rapport Technical Report, 2007.

24. Laine, J., "Condensation Pool Experiments with Non-Condensable Gas," Lappeenranta University of Technology, TOKE-2/2002, December 2002 (ADAMS Accession No. ML101410625).

25. Laine, J. "Supplementing Condensation Pool Experiments with Non-Condensable Gas," Lappeenranta University of Technology, YTY-01/2002, October 2002.

26. Tanskanen, V. and M. Puustinen, "CFD Simulation of Air Discharge Tests in the PPOOLEX Facility," Lappeenranta University of Technology, NKS-169, July 2008.

27. Timperi, A, et al., "Numerical Analyses of a Water Pool Under Loadings Caused by a Condensation Induced Water Hammer," VTT Industrial Systems, Finland, NKS-96, March 2004.

28. Timperi, A., et al., "Analysis of Loads and Fluid-Structure Interactions in a Condensation Pool," VTT Technical Research Center of Finland, NKS-154, April 2007.

29.   Pattikangas, T., et al., "CFD and FEM Modeling of PPOOLEX Experiments," VTT Technical Research Center of Finland, NKS-236, January 2011.

30.   Timperi, A., et al., "Modeling of Interaction of Multiple Vent Pipes in a Pressure Suppression Pool," VTT Technical Research Center of Finland, NKS-264, April 2012.

31.   Tanskanen, V., "CFD Modeling of Direct Contact Condensation in Suppression Pools by Applying Condensation Models of Separated Flow," Lappeenranta University of Technology, Thesis for the Degree of Doctor of Science (Technology), March 2012.

32.   Reference Deleted

33.   Ishii, M., et al., "Experimental Measurement of Suppression Pool Void Distribution during Blowdown in Support of Generic Issue 193," U.S. Nuclear Regulatory Commission, NUREG/CR-7186, September 2014 (ADAMS Accession No. ML14255A123).

34.   Smith, B.L., "A Numerical Investigation of Three-Dimensional Flows in Large Volumes in the Context of Passive Containment Cooling in BWRs," Nuclear Engineering and Design, Vol. 237, No. 11, pp. 1175–1184, 2007.

35.   Hart, J., et al., "TEPSS–Technology Enhancement for Passive Safety Systems," Nuclear Engineering and Design, Vol. 209, No. 1-3, pp. 243–252, 2001.

36.   Meier, M., "Numerical and Experimental Study of Large Steam-Air Bubbles Injected in a Water Pool," Swiss Federal Institute of Technology Zurich, PhD Thesis No. 13091, 1999.

37.   Meier, M., M. Andreani, and G. Yadigaroglu, "Experimental Study of Large Steam-Air Bubbles Condensing in a Suppression Pool," International Mechanical Engineering Congress and Exposition '98, ASME, Anaheim, 1998.

38.   "Experience and Qualifications for Nuclear Power Plant Studies," Alden Research Laboratories, Inc., January 2009.

39.   Padmamabhan, M., "Hydraulic Performance of Pump Suction Inlets for Emergency Core Cooling Systems in Boiling Water Reactors," U.S. Nuclear Regulatory Commission, NUREG/CR-2772, June 1982 (ADAMS Accession No. ML112440074).

40.   Kamath, P.S. et al., "An Assessment of Residual Heat Removal and Containment Spray Pump Performance Under Air and Debris Ingesting Conditions," U.S. Nuclear Regulatory Commission, NUREG/CR-2792, September 1982 (ADAMS Accession No. ML100110155)

41.   "NRC Generic Letter 2008-01: Managing Gas Accumulation in Emergency Core Cooling Decay Heat Removal and Containment Spray Systems," U.S. Nuclear Regulatory Commission, December 2007 (ADAMS Accession No. ML072910759).

42.   Rogers, R.M., "BWR Owners' Group Technical Report ECCS Pumps Suction Void Fraction Study," General Electric Hitachi Nuclear Energy, 0000-0101-3794-R0-NP, April 2009.

43. Killen, J.M and J.M. Wetzel, "Effect of Air Ingestion on Performance of a Centrifugal Pump," University of Minnesota, Final Report for Contract N00024-80-C-5944, Project Report No. 201, July 1981.

44. "Report of the Expert Panel on the Effect of Gas Accumulation on Pumps—'The Pump Roadmap,'" 1026498 Final Report, Electric Power Research Institute, August 2012.

45. "Guidelines for Effective Prevention and Management of System Gas Accumulation," NEI 09-10 (Rev1a-A), Nuclear Energy Institute, April 2013 (ADAMS Accession No. ML13136A129).

46. Sonin, A.A. and P.W. Huber, "On the Scaling Laws for Air Clearing in Water-Type Pressure Suppression Systems," Journal of Heat Transfer, Vol. 100, pp. 601-604, November 1978.

47. Emami, A. and C. Briens, "Study of Downward Gas Jets into a Liquid," AIChE Journal, Vol. 54, No. 9, September 2008.

48. McCauley, E., et al., "Multivent Effects in a Large Scale Boiling Water Reactor Pressure Suppression System," Lawrence Livermore Laboratory, UCRL-91369, Fifth International Meeting on Thermal Nuclear Reactor Safety, September 1984.

49. Puustinen, M and J. Laine, "Characterizing Experiments of the PPOOLEX Test Facility", Lappeenranta University of Technology, Finland, NKS-167, July 2008.

50. Zielke, W. and H-D Perko, "Gas Release in Transient Pipe Flow," Pressure Surges—Proceedings of the 6th International Conference, BHRA Fluid Engineering, Cranfield, Bedford, UK, pp. 3-14, 1990.

51. Kalra, A., "Task 5—Effects of Non-Condensable Gases on Seals (CVDS Pumps)," BWR Owners Group, BWROG-TP-12-013, Revision 0, August 2012 (ADAMS Accession No. ML12300A222).

52. Hutcherson, M.N. "Contribution to the Theory of Two-Phase Blowdown Phenomenon," Argonne National Laboratory, ANL-75-82, December 1975.

53. Kreith, F, *Principles of Heat Transfer*, International Textbook Company, Scranton, PA, 1965.

2. TITLE AND SUBTITLE

BWR ECCS Pump Suction Concerns following a LOCA

3. DATE REPORT PUBLISHED	
MONTH	YEAR
May	2016

4. FIN OR GRANT NUMBER

5. AUTHOR(S)

W. J. Krotiuk
C. Boyd
T. Zaki
W. Wang

6. TYPE OF REPORT

Technical

7. PERIOD COVERED (Inclusive Dates)

8. PERFORMING ORGANIZATION - NAME AND ADDRESS (If NRC, provide Division, Office or Region, U. S. Nuclear Regulatory Commission, and mailing address; if contractor, provide name and mailing address.)

Division of System Analysis
Office of Nuclear Regulatory Research
U. S. Nuclear Regulatory Commission
Washington, D.C. 20555-0001

9. SPONSORING ORGANIZATION - NAME AND ADDRESS (If NRC, type "Same as above", if contractor, provide NRC Division, Office or Region, U. S. Nuclear Regulatory Commission, and mailing address.)

Same as above

10. SUPPLEMENTARY NOTES

11. ABSTRACT (200 words or less)

This document describes a method to perform a plant specific assessment to determine whether an emergency core cooling system (ECCS) pump will acceptably operate following a loss of coolant accident (LOCA) in a boiling water reactor (BWR) pressure suppression pool using the analyses results and criteria presented in this report. The assessment approach uses the ECCS pump strainer location, the ECCS pump operation criteria, the ECCS pump startup and full operation timing information, and the transient pool void fraction information to make the determination.

In order to support the developed assessment method, this report describes the acceptable ECCS pump operating range necessary to prevent pump damage if noncondensable gas ingestion occurs or to permit recovery from noncondensable gas ingestion. Additionally, this report uses computational fluid dynamics (CFD) analyses to define a noncondensable gas bubble "exclusion zone" and provide the time dependent noncondensable void fraction distribution in the suppression pool outside the large gas bubble following a LOCA. The report also lists the test facilities used to test BWR pressure suppression systems and summarizes the test data available from these facilities which can be used to verify the acceptability of the CFD analyses.

12. KEY WORDS/DESCRIPTORS (List words or phrases that will assist researchers in locating the report.)

BWR, ECCS pump, pump gas ingestion, BWR suppression pool gas

13. AVAILABILITY STATEMENT
unlimited

14. SECURITY CLASSIFICATION
(This Page) unclassified
(This Report) unclassified

15. NUMBER OF PAGES

16. PRICE

BWR ECCS Pump Suction Concerns following a LOCA